

AD-A258 974



1

AFIT/GE/ENG/92D-35

DTIC
ELECTE
JAN 6 1993
S C D

ACQUISITION OF DIRECT SEQUENCE SPREAD
SPECTRUM SIGNALS USING DIGITAL
SIGNAL PROCESSING TECHNIQUES

THESIS

Ronald E. Schmitz, Captain, USAF

AFIT/GE/ENG/92D-35

012213
93-00124
HI

Approved for public release; distribution unlimited

93 1 04 004

Acquisition of Direct Sequence Spread
Spectrum Signals Using Digital
Signal Processing Techniques

THESIS

Presented to the Faculty of the School of Engineering
of the Air Force Institute of Technology
Air University
In Partial Fulfillment of the
Requirements for the Degree of
Master of Science in Electrical Engineering

Ronald E. Schmitz, B.S. E.E.
Captain, USAF

December 1992

Accession For	
NTIS GRA&I	<input checked="" type="checkbox"/>
DTIC TAB	<input type="checkbox"/>
Unannounced	<input type="checkbox"/>
Justification	
By	
Distribution/	
Availability Codes	
Dist	Avail and/or Special
A-1	

DTIC QUALITY INSPECTED 6

Acknowledgements

The purpose of this study is to develop an analytical model for the use of Fast Fourier Transforms in the acquisition of direct sequence spread spectrum signals. This thesis concentrated on the of the acquisition of GPS signals but the method of acquisition can be applied to other direct sequence spread spectrum systems using short PN sequences.

I'd like to thank my committee members, Major Mehalic and Lt Col Riggins for sacrificing many hours of their valuable time to help me in my attempt to complete this thesis. Special thanks are given to my advisor, Capt Joe Sacchini, for his patience and ability to supply a vector when needed. I would also like to thank my study partners, Jim H, Jim C, Dennis, Chaz, and Brian. Without their assistance and enlightenment I would not have been able to survive.

I especially want to thank my family for giving me the support and encouragement to attempt this thesis. I especially thank them for enduring the long hours that I spent away from them. To my wife Margaret and my son Brian, I give my love, appreciation, and a promise to spend more time with them.

Ronald E. Schmitz

Table of Contents

	Page
List of Figures	vi
List of Tables	x
List of Symbols	xi
Abstract	xiv
I. Introduction	1
1.1 Background	1
1.2 Problem Statement	3
1.3 Assumptions	3
1.4 Scope	4
1.5 Approach	5
1.6 Overview	6
II. Literature Review	7
III. Theory of Acquisition	10
3.1 Introduction	10
3.2 Global Positioning System Signals	10
3.3 Coarse Acquisition System	13
3.4 Correlation of the Received and Reference Code	17
3.4.1 Linear Correlation	17
3.4.2 Circular Correlation	20

	Page
3.5 Effects of Doppler Shift	33
3.6 Effects of Data Modulation	38
3.7 Effects of Noise	38
3.8 Conclusion	40
IV. Simulation Procedure	42
4.1 Introduction	42
4.1.1 Block Diagram Editor	42
4.1.2 Signal Display Editor	44
4.2 Block Descriptions	45
4.2.1 Coarse/Acquisition Code Generator	45
4.2.2 Correlation Block	46
4.2.3 Peak to Average Ratio Block	48
4.2.4 Vector Integrator Block	50
4.2.5 Delay Signal Generator	51
4.2.6 Peak Finder	51
4.3 Block Verification	51
4.3.1 Correlation Block	52
4.3.2 Peak-to-Average Ratio Block	52
4.4 Simulation of Code Offset	57
4.5 Simulation of the Received Signal with Noise	60
4.6 Simulation of the Received Signal with Doppler Shift	64

	page
4.7 Conclusion	70
V . Conclusions	71
5.1 Summary	71
5.2 Conclusions	71
5.3 Recommendations	73
5.4 Lessons Learned	73
Appendix A: Doppler Shift Calculations	75
Appendix B: SPW™ Block and Detail Drawings	77
Appendix C: Threshold Inputs For Various Doppler Frequencies	94
Bibliography	123
Vita	125

List of Figures

Figure	Page
1. Coarse Acquisition System	14
2. Sequences $x[n]$ and $G[n]$ when $\tau=0$	19
3. Sequences $x[n]$ and $G[n]$ when $\tau=\alpha$	19
4. Circular Correlation of $x[n]$ and $G[n]$	21
5. Normalized Correlation Peak	26
6. Correlation of $x[n]$ and $G[n]$ after padding and $\tau=0$	27
7. Correlation of $x[n]$ and $G[n]$ after padding and $\tau=\alpha$	29
8. Correlation of $x[n]$ and $G[n]$ after padding and $\tau=\alpha+2$	29
9. Correlation Peak for $\alpha=1022$	30
10. Correlation Peak of $x[n]$ and $G[n]$ for $\alpha<1022$	31
11. Correlation Peak of $x[n]$ and $G[n]$ for $\alpha>1024$	32
12. $r_s[n]$ with 500 Hz Doppler and $\xi=0$	35
13. $r_s[n]$ with 500 Hz Doppler and $\xi=1023$	36
14. SPW [™] Coarse Acquisition System	43
15. Auto-correlation of $x[n]$, 4096 Samples	53
16. Auto-correlation of $x[n]$, 20 Samples	54
17. Circular Auto-correlation of $x[n]$, 4096 Samples	55
18. Circular Auto-correlation of $x[n]$, 20 Samples	56
19. Number of Correlations versus Code Offset for $x[n]$ and $G[n]$	57

List of Figures (Continued)

Figure	Page
20. Peak to Average Ratio versus Code Offset for $x[n]$ and $G[n]$	58
21. Actual versus Detected Code Offset	59
22. Coarse Acquisition System with AWGN Simulator	61
23. Par versus Code Offset for Different SNRs	63
24. Coarse Acquisition System Simulator for Doppler Shift	65
25. Input and Output of the Threshold Detector	68
26. Gold Code Generator Symbol	78
27. Gold Code Generator Detail	79
28. g_1 Generator Symbol	80
29. g_1 Generator Detail	81
30. g_2 Generator Symbol	82
31. g_2 Generator Detail	83
32. Correlator Symbol	84
33. Correlator Detail	85
34. Maximum Finder Symbol	86
35. Maximum Finder Detail	87
36. Complex Vector Integrator Symbol	88
37. Complex Vector Integrator Detail	89
38. Peak To Average Ratio Symbol	90
39. Peak To Average Ratio Detail	91

List of Figures (Continued)

Figure	Page
40. Delayed Signal Generator Symbol	92
41. Delayed Signal Generator Detail	93
42. Input of Threshold Detector with 454 Hz Doppler and $\theta=0$	96
43. Input of Threshold Detector with 454 Hz Doppler and $\theta=0.1$	97
44. Input of Threshold Detector with 454 Hz Doppler and $\theta=0.2$	98
45. Input of Threshold Detector with 454 Hz Doppler and $\theta=0.3$	99
46. Input of Threshold Detector with 454 Hz Doppler and $\theta=0.4$	100
47. Input of Threshold Detector with 454 Hz Doppler and $\theta=0.5$	101
48. Input of Threshold Detector with 454 Hz Doppler and $\theta=0.6$	102
49. Input of Threshold Detector with 454 Hz Doppler and $\theta=0.7$	103
50. Input of Threshold Detector with 454 Hz Doppler and $\theta=0.8$	104
51. Input of Threshold Detector with 454 Hz Doppler and $\theta=0.9$	105
52. Input of Threshold Detector with 454 Hz Doppler and $\theta=1.0$	106
53. Input of Threshold Detector with 500 Hz Doppler and $\theta=0.5$	107
54. Input of Threshold Detector with 500 Hz Doppler and $\theta=0.0$	108
55. Input of Threshold Detector with 600 Hz Doppler and $\theta=0.5$	109
56. Input of Threshold Detector with 600 Hz Doppler and $\theta=0.3$	110
57. Input of Threshold Detector with 600 Hz Doppler and $\theta=0.8$	111
58. Input of Threshold Detector with 700 Hz Doppler and $\theta=0.5$	112
59. Input of Threshold Detector with 700 Hz Doppler and $\theta=0.3$	113

List of Figures (Continued)

Figure	Page
60. Input of Threshold Detector with 700 Hz Doppler and $\theta=0.8$	114
61. Input of Threshold Detector with 800 Hz Doppler and $\theta=0.5$	115
62. Input of Threshold Detector with 800 Hz Doppler	116
63. Input of Threshold Detector with 800 Hz Doppler and $\theta=0.6$	117
64. Input of Threshold Detector with 900 Hz Doppler and $\theta=0.5$	118
65. Input of Threshold Detector with 900 Hz Doppler	119
66. Input of Threshold Detector with 900 Hz Doppler and $\theta=0.6$	120
67. Input of Threshold Detector with 1000 Hz Doppler and $\theta=0.5$	121
68. Input of Threshold Detector with 1000 Hz Doppler	122

List of Tables

Table	Page
1. PAR Versus Phase Inversion Location	67
2 PAR for Frequencies from 500 Hz to 900 Hz	68

List of Symbols

A/D	Analog-to-Digital Converter
AGC	Automatic Gain Control
AWGN	Additive, White, Gaussian Noise
A_c	Amplitude of the received C/A code in volts
A_p	Amplitude of the received P-code in volts
C/A	Coarse/Acquisition code
CZT	Chirp Z Transform
BDE	SPW TM Block Diagram Editor
$D_i[n]$	Data on satellite i transmission
dB	Decibels
dBW	Decibels referenced to 1 Watt
DFT	Discrete Fourier Transform
DS	Direct Sequence
DSP	Digital Signal Processing
GHz	10^9 Hertz
GPS	Global Positioning System
g_1	A Maximal Length Sequence Generator for GPS Gold Codes
g_2	A Maximal Length Sequence Generator for GPS Gold Codes
IF	Intermediate Frequency
FFT	Fast Fourier Transform
$g_c[n]$	Data out of the cosine threshold Detector

List of Symbols (Continued)

$g_s[n]$	Data out of the sine threshold Detector
$G_i[n]$	Transmitted Gold code for Satellite i
kHz	10^3 Hertz
L1	1.5754 GHz Carrier Frequency of GPS Satellite Transmission
L2	1.2276 GHz Carrier Frequency of GPS Satellite Transmission
L	Length of a sequence in Chips
L_{FFT}	Length of a FFT in Samples
LO	Local Oscillator
NCO	Numerically Controlled Oscillator
N_o	Power Spectral Density of the Noise, One Sided, in watts
$n(t)$	Zero-mean, narrow-band, white noise with power spectral density of N_o
$n_m(t)$	Zero-mean, narrow-band, white noise with power spectral density of N_o after a mixer
$n[n]$	Sampled zero-mean, narrow-band, white noise with power spectral density of N_o
PAR	Peak-to-Average Ratio
PSD	Power Spectral Density
P-code	Precise-Code
PN	Pseudo-Noise

List of Symbols (Continued)

RSL	Received Signal Level
RF	Radio Frequency
R_{xy}	Cross-correlation of sequences x and y
$r[n]$	sampled sequence from $r(t)$
SDE	SPW TM Signal Display Editor
SPW TM	Signal Processing WorkStation TM Software
SS	Spread Spectrum
ω_d	Doppler shift in radians per second
ω_e	Difference Between the Estimate and Actual Doppler shift
ω_{est}	Estimate of the Doppler shift in radians per second
ω_{if}	Intermediate frequency in radians per second
ω_1	L1 in radians per second
ϕ	Satellite clock phase error in radians
α	Difference between reference and received code in samples
ξ	Location of a phase shift in samples
θ	Location of the Phase inversion in an Epoch

Abstract

This thesis investigates the use of digital signal processing (DSP) techniques to achieve initial synchronization with Global Positioning System (GPS) Pseudo-Noise (PN) signals. Synchronization with the transmitted PN signal is essential to the despreading of the transmitted Direct Sequence Spread Spectrum (DS/SS) signals and decoding of the transmitted satellite data. The use of DSP methods to decrease the time required to achieve initial synchronization is investigated. This thesis proposes an initial acquisition section of the GPS receiver and derives the equations to show the method is mathematically feasible. Computer simulations of the proposed receiver using received signals corrupted by Doppler shifts and noise and having various code offsets shows that coarse acquisition of GPS signals can be achieved using DSP methods. However, the correlation of the sequences is distorted by zero padding to allow the use of radix-2 FFTs. This distortion can be accounted for and proper coarse acquisition is still achieved.

Acquisition of Direct Sequence
Spread Spectrum Signals
Using Digital Signal Processing Techniques

I. INTRODUCTION

1.1 Background

Global Positioning System (GPS) satellites operate by transmitting spread spectrum (SS) signals to provide users with positioning information. The satellites use a special class of Pseudo-Noise (PN) sequences called Gold codes to spread the GPS signals in the frequency domain. These PN sequences were selected because the single peak correlation property enables precise delay measurements between the satellite and receiver and the low cross-correlation property enables all of the satellites to transmit on the same frequencies without causing interference [1]. However, the use of a PN code to spread the transmitted signal requires the receiver to accurately synchronize a local reference PN sequence to the received signal PN sequence[2]. In addition to the time ambiguity from the unknown transmission delay, the relative motion between the receiver and orbiting satellite Doppler shifts the transmitted GPS signal in frequency. Therefore, the receiver must search through both time and frequency to acquire the GPS signal. To decrease the acquisition time, the use of Digital Signal Processing (DSP)

techniques to perform the time search by using Fast Fourier transforms (FFTs) has been proposed [5, 9]. This thesis investigates the use of FFTs to achieve PN code synchronization.

Each satellite transmits a unique PN sequence: a short code for acquisition, the Coarse/Acquisition-code (C/A-code), and a long code for precise positioning, the Precise-code (P-code). The C/A-code is used for initial acquisition of the GPS signal and the P-code is used to obtain precise positioning information. After initial acquisition of the C/A code, the receiver uses the data from the satellite to acquire the P-code [1].

The process of synchronizing with the local PN sequence is normally performed in two steps. Initially, the coarse acquisition process brings the sequences to less than a single chip difference. This is called PN acquisition. Then the fine synchronization system takes over, reduces the time difference, and maintains synchronization. This process is called PN tracking [2]. The time required to acquire a PN sequence is determined by the number of possible time and frequency bins that must be searched and how the bins are searched. The number of time bins is determined by the length of the PN sequence. The GPS C/A code sequence is 1023 chips long. To reduce the time ambiguity to less than 1/2 of a chip required for coarse synchronization, two time bins must be searched for each chip. Therefore, 2046 time bins must be searched for each frequency. The Doppler shift can be up to ± 10 kHz. With 1 kHz steps, up to 20 different frequencies must be searched and in a worst case situation 40,960 different

combinations of time and frequency must be searched to achieve PN acquisition. Significant amounts of research has been done to reduce the search time required for PN acquisition by finding more efficient search strategies. This thesis examines the feasibility of decreasing the search time by simultaneously searching all possible time bins for a given frequency step. The proposed method uses FFTs to perform correlation and search through all possible time offsets in a single dwell for each possible frequency range. The time per dwell is set by the time required to sample the transmitted sequence for an epoch. An epoch is defined as one complete PN sequence. For the GPS C/A code an epoch takes 1 millisecond and is 1023 chips or 2046 samples in length.

1.2 Problem Statement

The use of FFTs to decrease the acquisition time for GPS receivers has been proposed. While papers have shown the feasibility of using FFTs to acquire the GPS signal, they have been limited in scope. The problems encountered when using FFTs to perform the correlation of GPS C/A codes were not addressed. The effects of the offset between the reference and received code, Doppler shift of the transmitted frequency, and noise need to be addressed before development of a GPS receiver using FFTs to perform the initial acquisition.

1.3 Assumptions

This study assumes a systems-level decision has been made as to which

satellites are in view and the receivers local PN generator is producing the correct code. A down converter is available to convert the incoming signal to an intermediate frequency (IF). The Radio Frequency (RF) front end of the receiver will perform the Automatic Gain Control (AGC) and amplify the receiver signal to the required levels. This study also assumes that an analog-to-digital (A/D) converter is available to digitize the down converted signal at 2.046 million samples per second or greater. The processor used to implement the receiver can compute the required three 2048 bit FFTs and the 2048 complex multiplies in less than 1 millisecond.

1.4 Scope

This thesis studies the application of DSP based methods to acquire the GPS C/A code. This study is divided into two parts. The first part presents the mathematical background for the coarse acquisition system. The second is the simulation of the coarse acquisition system.

The mathematical background explains the theory of achieving coarse acquisition. First, the GPS signals are introduced and the blocks of the proposed coarse acquisition system are explained. Next, the background on the use of FFTs to perform correlation and the difference between FFT-based and linear correlation is presented. Then, the effects of zero padding sequences on the correlation is explained. Next, the effects of Doppler shift and satellite data on the coarse acquisition process is explored. Finally, the effects of noise on the

ability of the coarse acquisition section to achieve initial code synchronization is explained.

The simulation section explains the software and procedures used to simulate the coarse acquisition system. First, the blocks custom-made to perform special mathematical functions for the coarse acquisition system are explained. Then, the verification procedures used to ensure the blocks perform the correct mathematical function are explained. Finally, the results of the simulations with code offset, noise, or Doppler frequency are discussed.

1.5 Approach

The approach is to develop a mathematical model of the coarse acquisition of the GPS C/A code then use a software package to simulate the model of the acquisition process. The correlation process using FFTs is developed. Then, the effect of padding sequences on the correlation process is developed. The effects of code offset, noise, Doppler shift, and data modulation are modeled. The coarse acquisition section of the GPS receiver is modeled using Signal Processing WorkStation™ (SPW™) software from ComDisco™ Corporation Incorporated [3]. First, the mathematical functions not provided by ComDisco™ are built. Then, the blocks are assembled into the coarse acquisition section of the GPS receiver. A system to simulate the GPS signal is assembled so the actual GPS Gold codes can be used in the simulations. The signal is input into the receiver after noise is added or the PN sequence is multiplied by a Doppler frequency. The output from

the simulations is recorded using the output blocks of the ComDisco™ software. The software is run on a SUN4™ workstation.

1.6 Overview

A literature review, given in Chapter 2, covers papers on the use of FFTs in PN code acquisition and gives some background on the acquisition of SS signals. Chapter 3 provides the background for the coarse acquisition of the GPS signals. First, the GPS signals and all of the individual parts of the signals are described. Then, the proposed coarse acquisition system block diagram and individual blocks are outlined. The correlation of the GPS signals and the use of FFTs in correlation is explained. The effects of Doppler shift, data modulation, and noise on the correlation of the GPS signals is explored. Chapter 4 describes the simulation of the proposed coarse acquisition system using SPW™. An overview of the blocks constructed to make the coarse acquisition system is given. The process of verification to ensure that each block performed the correct mathematical operations is detailed. Finally, simulations of the coarse acquisition process in the presence of Doppler shift, data modulation, and noise are presented. Three appendices are attached: Appendix A derives the maximum expected frequency of the Doppler shift, Appendix B contains the SPW™ detail and block diagrams, and Appendix C contains inputs to the Threshold detector for numerous Doppler frequencies.

II. LITERATURE REVIEW

The acquisition process is vital to the establishment of communications in any spread spectrum system [4] because data demodulation cannot begin until the synchronization process is complete. In addition, GPS receivers require fast acquisition to counteract intentional interference and to increase availability [5].

Serial search methods are normally used to initially acquire Direct Sequence (DS) SS systems that use long PN sequences [6]. The serial search methods use correlators to determine if the reference code is synchronized with the received code. The most common method is a sliding correlator. In this method, the local PN code is mixed with the incoming signal and the output of an integrate and dump circuit is monitored to determine if a threshold is exceeded. If the threshold is not exceeded, the reference PN code is adjusted in time and the process is repeated. The process of adjusting the reference PN code is continued until the threshold is exceeded. Other methods of acquisition include sequential estimation [7] and the use of digital sliding correlators[8].

In sequential estimation acquisition, the incoming signal is mixed with the reference PN code for a small portion of the PN sequence. The sequential estimator in [7] uses five bits for a 63-bit PN sequence. If the number of correlations exceeds a threshold, acquisition is attempted. If the threshold is not exceeded, the reference PN generator is adjusted and the process starts over. In sequential estimation, only a small portion of the sequence is examined to

determine if acquisition should be attempted instead of looking at the entire sequence as in the first method of acquisition[7].

The digital sliding correlator method begins by inputting the received signal into a one-bit A/D converter, and then loading the A/D converter output into a series of shift registers. The output of each shift register is modulo-two-added with a reference PN sequence. If the sum of the modulo two added outputs exceeds a threshold, acquisition is declared. If the threshold is not exceeded, the reference PN sequence is shifted 1/2 of a bit and the process is repeated [8].

The recent increase in the power of DSP chips is fueling the use of FFTs to decrease spread spectrum acquisition time. Papers [5] and [9] introduce the concept of using the FFT to perform the cross-correlation of the received GPS signal and the locally generated reference Gold code.

In his paper, Davenport shows that the FFT can be used to perform correlations. He then proposes that the Chirp-Z Transform (CZT) be used to perform the correlation. The CZT is used to compensate for the zero padding of the sequences. Padding of the sequences is required to lengthen the sequence to the next power of two. He demonstrates the use of the CZT to perform the cross-correlation of the received and reference PN sequence and shows that the cross-correlation produces an easily identifiable peak [9]. The article does not provide any in-depth mathematical development of FFT-based correlation but does show that the use of DSP methods to perform correlation is more computationally efficient than linear correlation.

The mean acquisition time of the FFT method of acquisition is discussed by Van Nee. He discusses how the FFT performs a parallel search in time by correlating the incoming signal with the local reference. He then presents a formula used to compute the mean acquisition time using the FFT acquisition method. He concludes that the acquisition time of the GPS receiver can be reduced through the use of the FFT [5].

Numerous articles have been written about the acquisition of SS signals. A decrease in acquisition time, probability of a false acquisition, and complexity of the receiver are the goals of the research. The theory of using FFTs to perform correlation is well known and is published in at least two books [10, 11], but the use of FFTs to perform coarse acquisition of SS signals is not well established. The two articles [5,9] that address the use of FFTs to perform SS acquisition indicate the process has the desired characteristics of faster acquisition and less complex receivers.

III. THEORY OF ACQUISITION

3.1 Introduction

This chapter provides the mathematical background for the coarse acquisition for the GPS C/A-code. The signal transmitted by a GPS satellite is presented and each component of the signal is explained. An overview of the proposed coarse acquisition section of the GPS C/A-code receiver is given. Next, the theory of correlation using FFTs and the effects of padding sequences on cross-correlation is discussed. Finally, the effects of Doppler shift, noise, data modulation, and code offset on the coarse acquisition process is explained. As with any spread spectrum system, the coarse acquisition of the GPS C/A-code is required before data can be decoded. This chapter provides an understanding of the difficulties in achieving coarse acquisition.

3.2 Global Positioning System Signals

Every GPS satellite transmits a complex signal on the same two frequencies with different data and PN codes. The two frequencies are designated L1 and L2. The transmitted signal on L1 is [1]:

$$\begin{aligned} S(t) = & A_p P_i[n] D_i[n] \cos(\omega_f t + \phi) \\ & + A_c G_i[n] D_i[n] \sin(\omega_f t + \phi) \end{aligned} \quad (1)$$

where

A_p = Amplitude of the P-code

$P_i[n]$ = P-code at 10.23 Mbps

$D_i[n]$ = 50 bps data

ω_1 = $2\pi 1.57542$ GHz

ϕ = Satellite Clock Phase Error

A_c = Amplitude of the C/A-code

$G_i[n]$ = C/A-code at 1.023 Mbps

The transmitted power of the C/A-code, determined by the amplitude of A_c , is three to six decibels higher than the power of the P-code set by A_p . The frequency 1.2276 GHz is designated as L2 in the GPS system. The signal transmitted on frequency L2 consists of the same P-code as on L1, and satellite data as transmitted on frequency L1. The signal at frequency L2 is transmitted with the same power as the P-code transmitted on frequency L1. The minimum Received Signal Level (RSL) is -160 dBW for the C/A-code and -166 dBW for the P-code signals[1]. The C/A-Code correlation process effectively decreases the amplitude of the P-code signals by 30 dB [12]. After the C/A-code despreading process the P-code signal appears as additional noise in the received signal. The additional 30 dB loss from the correlation process decreases the effective power of the P-code signals beneath the power of thermal noise. Therefore the P-code on L1 and L2 does not effect the C/A-code acquisition process [1] and the effects of

the P-code on the acquisition process are not addressed in this thesis. The satellite clock phase error, ϕ , is the difference between the phase of the satellite and the local oscillator. Subscripts i on the data, P-code, and C/A-symbols are to show that data and PN codes are satellite specific. For the rest of this document the subscripts are dropped unless needed for clarity. For acquisition, the received signal is:

$$r(t) = A_r G[n] D[n] \sin[(\omega_c - \omega_d)t + \phi] + n(t) \quad (2)$$

where

A_r = Amplitude of the Received Signal

ω_d = Doppler Shift

$n(t)$ = Zero-mean, Narrow-Band, White Noise with
Power Spectral Density of N_o (one-sided)

The Doppler shift, ω_d , can range up to ± 9.6 kHz depending on the relative speed of the receiver and the location of the satellite. The computations of the maximum Doppler shift are derived in Appendix A. The Doppler shift can have a significant impact on the time required to achieve initial synchronization.

The signal in Equation 2 is used as the received signal for the rest of this document. The power of the input noise and the received signal is not addressed

because the receiver RF front end is assumed to have AGC circuitry and A_r is assumed to be one for the rest of this document. The relative power of the noise and signal is addressed in Section 3.6.

3.3 Coarse Acquisition System

Figure 1 shows a block diagram of the proposed coarse acquisition section for the GPS receiver. After reception by the antenna, the signal is mixed with the Local Oscillator (LO). The output of the mixer is filtered to remove the sum components and amplified with a gain of two. The amplifier gain of two is chosen to simplify the mathematics and is not meant to be representative of the gain of the actual receiver. The bandwidth of the filter needs to pass the intermediate frequency (IF) but preserve the power spectral density of the received signal around the IF frequency. The bandwidth of the transmitted GPS signal is 20.46 MHz null-to-null but the C/A-code is only 2.046 MHz null-to-null [1]. The filter bandwidth is not addressed in the document but is assumed to be wide enough to preserve the power spectral density (PSD) of the received signal. The signal out of the mixer is:

$$r_m(t) = G[n]D[n]\cos\{(\omega_f + \omega_d)(t) - \phi\} + n_m(t) \quad (3)$$

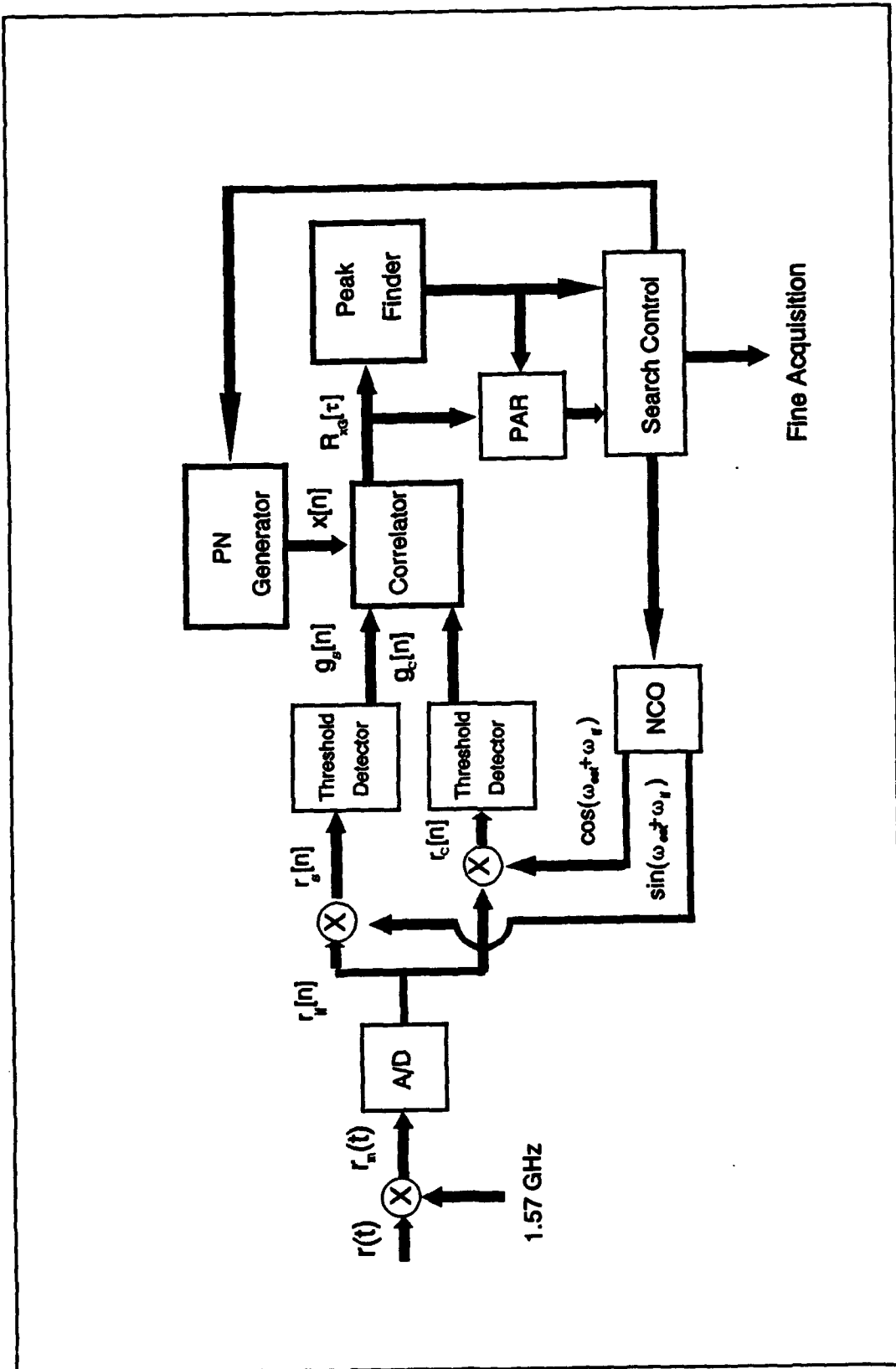


Figure 1 Coarse Acquisition System

where:

ω_{if} = Difference Between the L0 and L1

$n_m(t)$ = Band pass Filtered Noise Frequency Shifted

The LO frequency must be chosen so that when $r[n]$ is mixed with the frequency $\omega_{if} + \omega_{est}$, the output of the mixer can be filtered to remove the sum terms, where ω_{est} is the estimate of the Doppler shift frequency. The noise term, $n_m(t)$, can be considered a frequency shifted version of $n(t)$ with the same PSD [13]. The signal is then sampled at 2.046 MHz, the Nyquist rate for $G[n]$, and the resulting signal is:

$$r_{if}[n] = G[n]D[n]\cos\{(\omega_{if} + \omega_{est})n - \phi\} + n_m[n] \quad (4)$$

Sampling at 2.046 MHz generates two samples per chip of the GPS C/A-code. The sampling rate limits the time resolution of the coarse acquisition system to 1/2 of a chip. Then $r_{if}[n]$ is mixed with $\sin\{(\omega_{if} + \omega_{est})n\}$ and $\cos\{(\omega_{if} + \omega_{est})n\}$. Assuming that ω_{est} the estimate of the Doppler shift, is not the same as ω_d , the Doppler shift, the output of the mixer after filtering and amplification is:

$$r_s[n] = G[n] D[n] \sin\{\omega_e n + \phi\} + n_s[n] \quad (5)$$

and

$$r_c[n] = G[n] D[n] \cos\{\omega_e n + \phi\} + n_c[n] \quad (6)$$

where

$\omega_e =$ difference between the actual Doppler shift and estimate of the Doppler shift

The signals $r_s[n]$ and $r_c[n]$ represent orthogonal channels. If the estimate of the Doppler frequency, ω_{est} , is correct, then $r_s[n]$ and $r_c[n]$ are scaled by ϕ . If ω_{est} is not equivalent to ω_a , the input to the threshold detector is amplitude modulated by the frequency ω_e . Because of orthogonality, as the power in one channel decreases, the power in the other channel increases. Therefore, inputting both $r_s[n]$ and $r_c[n]$ ensures all of the power in the received signal reaches the correlator. Prior to the correlator, the signal is sent through a threshold detector. The output of the threshold detector is defined as:

$$g[n] = \begin{cases} 1 & r[n] \geq 0 \\ -1 & r[n] < 0 \end{cases} \quad (7)$$

The actual input to the correlator is $g_s[n]$ and $g_c[n]$. If the effects of the noise, data, and Doppler are ignored, then $g_s[n] = r_s[n]$ and $g_c[n] = r_c[n]$. The correlator cross-correlates $g[n]$ and $x[n]$. The output of the correlator is a vector that contains the value of the correlation for each τ , where τ is the offset between $x[n]$ and $g[n]$. The peak finder locates the peak value in the vector and sends the index of the peak value to the search control and Peak-to-Average Ratio (PAR) block. The PAR block computes the PAR of the vector at the output of the correlator and sends the PAR to the search control block. The search control block determines if coarse acquisition has occurred. If acquisition has not occurred, the search control block adjusts the Numerically Controlled Oscillator (NCO) and begins another search. If coarse acquisition is achieved, the search control block provides the time difference between the reference and received PN codes to the rest of the GPS receiver. This enables the fine acquisition circuitry to lock onto and track the C/A-code. The search control block was not developed as part of this thesis but is shown for completeness of the coarse acquisition system. This overview of the receiver presents an introduction of the functionality of the main blocks in the coarse acquisition process.

3.4 Correlation of the Received and Reference Code

3.4.1 Linear Correlation. The reference PN sequence is $x[n]$, where $x[n]$ is defined as the satellite's Gold code sampled at two samples per chip, and $x[0]$ is defined as the output when the g_1 and g_2 shift registers of the Gold code

generator contain all ones. Recall that Gold codes are a combination of two maximal length sequences. The received signal, $G[n]$, is generated using the same generator polynomials as $x[n]$ [14], but values of the $g1$ and $g2$ shift registers are unknown for $G[0]$, where $G[0]$ is defined as the first bit in the epoch of received data sequence. The cross correlation of $G[n]$ and $x[n]$ is defined as:

$$R_{xG}[n]=x[n]*G_i[n]=x[n]*x[n+\alpha] \quad (8)$$

where

α = Offset Between $x[0]$ and $G[0]$

$*$ = Linear Correlation Operator

Figure 2 shows the sequences $x[n]$ and $G_i[n]$ when $\tau=0$. As τ increases $G[n]$ slides to the right, and when $\tau = \alpha$, as shown in Figure 3, the two sequences produce a correlation peak of 2046. Properties of Gold codes include an auto-correlation that has a normalized peak value of one [1], and instead of the two-level auto-correlation of a maximal length PN sequence, the Gold code has a four-level auto-correlation function. The Gold code properties are for sequences that are sampled at one bit per chip and the GPS code are sampled at two bits per chip. To determine the value of α in Equation 8, the vector out of the correlator is searched for the maximum value:

$$x[n] = \boxed{x[0], x[1], \dots, x[2044], x[2045]}$$

$$G[n + \tau] = \boxed{x[\alpha], x[\alpha+1], \dots, x[2045] \mid x[0], \dots, x[\alpha-2], x[\alpha-1]}$$

For $\tau=0$

Figure 2 Sequences $x[n]$ and $G[n]$ when $\tau=0$

$$x[n] = \boxed{x[0], x[1], \dots, x[2044], x[2045]}$$

$$G[n + \tau] = \boxed{x[0], x[1], \dots, x[\alpha], x[\alpha+1], \dots, x[2044], x[2045]}$$

For $\tau=\alpha$

Figure 3 Sequences $x[n]$ and $G[n]$ with $\tau=\alpha$

$$\tau = \alpha \quad \text{When } R_{xG}[\tau] = M \quad (9)$$

where:

$M =$ Maximum value of $R_{xG}[n]$ for $n = 0$ to 2045

This assumes that $x[n]$ is periodic, and that $G[n]$ is slid to the right until the peak occurs. However, the proposed acquisition method uses FFTs to perform correlation and the result is not linear but circular correlation [10]. The differences are discussed in the next section.

3.4.2 Circular Correlation. The use of the FFT to perform convolution or correlation requires the periodicity of the FFT be taken into account. The results of the FFT-based correlation is called circular because the periodicity of the FFT causes periodicity in the correlation. The length of the periodicity of the correlation corresponds to L_{FFT} , the length of the FFT used to perform the correlation. Circular correlation differs from linear correlation in the following ways: circular correlation is periodic on L_{FFT} , and aliasing occurs in circular correlation [10]. Figure 4 shows circular correlation graphically. Note that instead of sliding as in linear convolution, a sequence is rotated about another sequence. The correlation repeats every L_{FFT} , as shown in Figure 4. In the case of $x[n]$ and $G[n]$, there is aliasing during the entire correlation. The aliasing can be avoided by padding the sequences to 4092, but that increases the number of computations required to perform the correlation. In many applications, the aliasing is intolerable but 1023 chip Gold codes have a maximum value of 65 when the Gold code sequences are not aligned [15]. Therefore, the maximum values of the correlation when $\alpha \neq \tau$ is two orders of magnitude less than the maximum value correlation when $\alpha = \tau$. The circular correlation of $x[n]$ and $G[n]$

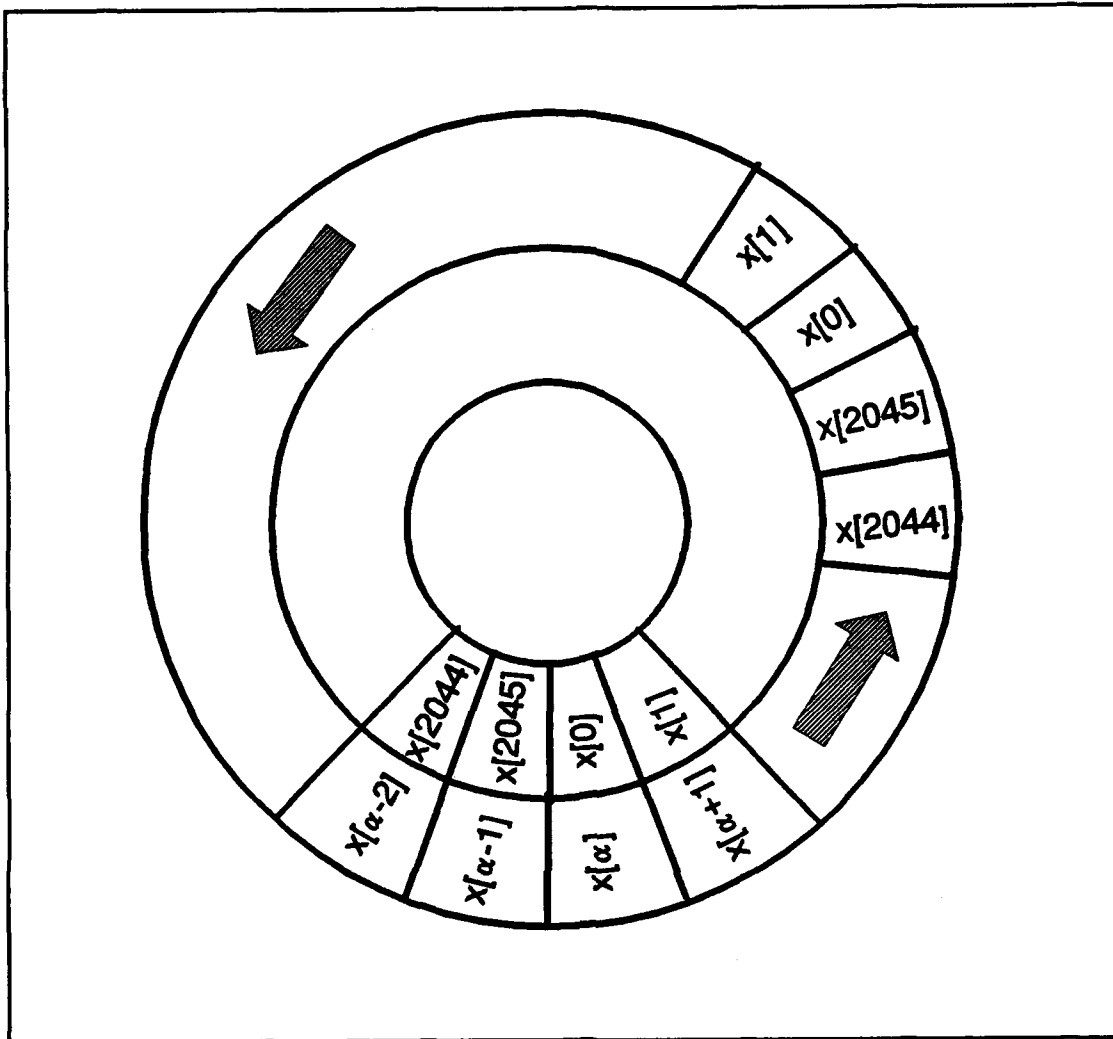


Figure 4 Circular Correlation of $x[n]$ and $G[n]$

is a maximum value when $\alpha = \tau$ and the indices of the maximum value correspond to the amount of offset between the received and reference code. This α , the amount of code offset in samples, can be passed to the tracking circuit of the GPS receiver which performs fine synchronization with the received C/A-code.

the Discrete Fourier transform (DFT) is [10]:

$$X[k] = \sum_{n=0}^{N-1} x[n] e^{-j\frac{2\pi kn}{N}} \quad (10)$$

where

$x[n]$ = Input Sequence

N = Number of Samples of $x[n]$

$X[k]$ = Periodic Frequency Representation of $x[n]$

k = Indices of the DFT Ranging from 0 to $N-1$

The inverse DFT is defined as [10]:

$$x[n] = \frac{1}{N} \sum_{k=0}^{N-1} X[k] e^{j\frac{2\pi kn}{N}} \quad (11)$$

The FFT of a sequence is also given by solving Equation 10. The distinction between the DFT and FFT is the algorithms used to perform the calculations. The DFT is solved using direct calculation and requires more computation than the FFT, but the value of N has no restrictions. FFTs reduce the number of calculations but restrict the values of N that can be used. For example, the FFT used to simulate the GPS coarse acquisition receiver requires the input sequence length to be a power of two [3].

The circular convolution of sequences $x[n]$ and $y[n]$ using the Fourier transform is defined as [10]:

$$x[n] \otimes y[n] = \mathcal{F}^{-1}\{X[k]Y[k]\} \quad (12)$$

where

\mathcal{F}^{-1} = Inverse Fourier Transform Operator

$X[k]$ = Fourier transform of $x[n]$

$Y[k]$ = Fourier transform of $y[n]$

\otimes = Circular Convolution Operator

Using the properties from Table VI of [11] circular correlation is defined as:

$$x[n] \bullet y[n] = x[-n] \otimes y[n] = \mathcal{F}^{-1}(X[-k]Y^*[-k]) \quad (13)$$

where

$Y^*[-k]$ = Complex Conjugate of $Y[-k]$

\bullet = Circular Correlation Operator

The C/A-code is 1023 chips long and is sampled at two samples per chip. The resulting sequence, $x[n]$, is 2046 samples long. Because 2046 is not a power

of two, the algorithm used to transform $x[n]$ would require more computations than a 2048 bit sequence. For computational efficiency, the sequence is padded with two zeros, making the sequence 2048 bits in length [8].

First, the correlation of $x[n]$ and $G[n]$ without zero padding is explained.

The received sequence $G[n]$ is defined as:

$$G[n] = (x[\alpha], \dots, x[2045], x[0], \dots, x[\alpha-1]) \quad (14)$$

where

$x[n]$ = C/A-Code Sampled at 2 Samples Per Chip

α = Value of Offset, Between 0 and 2045.

The offset value α represents an delay in samples between the start of the reference and received C/A-code. The delay is a between 0 and 2045 samples, and is dependant on the distance between the satellite and the GPS receiver. The cross-correlation of $x[n]$ and $G[n]$ can be defined as:

$$R_{xG}[\tau] = \sum_{n=0}^{2045} x[n] G[n+\tau] \quad (15)$$

Because $G[n+\tau] = x[n+\alpha+\tau]$, Equation 15 can be rewritten as:

$$R_{xG}[\tau] = \left[\sum_{n=0}^{\alpha} x[n]x[n+\alpha+\tau] \right] + \left[\sum_{n=\alpha+1}^{2045} x[n]x[n-\alpha+\tau] \right] \quad (16)$$

The length of the sequences is 2046 and they are circularly correlated; therefore, the argument for the summation and sequences is modulo 2046. The result of the cross-correlation of $x[n]$ and $G[n]$ without zero padding, as defined in Equation 8, is a peak, when $\tau = \alpha$, as shown in Figure 5. The width of the peak is three samples and the amplitude at ± 1 sample from the peak is 0.5 of the normalized value. Recall that for a PN sequence correlated using continuous time, the width of the pulse would be one chip. The expansion of the correlation peak shown in Figure 5 is because the sequences correlated in the coarse acquisition section of the GPS receiver are sampled at two samples per chip.

Now, the effects of zero padding on the correlation $x[n]$ and $G[n]$ are investigated. When the sequences $x[n]$ and $G[n]$ are zero padded from 2046 to 2048 to reduce the number of computations required to perform the correlation [8], the new sequences are:

$$G_p[n] = (x[\alpha], \dots, x[2046], x[0], \dots, x[\alpha-1], 0, 0) \quad (17)$$

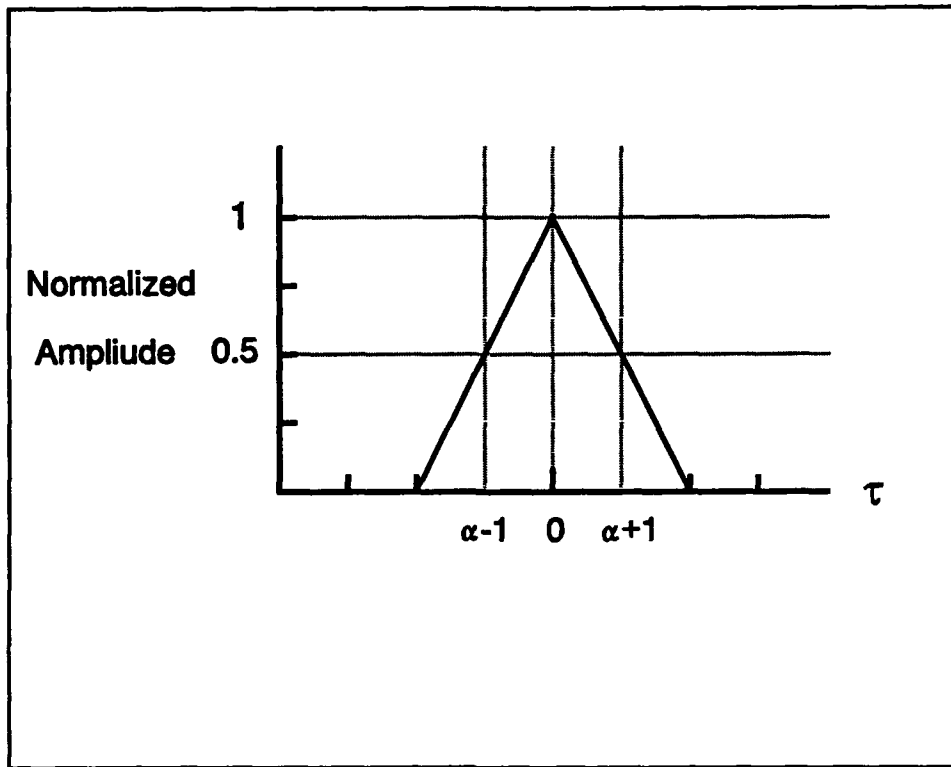


Figure 5 Normalized Correlation Peak

and

$$x_p[n] = (x[0], \dots, x[2045], 0, 0) \quad (18)$$

Then the cross-correlation of $x_p[n]$ and $G_p[n]$ is:

$$R_{xG}[\tau] = \sum_{n=0}^{2047} x_p[n] G_p[n+\tau] \quad (19)$$

$R_{xG}[\tau]$ has a maximum value of 2046 instead of 2048 when α and τ are equal to zero, because two of the samples are zero instead of ± 1 . Figure 6 shows the sequences $x[n]$ and $G[n]$ after the zero padding. The zeros are inserted at the end of the sequences $x[n]$ and $G[n]$. But when $G[n]$ is redefined in terms of $x[n]$, as shown in Figure 6, the zeros are inserted randomly into the middle of the

$$\begin{array}{l}
 x[n] = \boxed{x[0], x[1], \dots \quad \dots, x[2045], 0, 0} \\
 \\
 G[n+\tau] = \boxed{x[\alpha], x[\alpha+1], \dots \quad \dots, x[2045], x[0], \dots \quad \dots, x[\alpha-1], 0, 0} \\
 \\
 \text{For } \tau=0
 \end{array}$$

Figure 6 Correlation of $x[n]$ and $G[n]$ after padding and $\tau=0$

sequence $x[n]$. Recall that the sequences are circularly correlated but the correlation results are shown as linear correlation for clarity. The insertion of the zeros distorts the correlation of $G[n]$ and $x[n]$. For values of α greater than 0, $R_{xG}[\tau]$ has two peaks instead of the one peak for the unpadded correlation of PN sequences. Figure 7 shows that the first peak occurs at $\tau=\alpha$. The amplitude of the first peak of the correlation is:

$$A_{peak1} = [2045 - \alpha] + \lambda \quad (20)$$

where

A_{peak1} = Amplitude of the Correlation Peak

α = Offset between the Start of $G[n]$ and $x[n]$

λ = Number of Correlations - Number of Non-Correlations (In the Non-Aligned Portion of the Sequences)

For the sequences $x[n]$ and $G[n]$, as shown in Figure 7, the samples for $x[\alpha]$ to $x[2045]$ are aligned and, using the sequence $x[n]$ as a reference, the samples from $x[0]$ to $x[\alpha-1]$ are not aligned with the corresponding sample in $G[n]$. The second peak of the correlation occurs when $\tau = \alpha + 2$, and the sequences are shown in Figure 8. The amplitude of the second peak is:

$$A_{peak2} = \alpha + \lambda \quad (21)$$

When $\tau = \alpha + 2$, the samples from $x[0]$ to $x[\alpha-1]$ are aligned. The amplitude of both peaks, A_{peak1} and A_{peak2} , is dependant on α and λ . As the value of α increases, A_{peak1} decreases and A_{peak2} increases. But the value of λ is unknown for

$$\begin{array}{l}
 x[n] = \left[\begin{array}{c|c} x[0], x[1], \dots & \dots, x[\alpha-1], x[\alpha], \dots \\ \hline \dots, x[2045], 0, 0 \end{array} \right] \\
 G[n] = \left[\begin{array}{c|c} x[2], x[3], \dots & \dots, x[\alpha-1], 0, 0, x[\alpha], \dots \\ \hline \dots, x[2045], x[0], x[0] \end{array} \right] \\
 \text{For } \tau = \alpha
 \end{array}$$

Figure 7 Correlation of $x[n]$ and $G[n]$ after padding and $\tau = \alpha$

$$\begin{array}{l}
 x[n] = \left[\begin{array}{c|c} x[0], x[1], \dots & \dots, x[\alpha-1], x[\alpha], \dots \\ \hline \dots, x[2045], 0, 0 \end{array} \right] \\
 G[n+\tau] = \left[\begin{array}{c|c} x[0], x[1], \dots & \dots, x[\alpha-2], x[\alpha-1], 0, 0, x[\alpha], \dots \\ \hline \dots, x[2044], x[2045] \end{array} \right] \\
 \text{For } \tau = \alpha + 2
 \end{array}$$

Figure 8 Correlation of $x[n]$ and $G[n]$ after padding and $\tau = \alpha + 2$

Equations 19 and 20. The length of the non-aligned portion of the sequences varies from 0 to 1023 and the length of the non-aligned portions of the sequences is dependent on α . While the exact value of λ is impossible to predict, the maximum value of the auto-correlation function for a complete GPS Gold code sequence when non-aligned is 65 [14]. If λ is ignored, the values of $A_{\text{peak}i}$ and

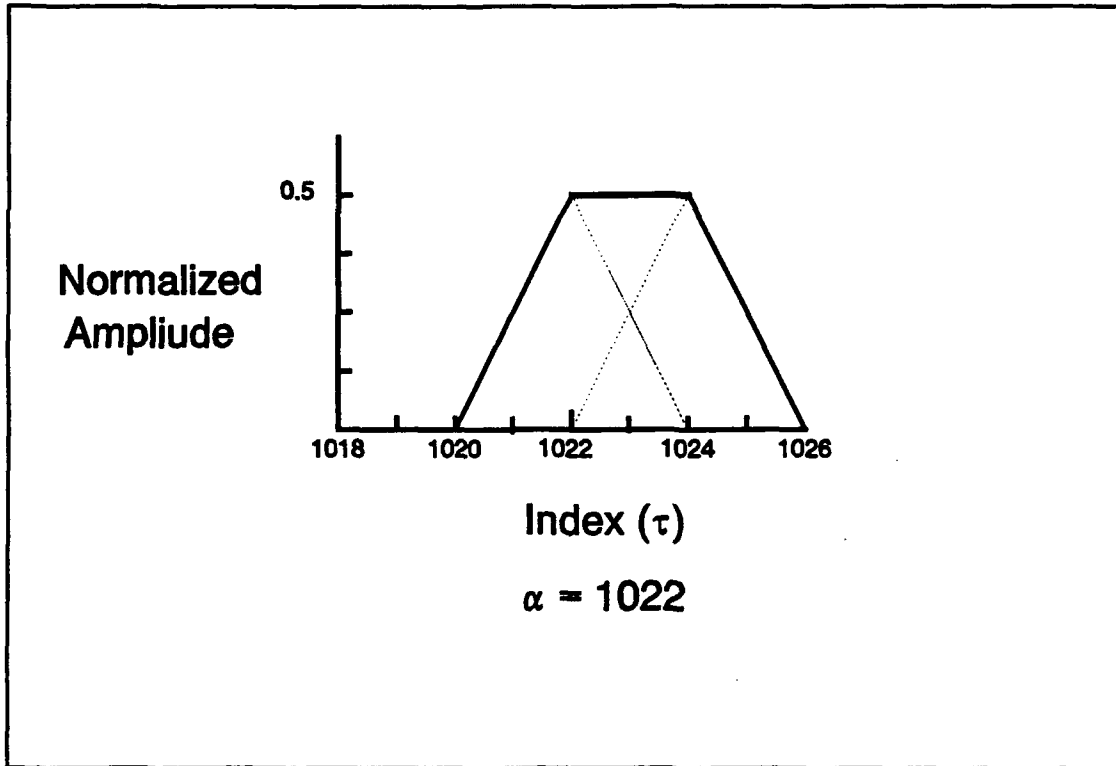


Figure 9 Correlation Peak for $\alpha = 1022$

A_{peak2} are equal when $\alpha = 1023$, and the resulting peak is shown in Figure 9. The solid lines represent the output of the correlator and the dashed lines represent the contribution by each individual correlation peak. For values of α less than 1023, the peak out of the correlation of $x[n]$ and $G[n]$ is shown in Figure 10. Figure 11 shows the output of the correlator when α is greater than 1024. Both figures show that the output of the correlator is the sum of two peaks where the dashed lines show the value of the individual peaks and the solid line shows the sum of the peaks. The value of α determines which peak has the maximum amplitude and the slope of the line connecting the two peaks. The slope of the

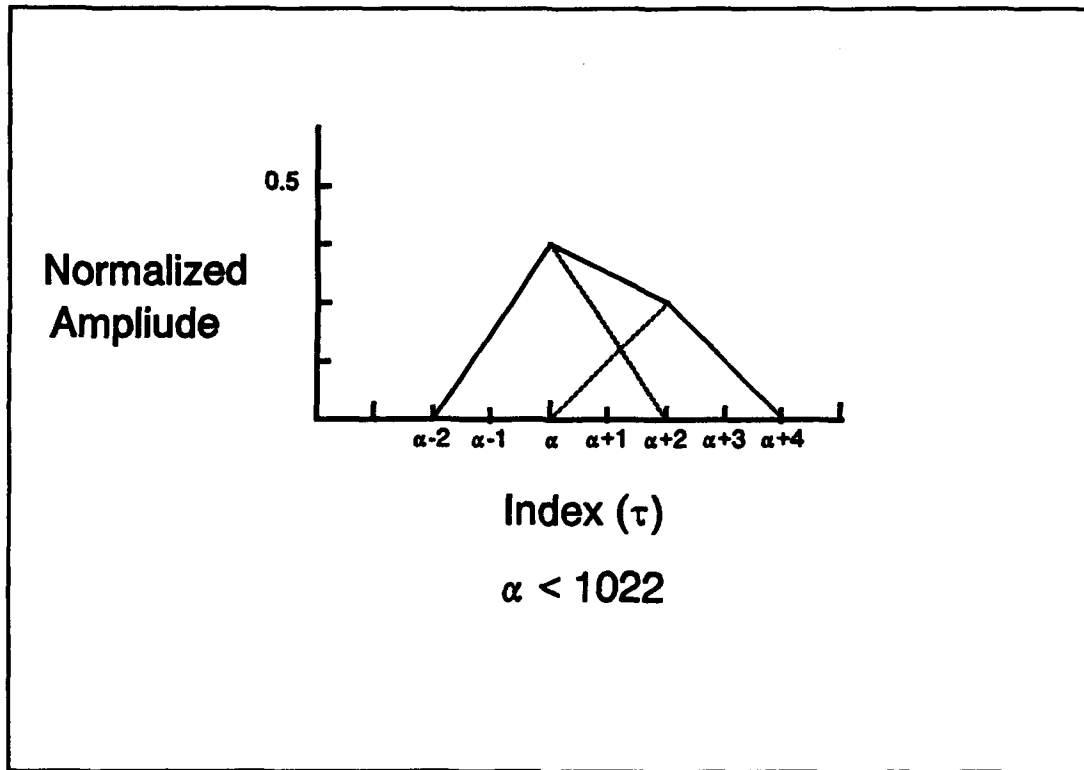


Figure 10 Correlation peak of $x[n]$ and $G[n]$ for $\alpha < 1022$

line between α and $\alpha+2$ is determined by how close α is to 1023 and as shown in Figure 9, when $\alpha=1023$ the line has zero slope. When $\alpha < 1023$, the slope of the line connecting α and $\alpha+2$ is negative and the peak of the correlation is at α . When $\alpha > 1023$, the line connecting α and $\alpha+2$ has positive slope and the peak of the correlation is at $\alpha+2$. The coarse acquisition receiver determines the amount of offset between $x[n]$ and $G[n]$ by locating the peak of the correlation. The index of the peak is the offset in number of chips. But when $\alpha = 1023$, the ambiguity of the peak is three samples or $3/2$ chips. The code tracking loop of the fine acquisition section of the receiver requires the sequences' offset to be less than

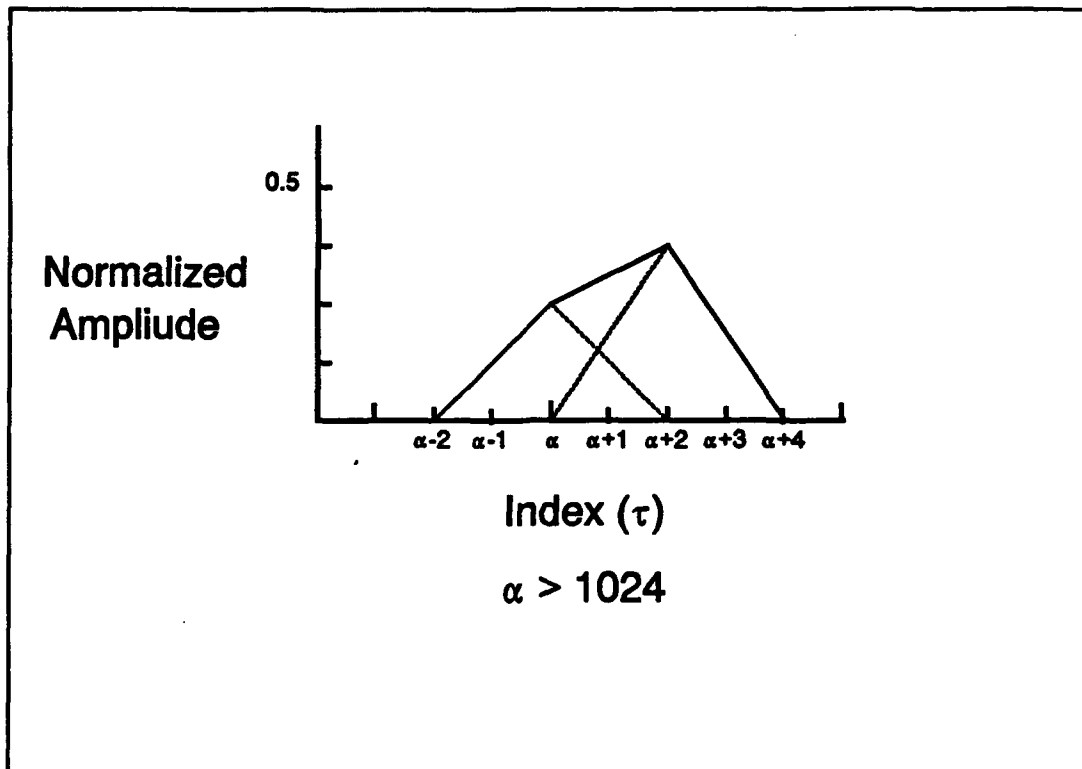


Figure 11 Correlation Peak for $x[n]$ and $G[n]$ for $\alpha > 1024$

one chip or the code loop cannot perform fine synchronization. Therefore, the coarse acquisition receiver cannot reduce the time ambiguity to less than one chip when $\alpha = 1023$. When $\alpha > 1023$ the peak is at $\alpha + 2$ and the receiver must subtract two from the location of the peak to determine the code offset. Recall this discussion does not include the effects of λ . The actual location of the change of the correlation peak index from α to $\alpha + 2$ is determined by λ and α .

The correlation of sequences using FFTs results in circular correlation instead of linear correlation. The use of Gold code sequences ensures that the overlapping portions of the code do not produce a significant peak except when

the sequences align [16]. The padding of the sequences to reduce the computations introduces distortion into the correlation. The change in the number of peaks from one to two introduces ambiguities into the location of the actual index of the peak when $\alpha=1022$. Also, the unknown value of λ could shift the actual area of ambiguity from $\alpha=1022$.

3.5 Effects of Doppler Shift

Doppler shift can have a significant impact on the PAR at the output of the correlator. Equations 5 and 6 show the input to the threshold detector with Doppler. In this section, the signal is assumed to be totally contained in $r_s[n]$ and $r_c[n]$ is ignored during the discussion on Doppler shift. Additional assumptions for this section are: the phase error is zero, the code offset is zero, and the data is a one. The code offset is set to zero to eliminate the distortion of the correlation from zero padding. Recall that when $\omega_e = 0$, all effects from Doppler are removed by the threshold detector, where ω_e is defined as the difference between the estimate of the Doppler shift frequency and the actual Doppler shift frequency. When $\omega_e \neq 0$, the frequency of ω_e and the locations of the phase inversions from ω_e determine the effect of the residual Doppler frequency ω_e . Using Equation 5 and eliminating the noise, the input to the threshold detector is:

$$r_s[n] = G[n] \cos(\omega_c[n]) \quad (22)$$

Ignoring amplitude scaling of the cosine because of the threshold detector, the effect of ω_c is to cause data inversions during data accumulation. The inversion during data accumulation decreases the amplitude of the correlation peak. The effect of a single inversion is:

$$R_{xx}[\tau] = \left[\sum_{n=0}^{\zeta} x[n]x[n+\tau] \right] - \left[\sum_{n=\zeta+1}^{2045} x[n]x[n+\tau] \right] \quad (23)$$

where

ζ = Location of the Inversion in Samples

The receiver takes 1 millisecond to accumulate the one epoch of data required for correlation. Recall that an epoch of a PN code is one complete code sequence and for the GPS coarse acquisition receiver an epoch is 2046 samples. Figure 12 shows the input to the threshold detector for one epoch of data when $\omega_c = 500$ Hz and $\xi = 0$. In this case, no inversions occur during data accumulation and the threshold detector removes all of the amplitude modulation. Thus, the amplitude of the correlation peak is not affected. Figure 13 shows the input to the threshold detector for $\omega_c = 500$ Hz and $\xi = 1023$. In this case the an inversion

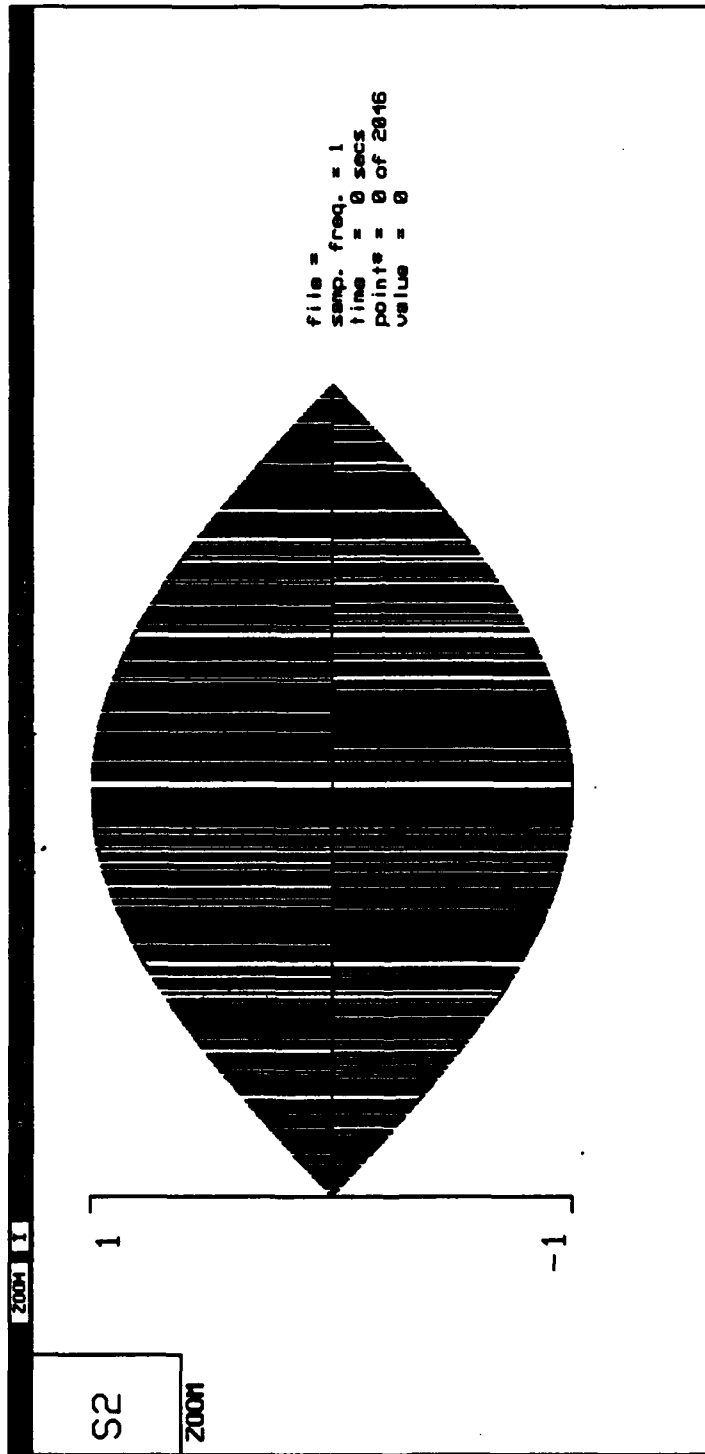


Figure 12 $r_r[n]$ With 500 Hz Doppler and $\xi=0$

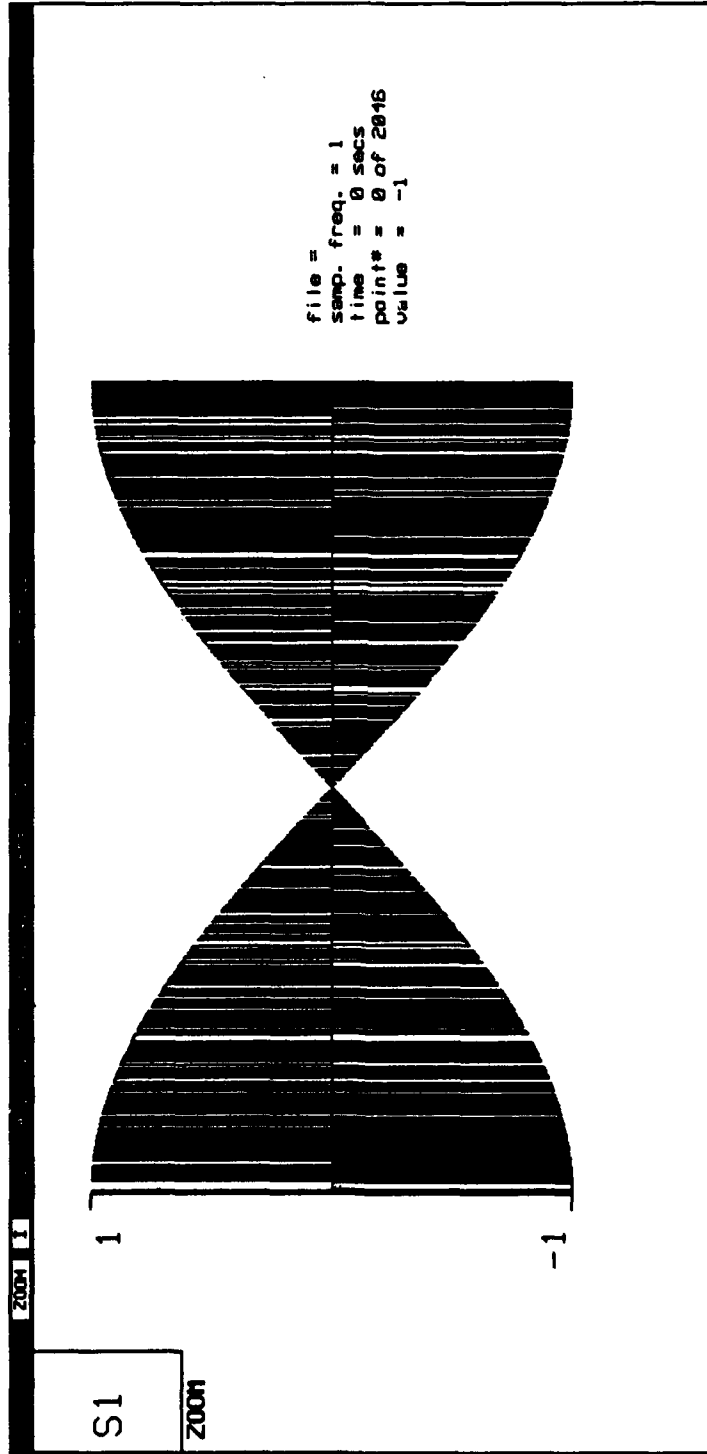


Figure 13 $r_s[n]$ With 500 Hz Doppler and $\xi = 1023$

of the data occurs during data accumulation, and the amplitude of the correlation peak is affected. For the case presented in Figure 13, the correlation of the samples after the phase inversion has the opposite sign of the correlation of the samples before the inversion. The effect of the phase inversion is described in Equation 22, and the correlation peak is predicted to be zero. In both Figures 12 and 13, $\omega_e = 500$ Hz and the value of ξ determines the effect of the Doppler shift on the correlation peak. This is significant because any Doppler left after mixing with the estimate can prevent acquisition.

For frequencies of ω_e below 500 Hz, the phase inversions from Doppler occur less than once per data accumulation on average, and the correlation peak of a data accumulation without a phase inversion is unaffected. When ω_e is greater than 500 Hz, at least one inversion occurs during each data accumulation. When ω_e is greater than 1000 Hz, there are at least two data inversions per accumulation cycle.

The effects of ω_e on the correlation peak can be significant. While ω_e determines how often a data inversion occurs, ξ determines the effect that an inversion has on the correlation process. The step size, of the frequency search control can be set to 1000 Hz steps to ensure that ω_e is less than or equal to 500 Hz for at least one acquisition attempt. But $\omega_e < 500$ Hz does not ensure that the effects of ξ do not prevent acquisition. When determining the effects of ω_e on the ability of the coarse acquisition receiver to determine the code offset, more than the frequency of the Doppler must be considered.

3.6 Effects of Data Modulation

The GPS data message is 1500 bits long and has five subframes. The GPS frame is sent once every 30 seconds as the data, $D[n]$, modulates the GPS bit stream at 50 bps. This means that an inversion in the PN sequence from the data is possible once every 20 milliseconds. The effect on a correlation from satellite data changing during data accumulation is described by Equation 23. The only difference is the source of the phase inversion. The effect of data modulation is equivalent to $\omega_e=25$ Hz, if the 50 bps data changed states every 20 milliseconds. The actual data does not change every 20 milliseconds. Therefore, on the average, the effects of the data modulation are less than $\omega_e=25$ Hz. But the effects of the GPS message data on a single correlation is determined by ξ , the location of the phase inversion. While not significant in terms of how often the GPS message data causes a phase inversion, the effect of the inversion from data on a single epoch can be significant.

3.7 Effects of Noise

The effects of noise on the correlation process are discussed without considering the effect of ω_d or τ . The input noise is assumed to be additive, white, Gaussian noise as introduced in Equation 2. The frequency shift to base band does not affect the Gaussian distribution of the noise [13]. The probability of a bit error can be described as [12]:

$$P_e = P[1]P_e[1] + P[-1]P_e[-1] \quad (24)$$

where

P_e = probability of a bit error

$P[1]$ = probability a 1 is sent

$P_e[1]$ = probability the 1 is received in error

$P[-1]$ = probability a -1 is sent

$P_e[-1]$ = probability the -1 is received in error

$G[n]$ is a PN sequence and one of the properties of a PN sequence is that a PN sequence has one more zero than one per epoch. In this case zeros are represented as -1. Sampling at two samples per bit results in:

$$P[1] = \frac{1024}{2046} = 0.500488 \approx 0.5$$

$$P[-1] = \frac{1022}{2046} = 0.499512 \approx 0.5 \quad (25)$$

The zero-mean, Gaussian white noise allows the probability of error for the individual symbols to be defined as:

$$P_e[1]=P_e[-1]=Q\left(\frac{1}{\sigma}\right) \quad (26)$$

where

Q = complimentary error function.

σ = standard deviation of the noise

The 1 in the complementary error function represents the power in the signal. This derivation assumes that the power in the signal is normalized to 1.

Using Equations 24, 25 and 26, P_e can be redefined as:

$$P_e = Q\left(\frac{1}{\sigma}\right) \quad (27)$$

Then from Equation 14, as P_e increases, $R_{xG}[\tau]$ for $\tau = \alpha$ decreases, because each bit error decreases the number of samples that match when $\tau = \alpha$. The findings of Equation 14 can be extended to each of the peaks from the partial correlations of Equation 16.

3.8 Conclusion

The FFT can be used to perform correlation and obtain coarse acquisition of the GPS C/A code. However the code offset, Doppler shift, and received signal SNR can have a significant impact on the ability to correlate the received signal

with the reference PN sequence. The zero padding decreases the number of computations required to perform the correlation using radix-2 FFTs. But the zero padding distorts the circular correlation of the received signal and reference PN code. The code offset causes ambiguity as to which peak should be used to determine the code offset when the code offset is near 1023. The Doppler shift decreases the amplitude of the peak by causing inversions during data accumulate and the effect is determined by the location of the inversion. Data modulation can cause inversions up to once every 20 epochs and has the same effect as an inversion from Doppler shift. The noise at the input is predicted to decrease the PAR, but the effect of the noise on the uncorrelated portion of the code cannot be predicted. The individual effects of the data, noise, code offset, and Doppler on the coarse acquisition process can affect the ability of the coarse acquisition section of the GPS receiver to achieve coarse acquisition with the C/A-code.

IV. SIMULATION PROCEDURE

4.1 Introduction.

Signal Processing WorkSystem SPW™, from Comdisco System Incorporated, is the software tool used to model the GPS receiver C/A code coarse acquisition system. In addition to modeling the acquisition section, SPW™ is used to generate the input signals and record the output files. SPW™ is an interactive computer aided tool for digital signal processing simulation and design. SPW™ has many different packages available for use in simulation, and the two used in this thesis were the Block Diagram Editor (BDE) and the Signal Display Editor (SDE). The coarse acquisition system, shown in Figure 14, was assembled using the BDE and is the basic system for all simulations.

4.1.1 Block Diagram Editor. The BDE enables construction of systems from libraries of basic signal processing blocks. The BDE Graphical User Interface (GUI) represents the blocks as symbols and allows groups of symbols to be combined to create a new symbol. Symbols are customized to the specific application by changing block parameters. Examples of parameters are the length of an input vector or the frequency of an oscillator. Also, parameters can be calculated using other parameters. An example of this is the difference vector length in the correlation block. The difference vector parameter is automatically

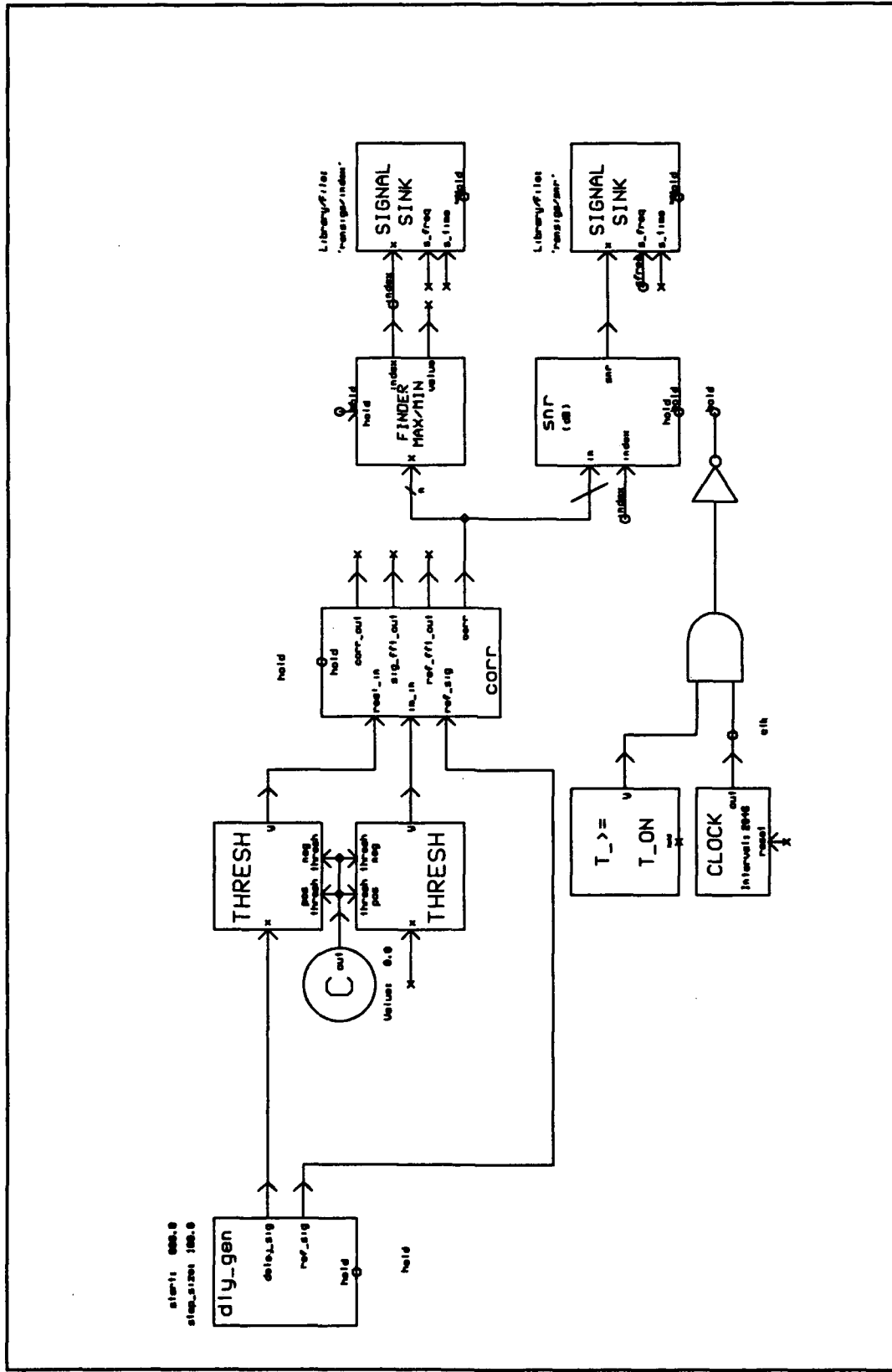


Figure 14 SPW™ Coarse Acquisition System

computed as the difference between the input and output vectors. The hold input on SPWTM blocks is used to disable the operation of the block when the output is not needed. The hold input is also used to decrease the simulation time by eliminating unneeded computations. The clock that drives the hold is set to enable the block operations once every 2046 samples. This corresponds to the length of an epoch of the C/A code. The use of the hold on the correlation block allows the computation of the correlation once for each epoch of data. The "T_>= T_ON" block disables the operation of the blocks for time equal to zero. At time equal to zero, no data has been input into the tapped delay lines (TDLs) of the correlator, and the output of the correlation block does not contain any valid data; therefore, the output of the correlation block at time zero was disabled.

The input and output files can be specified by the type and location of the data through the use of signal sinks. The data recorded can be synchronized with the output of the correlation block by the hold input to the data sink. Each simulation can be set to run a specific number of iterations or run interactively and stop when requested.

4.1.2 Signal Display EditorTM. The SDETM module is used to display, edit and create waveforms. The SDETM GUI allows signals from a simulation to be viewed, modified, analyzed, and resaved. Also, signals needed in a simulation can be constructed and saved. The window size of the SDETM can be adjusted to allow inspection of individual samples of the signals or to allow viewing the entire

signal. The SDE™ also contains mathematical functions such as log and square root and can modify an entire signal or just specific samples.

4.2 Block Descriptions

This section discusses the blocks custom-made to fulfill the specific requirements of the GPS coarse acquisition receiver. In all cases the blocks are made up of SPW™ blocks and combined into a single entity for each of the needed operations. Several of the blocks are more than one level deep. When a custom block is made, all parameters are placed one level below the symbol. On many of the blocks, parameters are automatically calculated using other user input parameters. The SPW™ detail block drawings for the blocks described in this section are shown in Appendix B, Figures 26 through 41.

4.2.1 Coarse/Acquisition Code Generator. To enable simulation using the actual GPS codes, a GPS Gold code generator is constructed. A Gold code is the combination of two maximal length sequences and in the GPS system, the sequences are designated g1 and g2 [1]. The sequence g1 and two taps from g2 are modulo two added to make the GPS Gold code. GPS uses the same g1 for all of the satellites. The Gold code is changed by selecting two taps from the g2 generator and modulo-two adding them with g1 to make a unique Gold code. The C/A code generator includes the g1 and g2 generators and a modulo-two adder. The g1 generator generates a maximal length sequence. The all-ones state

is used as a common starting point for all GPS satellite C/A codes, so the g1 and g2 tapped delay lines (TDLs) are pre-loaded with all ones. After the initial load of all ones, the Gold code generator will continuously cycle through the 1023-bit sequence. The epoch detector will output a pulse every time the g1 TDL is all ones to signal the start of new epoch. The g2 generator also generates a maximal length sequence, but the output is two taps of the TDL.

The tap_1 and tap_2 inputs are used to select the specific satellite PN sequences. The tap settings are listed in [14] but the listing is for GPS Pseudolite signals. GPS Pseudolites are ground based transmitters of the GPS signals. The only difference between a pseudolite and a satellite code is the initial load of the TDL. The gold code generator modulo-two adds the outputs from the g1 and g2 blocks. All of the blocks used to generate the Gold code output binary data as ones and zeros. The last block in the generator maps the ones and zeros of the binary data to a 1 for a binary one and a -1 for a binary zero.

4.2.2 Correlation Block. The correlation block performs the correlation of the received signal with the reference Gold code. This block performs the mathematical function described in Equation 14. The TDLs are used to convert the serial input data to vector data. All blocks prior to the vector padding have vectors of length 2046. After padding, the vector length is 2048, and the difference between the vector lengths is used to compute the length of the difference vector. Both the reference and signal vectors are Fourier transformed.

SPW™ [3] defines the forward FFT as:

$$Y(k) = \frac{1}{N} \sum_{j=0}^{N-1} X(j) e^{-i \frac{2\pi k j}{N}} \quad (28)$$

where:

$X(j)$ = Input Sequence

$$i = \sqrt{-1}$$

The inverse FFT has the form [3]:

$$Y(k) = \sum_{j=0}^{N-1} X(j) e^{i \frac{2\pi k j}{N}} \quad (29)$$

Note that the location of the scale factor, $1/N$, is in the forward transform instead of the inverse transform as defined in Equations 10 and 11. In the correlator block, both the forward and reverse FFT are performed, and the actual location of the scaling does not affect the amplitude final output. In both the forward and reverse transform, the vector length, N , must be a power of two. After the forward FFT operation, the indices of both the reference and signal vectors are

reversed. Both signals are changed from real and imaginary to complex, and the complex conjugate of the input signal is computed. Next, the signals are complex multiplied point-by-point. The output of the complex multiplication is inverse transformed and the result is a vector representing the correlation of the input signal and the reference Gold code. The output of the inverse FFT is point-by-point squared and summed. The squaring and summing is not explained in Chapter 3.3, but the sign and phase of the signal is not needed to achieve coarse acquisition. The only output needed is the relative time difference between the reference and received sequences. The squaring ensures that values at all indices in the vectors are positive. The summing is to combine the correlation output of the real and imaginary output of the inverse FFT. Recall that, as explained in Section 3.3, the exact phase of the input signal is not known, and the input to the correlator is two orthogonal channels. The summing combines the output of the two orthogonal channels into a single vector. The output of the correlator block is a vector that has a peak and the index of the peak can be used to determine the offset between the input signal and the reference Gold code.

4.2.3 Peak-to-Average Ratio Block. The Peak-to-Average Ratio (PAR) block computes the average peak power to average power in all other indices ratio for the vector at the output of the correlator. The vector out of the correlation block is in volts squared and assumes normalized power in an one-ohm resistor. The PAR is computed by:

$$PAR = \frac{2045}{3} \left[\frac{\sum_{n=p-1}^{p+1} y[n]}{\sum_{n=0}^{2048} y[n] - \sum_{n=p-1}^{p+1} y[n]} \right] \quad (30)$$

where

$y[n]$ = Vector Output of Correlator Block

p = Index of the Peak Value in the Vector

2045 = Length of the Vector Minus 3

3 = Number of Points with Signal Power

The top summation is the peak power and the bottom is the total power in the vector minus the signal power. The correction factor is correct for the fact that the peak power is summed over three points and the average power is summed over 2045 points. The real-to-decibels block computes:

$$dB = 20 \log_{10} x \quad (31)$$

But the output of the correlation block is power. To correct for computations of the real-to-decibels block the output of the real-to-decibels block is divided by two.

The clippers are required before the extract component blocks to prevent

underflow and overflow. The index input of the extract component block is the index of the peak value in the correlation vector and ranges from 0 to 2047. Because points on both sides of the peak are used in the computation of the PAR, underflow will occur when the correlation peak is at the zero index and one is subtracted. Overflow will occur when the correlation peak is at index 2047 and one is added. If underflow or overflow occurs the simulation is aborted. Therefore, the clippers are required.

4.2.4 Vector Integrator Block. The vector integrator block performs a point wise summation of a vector and holds the summation as an output. The vectors are summed until the reset is set true. The block performs the function:

$$y(n) = \sum_{z=1}^r x(n) \quad \text{For } n = 0, 1, \dots, L-1, L \quad (32)$$

where

$x[n]$ = Input Vectors

$y[n]$ = Output Vectors

r = Number of Vectors to be Integrated

When reset this block will output the values of the present input vector.

4.2.5 Delay Signal Generator. This block generates a reference Gold code and a delayed Gold code. The delay input sets the delay between the reference and the delay sequence in samples. Inside the block, a Gold code generator, described in Section 4.2.1, is used to generate the Gold code. A SPW™ clock block is used to set the number of samples per bit to two. The Gold code is sent into a TDL and is output as a vector. Then, the component selected by the delay input is output as the reference signal. It will take at least one epoch of data to fully load the TDL. This will prevent using any of the delayed signals except zero delay for the first epoch. The TDL delays the reference signal to match the development of correlation in Chapter 3 and enables the location of the peak to directly represent the amount of offset between the input and reference code.

4.2.6 Peak Finder. The Peak Finder locates the peak of the numbers in the correlation vector. The block outputs the index of the peak when the index is less than 993, and subtracts 2 from the index when the index of the peak is greater than 995.

4.3 Block Verification

Preliminary testing was performed to ensure the individual blocks were performing the required operations, and this section outlines the testing performed prior to implementing the entire coarse acquisition system. Once confidence in the output of the system is established, additional simulations were run to determine effects of the code offset, Doppler shift, and noise on the ability of the

proposed coarse acquisition system to determine the code offset.

4.3.1 Correlation Block. To test the correlation block, the output was compared to linear correlation. The SPWTM SDETM is used to perform the linear correlation of $x[n]$, and the output is shown in Figures 15 and 16. The correlation block was used to perform circular auto-correlation of $x[n]$ with $\alpha=0$, and the results are shown in Figure 17 and 18. Figures 15 and 17 display 4096 samples, while Figures 16 and 18 display 20 samples centered on the peak of the correlation. The values of $R_{xx}[\tau]$ for $\tau \neq 0$ is on the same order of magnitude for the circular and linear correlation while the value of $R_{xx}[0]$ is identical. Then, the input was changed from the real to the imaginary input of the correlator and the output correlation was observed on the imaginary output. The blocked passed the testing because all observed outputs matched theoretical predictions.

4.3.2 Peak to Average Block The PAR ratio block was tested using known input signal. The PAR block did compute the average PAR correctly for all indexes except 0 and 2047. The clippers in the PAR cause the value in the indices of 0 and 2045 to be used twice in the PAR computations and the result is a calculated PAR higher than the actual PAR. The PAR block computes the PAR as 33.4 dB when $\alpha=0$ and $\alpha=2045$, and the actual PAR is 31.4 dB. The actual PAR at indices 0 and 2045 is used in all data presented in this thesis.

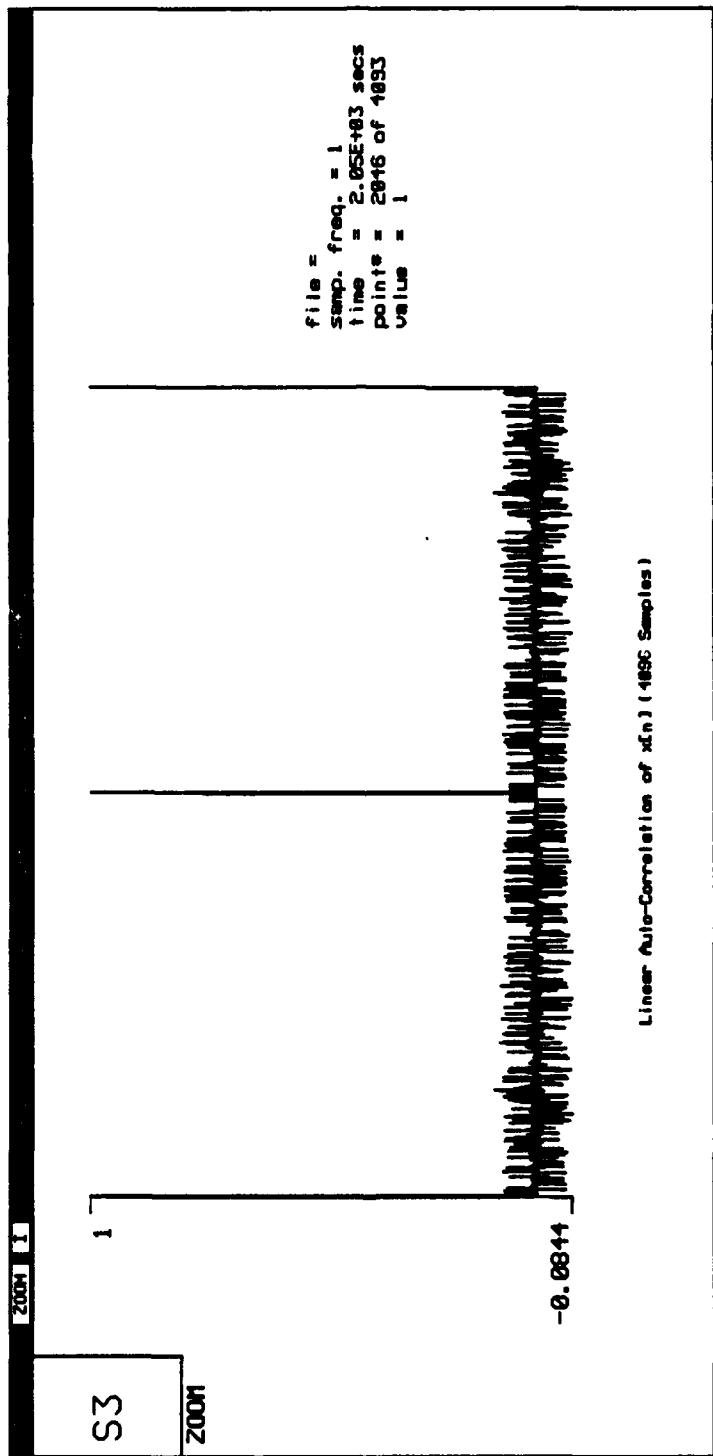


Figure 15 Linear Auto-Correlation of $x[n]$, 4096 Samples

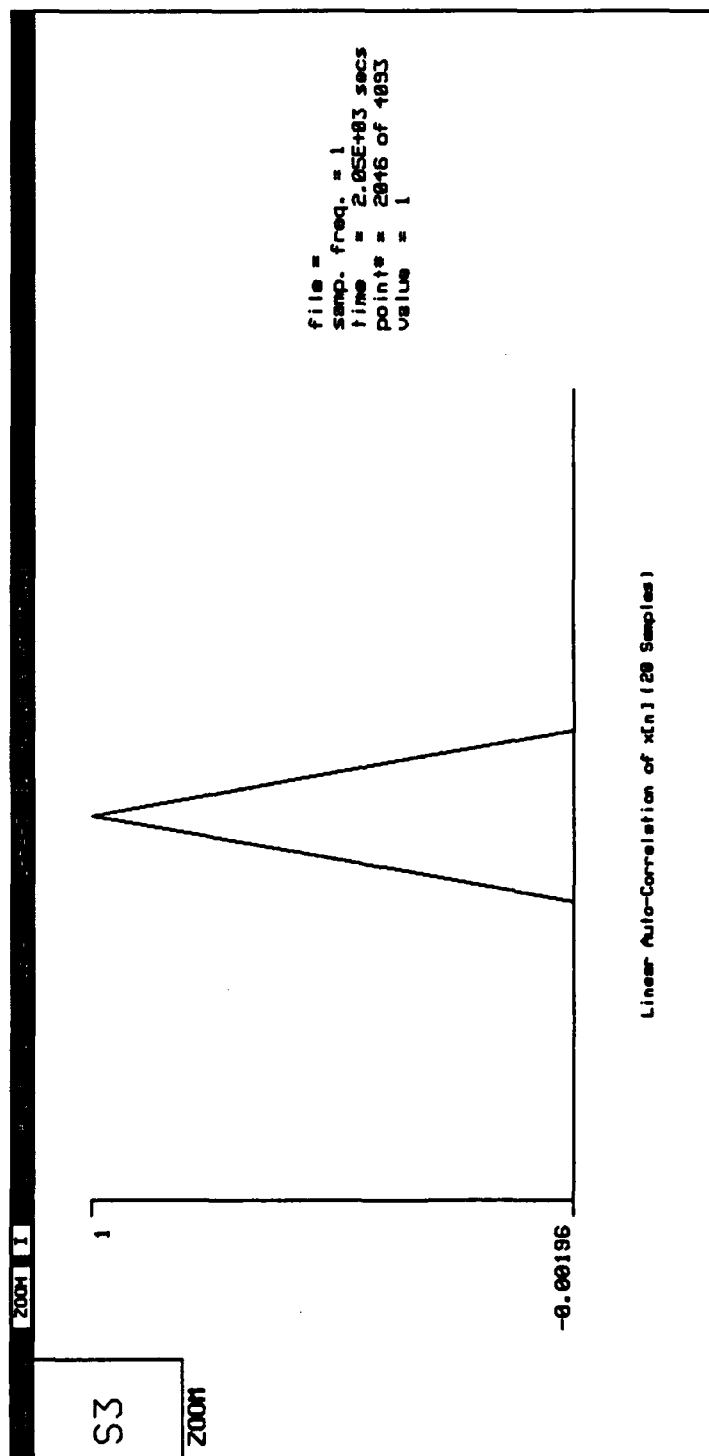


Figure 16 Linear Auto-Correlation of $x[n]$, 20 Samples

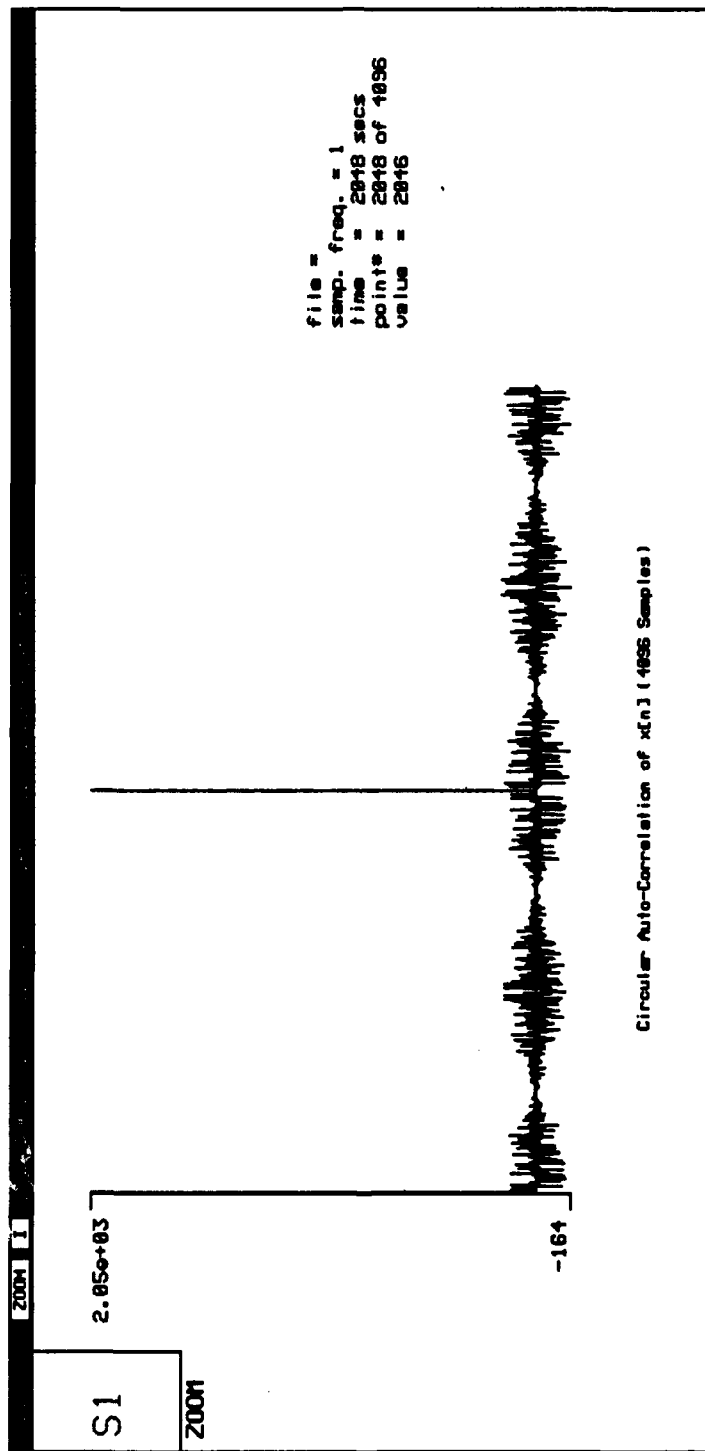


Figure 17 Circular Auto-Correlation of $x[n]$, 4096 Samples

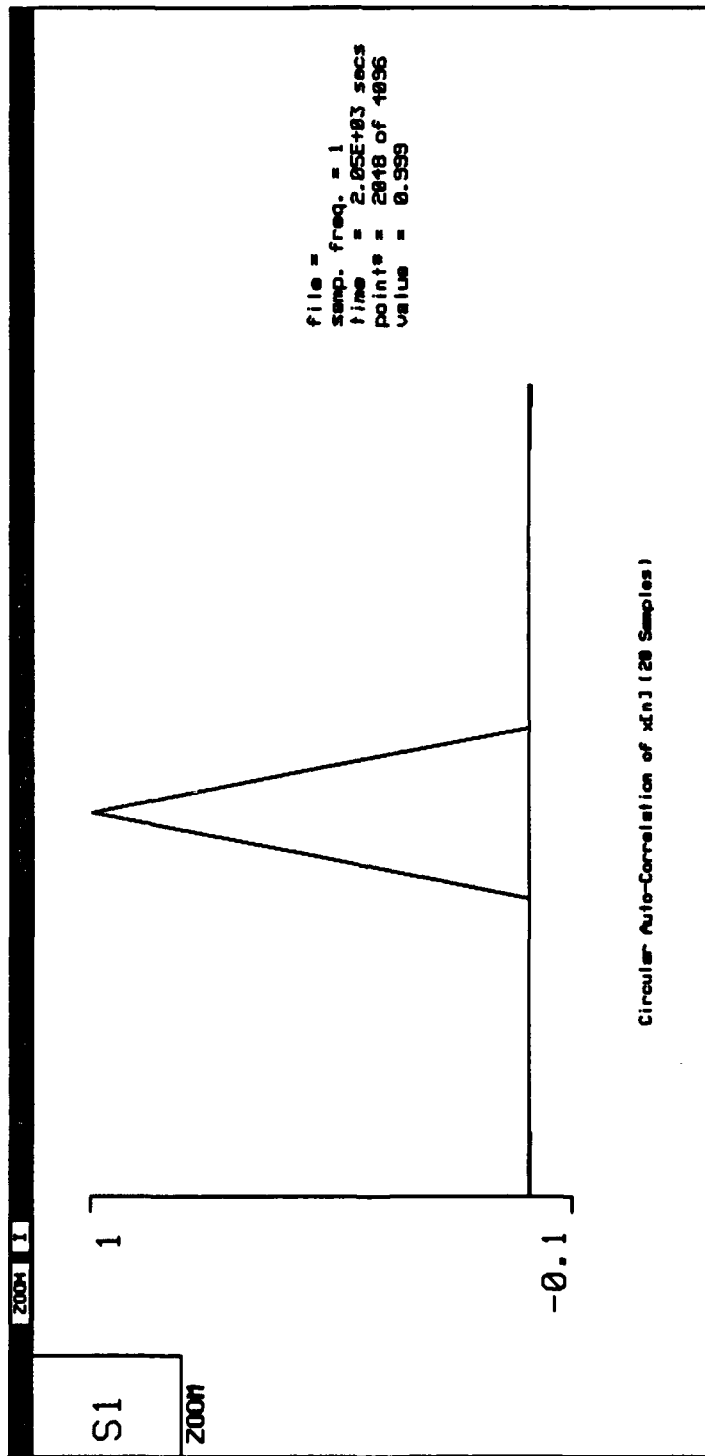


Figure 18 Circular Auto-Correlation of $x[n]$, 20 Samples

4.4 Simulation Of Code Offset.

The effects of the code offset is investigated to determine if the simulation results matched the prediction of Equation 15. Figure 19 shows the number of

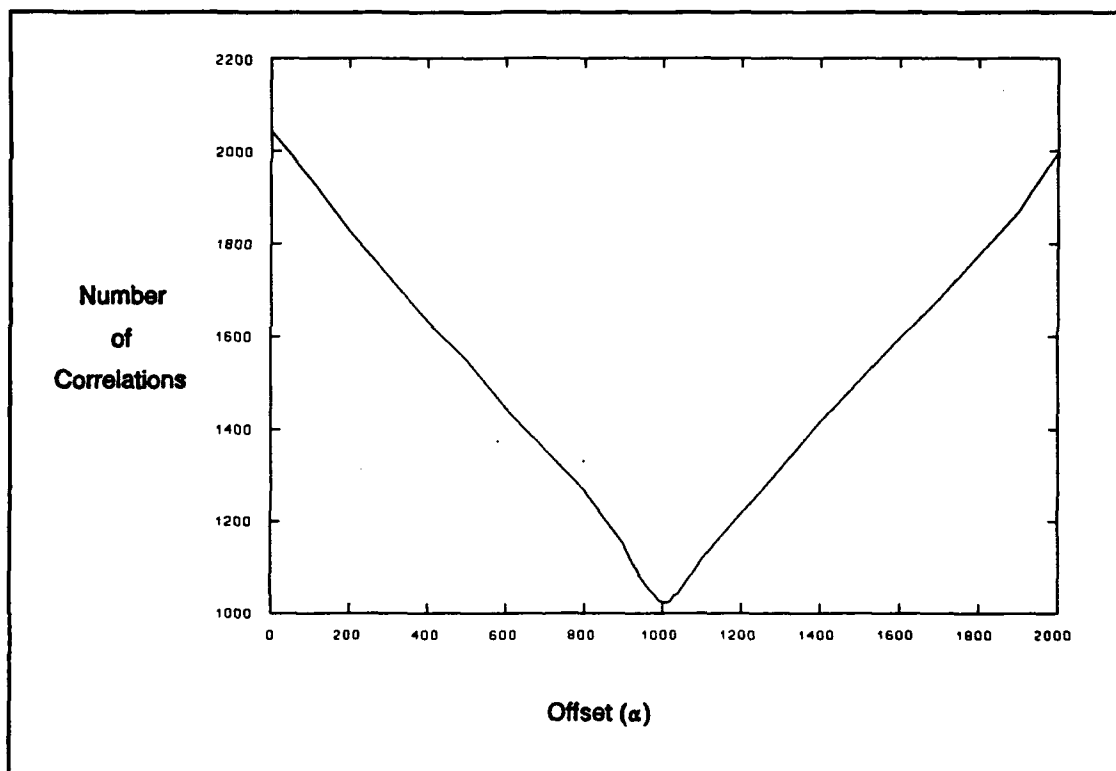


Figure 19 Number of Correlations versus Code Offset for $x[n]$ and $G[n]$

correlations verses code offset, and Figure 20 shows the computed PAR versus code offset. The number of correlations is the maximum value of the correlation. The data in these figures is computed without noise or Doppler shift. The PAR decreases as α increases until $\alpha=980$, and when $\alpha=1020$, the PAR starts to increase. The minimum value for the PAR is 23.5 dB. The number of

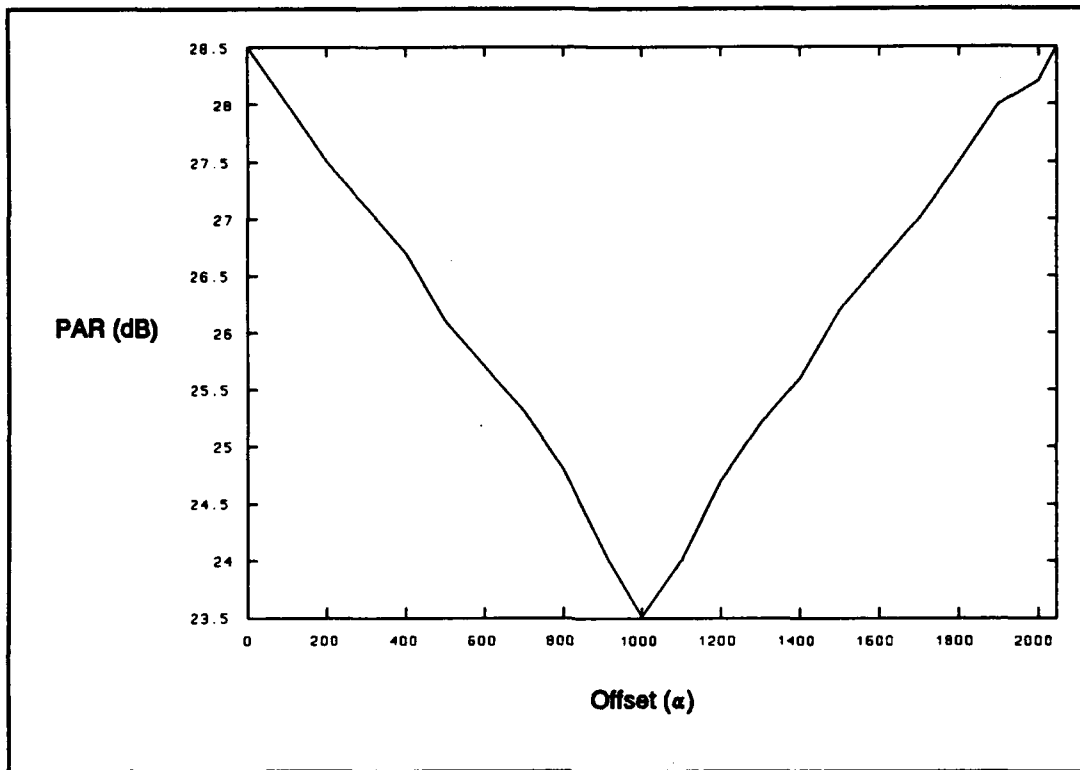


Figure 20 Peak To Average Ratio versus Code Offset for $x[n]$ and $G[n]$

correlations decreases as α increases until $\alpha=1003$, and when $\alpha=1010$, the number of correlations begins to increase. The minimum number of correlations is 1023. The two peaks predicted in Section 3.4.2 did exist. The peak value of the correlation did occur at α for values less than 1023. But the transition of the index of the peak from α to $\alpha+2$ did not occur at $\alpha=1023$. The value of the transition was at $\alpha=994$, as shown in Figure 21. The value of the index of the peak is equal to the offset up to 993, and then jumps by 3 to 996 when the offset is 994. This is 29 samples or 14.5 chips earlier than predicted in Section 3.4.2 when the effects of λ were ignored. Recall that λ is the number of

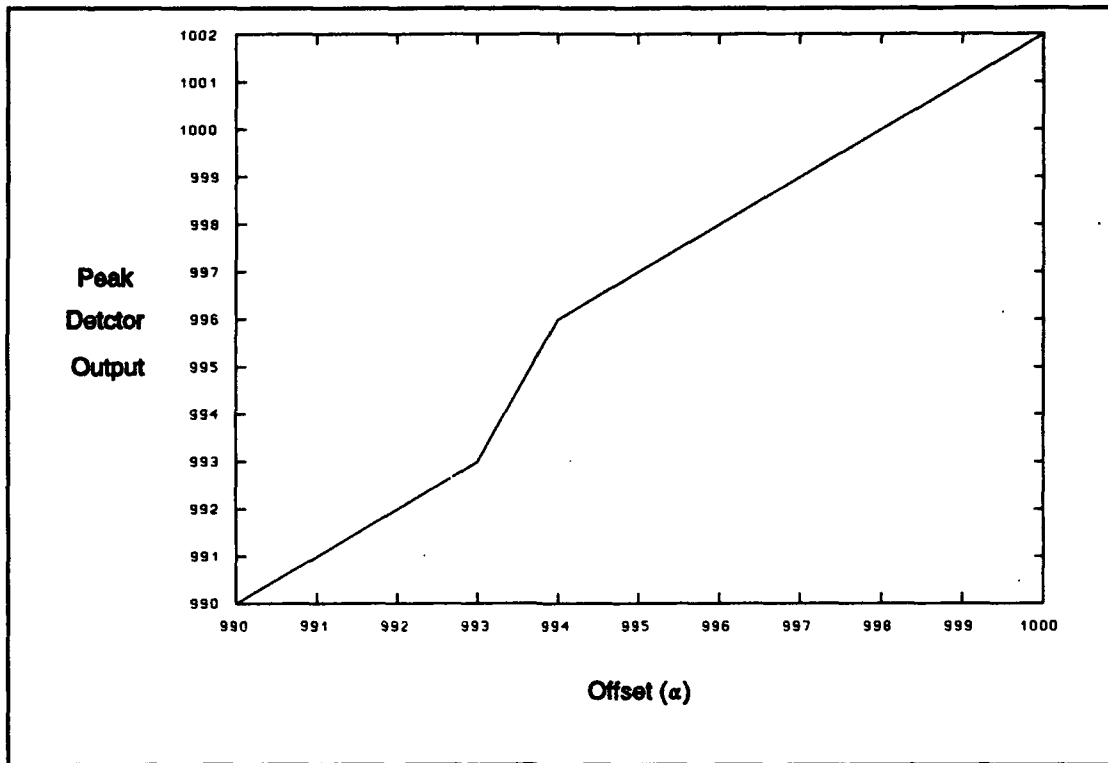


Figure 21 Actual versus Detected Code Offset

correlated samples minus the number of uncorrelated samples for the non-aligned portion of the sequences. As explained in Section 3.3, the effects of λ will shift the location of the index of the correlation peak from α to $\alpha+2$. Note that these computations are done with the Gold code for satellite number one, and the sequences from other satellites may change the index of the peak to slightly different values.

For the code offset, the results are as predicted by theory except for the ambiguity of when the index of the correlation peak changes from α to $\alpha+2$. When the index of the peak changes from α to $\alpha+2$, the Maximum Finder block

subtracts 2 from the index and sends the corrected index value to the fine synchronizer. But the index value at which the Maximum Finder block begins to subtract two from the index number of the maximum value is preset and must be set before the coarse receiver is simulated.

4.5 Simulation of the Received Signal with Noise.

The noise in the input signal is simulated by injecting Gaussian noise at the input to the threshold detector as shown in Figure 22. The probability of bit error is derived in section 3.6 for the input to the threshold detector. The SNR at the input to the threshold detector was computed using:

$$SNR = 10 \log_{10} \left[\frac{1^2}{\sigma^2} \right] \quad (33)$$

where

1^2 = Normalized Signal Power

σ^2 = Noise Power

The SPWTM Gaussian noise generator is used as the noise source. The noise generator's user-definable parameters are sample frequency, mean, and variance. The sample frequency is set to one and the mean is set to zero for all simulations. The noise generator's variance is set to achieve the desired SNR at

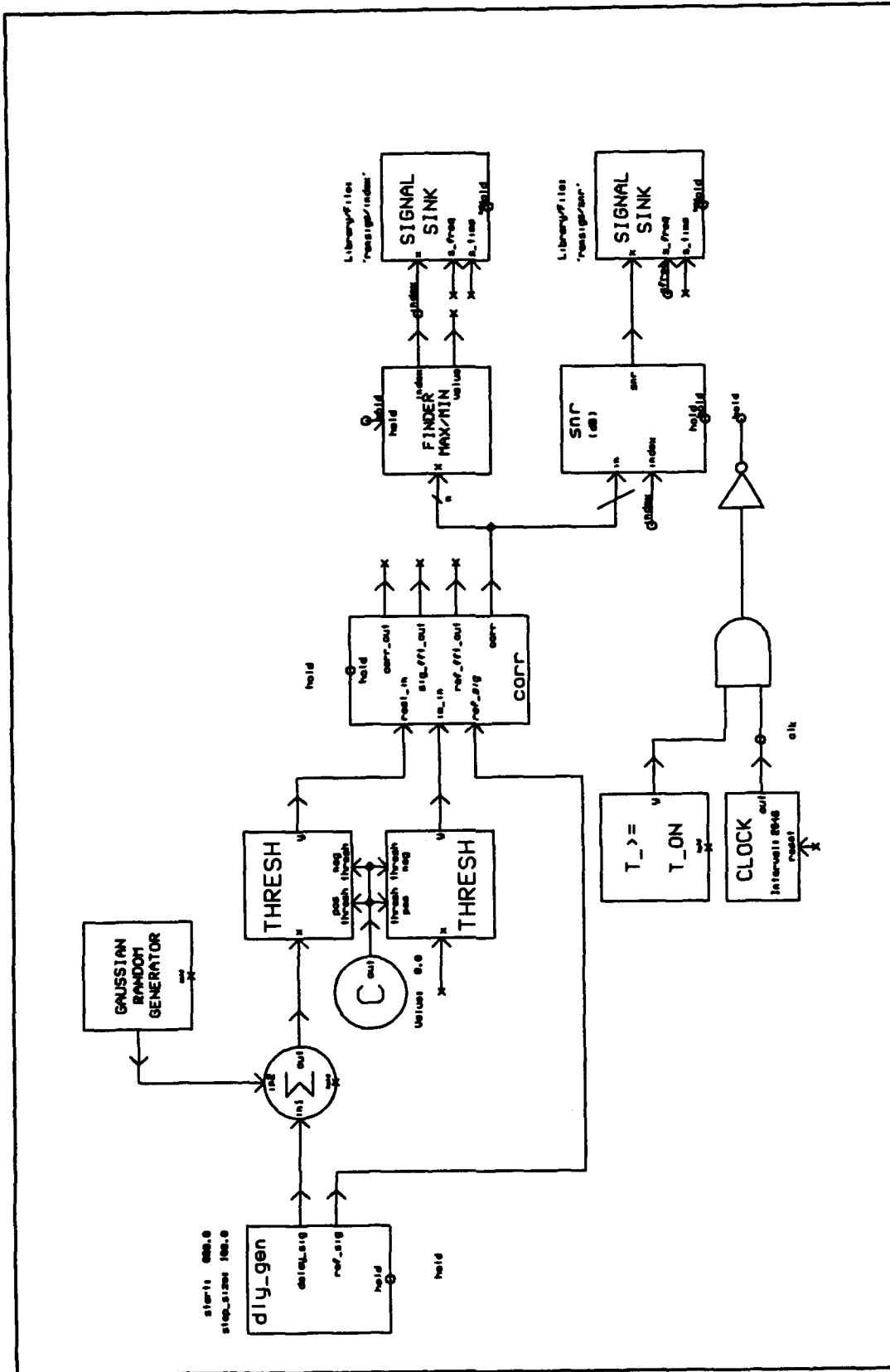


Figure 22 Coarse Acquisition System with AWGN Simulator

the input to the correlator. For zero-mean, additive white, Gaussian noise, the variance, defined as σ^2 , is the noise power. Therefore, the SNR at the input to the threshold detector can be set by adjusting the variance of the noise [15]. The signal power is set at 1^2 or 1 for all simulations. For each simulation with noise, the bit error rate (BER) at the input to the correlator is recorded.

To establish a reference, noise alone is input into the correlator for 10 epochs. The PAR of the noise ranged from 9.61 dB to 6.95 dB, with a mean of 8.2 dB. The number of correlations at the peak value ranged from 145 to 172, with a mean of 163. A second reference is a signal with no noise. For no noise, the number of correlations at the peak varies from 2042 to 1023, and the PAR varies from 28.5 dB to 23.5 dB as α varies from zero to 2000.

The effect of noise on the ability of the coarse acquisition receiver to determine α was investigated. Figure 23 shows the plots of the PARs at the output of the correlator for various SNRs at the input to the threshold detector as α ranges from 0 to 2000. The top line on Figure 23 is for infinite SNR, no noise, and the dashed line at the bottom is the average PAR for noise. The plots show that the effect of α on the PAR is similar for every SNR at the input to the correlator. Note that the decrease in the PAR at the output of the correlator corresponds to the decrease in SNR at the input. When the SNR of the input is decreased to -18 dB, α could not be reliably determined for all values of α .

The lines for the PARs with noise do not exactly parallel the PAR values without noise because the BER is not a constant for all ten epoch of the noise.

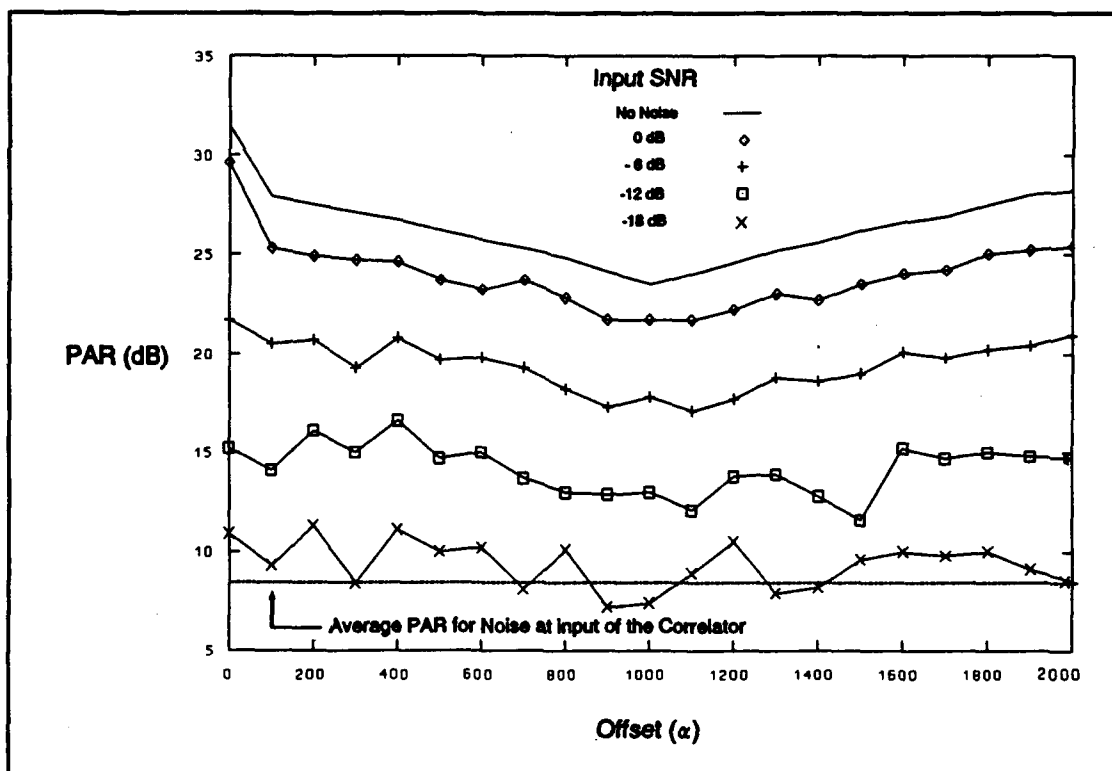


Figure 23 PAR versus Code Offset for Different Input SNRs

For this simulation, a data bit was considered in error when the output of the delay generator did not agree with the output of the threshold detector. For a SNR of 0 dB, the BER was 0.1584 when averaged over the 20 epochs data. Theory predicts the BER to be 0.1587. So the overall BER was within 0.02% of the theoretical BER, but the BER of the individual epochs ranged from 0.141 to 0.169. The variation in the BER at the input of the correlator affected the PAR of the output. The variation in the input BER is important because each point on Figure 23 is the result of a single correlation.

This simulation demonstrated that the proposed coarse acquisition method

can achieve acquisition for input SNRs greater than -18 dB without any Doppler shift. The effects of Doppler on the acquisition process were ignored during this portion of the simulations, and the receiver may not be able to acquire the GPS C/A code when the input SNR is -18 dB and the received signal contains Doppler at the input to the threshold detector.

4.6 Simulation of the Received Signal with Doppler Shift.

The effects of Doppler shift is simulated using the system shown in Figure 24. For this portion of the simulations, α was set to 0, the SNR = ∞ , and the satellite data is assumed to be constant one. The effect of Doppler shift is separated into two parts. The frequency of the Doppler determines the number of possible phase inversions during data accumulation, and the location of the inversions determines the effect of the inversions on the PAR. First, the effects of location of phase inversion, θ , is investigated. Then the effects of increasing the Doppler frequency is investigated. The location of the phase inversion, θ , is defined as:

$$\theta = \frac{\xi}{L} = \frac{\xi}{2048} \quad (34)$$

where

θ = Location of a Phase Inversion

ξ = Location of a Phase Inversion in Samples

L = Length of an Epoch of Data in Samples

This redefinition of the location of a phase inversion enables easier visualization of what occurs at the input of the threshold detector for Doppler shift. The value of the peak of the correlator output is affected by the location of the phase inversion from the residual Doppler. To examine the effects of θ , the residual Doppler frequency of 454 Hz was chosen so that as 10 continuous epochs of data were collected, θ increases from 0 to 1 in increments of 0.1. When $\theta=0$, the inversion occurs at sample number 0, and when $\theta=1$, the phase inversion occurs at sample number 2045. Appendix C, Figures 42 through 52, shows the input to the threshold detector for 10 epochs of 454 Hz Doppler frequency, and Table 1 shows the PAR at the output of the correlator. For all values of θ except $\theta=0.5$, the correlator is able to determine the correct value of α . When $\theta = 0.5$, the PAR at the output of the correlator is 8.4 dB and the number of correlations is 187. The value of PAR and number of correlations is equivalent to noise. The number of correlations is the maximum value for any index in the output vector of the correlator. For residual Doppler frequencies less than 500 Hz, a phase inversion does not occur every epoch of data. Only one inversion from Doppler shift can occur in an epoch of data acquisition, but the satellite data may cause a

second inversion in an epoch. For residual Doppler shift frequencies less than 500 Hz the location of the phase inversion from the Doppler shift is more important than the frequency of the residual Doppler shift. Figure 25 shows the input and output of the threshold detector for 100 Hz of Doppler shift. The SNR at the output of the correlator is the same as the SNR for no Doppler shift.

Table 1. PAR Versus Phase Inversion Location

θ	PAR (dB)	Detected Peak Location
0.0	31.4	0
0.1	30.2	0
0.2	27.8	0
0.3	22.8	0
0.4	16.4	0
0.5	8.4	1377
0.6	16.0	0
0.7	22.3	0
0.8	26.4	0
0.9	29.8	0
1.0	31.4	0

Next, the effect of residual Doppler frequencies from 500 Hz to 900 Hz is examined. This frequency range is chosen because in this range at least one

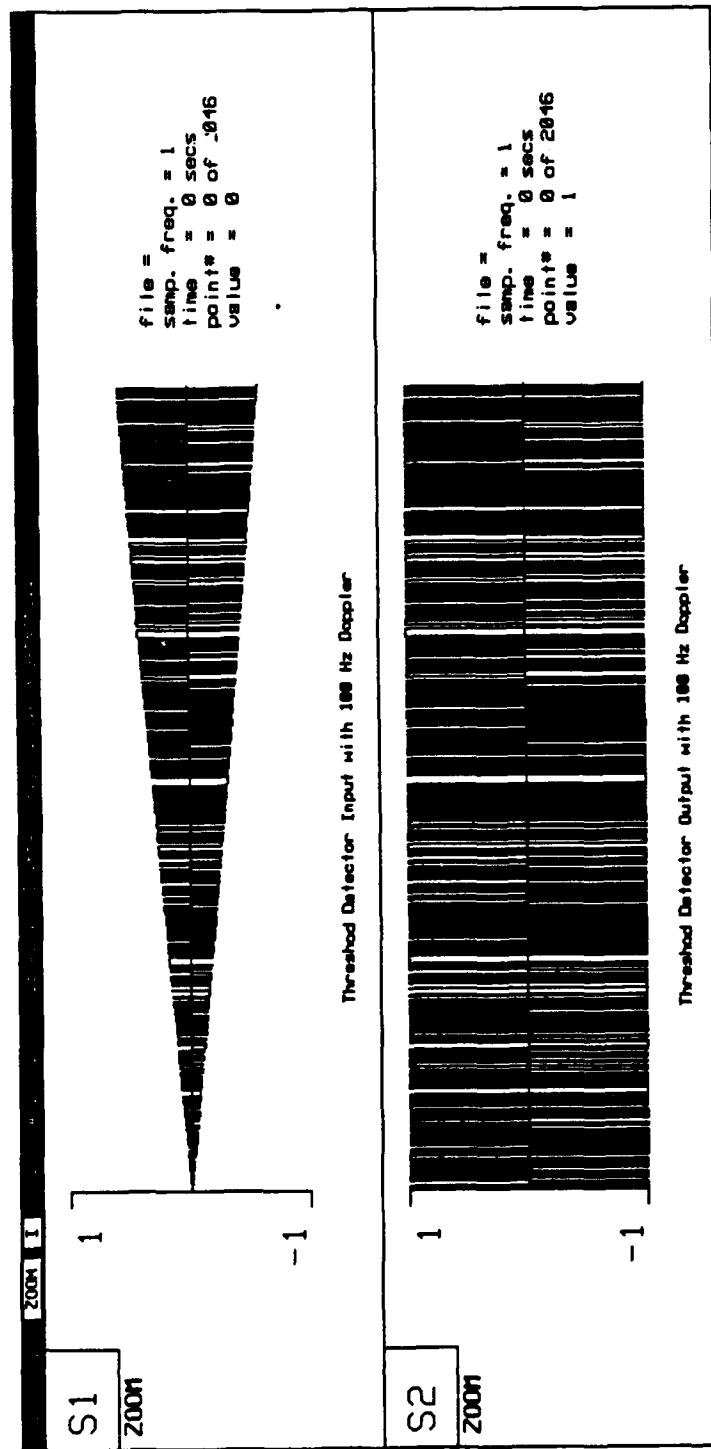


Figure 25 Input and Output of the Threshold Detector with 100 Hz Doppler

inversion would occur every epoch, and at frequencies equal to or greater than 1000 Hz at least two phase inversions occur every epoch. In this frequency range, the location of the phase inversion determines the effect on the PAR at the output of the correlator. Two epochs of data is shown for 500 Hz of residual Doppler shift, Figures 53 and 54. Because the location of the phase inversion does not change in the epoch following the lowest PAR a third sample of the input to the correlator is not shown for 500 Hz. Three epochs of data is shown collected for frequencies from 600 Hz to 900 Hz in 100 Hz steps. For each frequency, the value of θ was chosen to give the worst SNR at the output of the correlator on the first epoch, then the next epoch of data was examined, and the third epoch of data is for $\theta=0$. The inputs to the threshold detector are in Appendix C, Figures 55 through 66 and the results are tabulated in Table 2.

Table 2. PAR for Frequencies from 500 Hz to 900 Hz

Frequency (Hz)	Lowest PAR (dB)	PAR of Next Epoch (dB)	PAR for $\theta=0$
500	7.3	7.3	31.4
600	7.3	21.2	27.8
700	7.4	23.4	23.0
800	8.4	17.8	18.0
900	7.4	9.7	9.1

For residual Doppler shifts of 500 Hz, the effect of the Doppler is dependant only on θ , and θ does not change for the next epoch because the frequency of data acquisition is 100 Hz. For frequencies between 600 and 800 Hz, the SNR of the epoch following the lowest SNR is high enough to enable coarse acquisition. But when the residual Doppler shift is 900 Hz, the PAR for the epoch after the lowest possible PAR is equivalent to the PAR for noise. Appendix C, Figures 67 and 68, also includes plots of 1000 Hz Doppler, for $\theta = 0$ and 0.5. The PARs are 8.4 dB and 8.5 dB respectively. Neither of these PARs is high enough to achieve coarse acquisition.

4.7 Conclusion

The effects of code offset, noise, and Doppler frequency on the ability of the proposed GPS coarse acquisition system are examined in this chapter. Each affects the ability of the system to acquire the GPS C/A code. The acquisition in noise is possible for all code offsets, but the PAR is decreased by 5.5 dB when the code offset is at 954 samples. Noise can prevent the acquisition of the GPS signals when the SNR at the input to the threshold detector is lower than -18 dB. The phase inversion from the residual Doppler shift can reduce the PAR for any epoch of input data to the same level as noise. For frequencies less than 900 Hz, the epoch of data following the lowest PAR epoch has a high enough PAR to achieve coarse acquisition. The coarse acquisition system simulations shows that the use of the FFT to perform the correlation of the GPS C/A code is possible.

V. CONCLUSIONS

5.1 Summary

This thesis explored the use of radix-2 FFTs to perform the coarse acquisition of the GPS C/A code. The proposed coarse acquisition portion of the GPS receiver were explained at the block level. The theory of the using radix-2 FFTs to perform correlations were explained and the difference between linear and circular convolution was addressed. The effects of padding sequences to obtain a power of two prior to the radix-2 FFT-based correlation process was discussed. Then, the effects of doppler shift, code offset, and noise on the coarse acquisition process were presented. The coarse acquisition section of the GPS receiver was simulated with different code offsets for noise and doppler. Finally, the effects of the noise, doppler, and code offset on the ability of the coarse acquisition section of the receiver to determine the code offset were explored.

5.2 Conclusions

The simulation of the proposed acquisition method for the GPS C/A code demonstrated that the GPS C/A code can be acquired using the radix-2 FFT to perform correlation. The noise, Doppler shift, and code offset decreased the Peak-to-Average Ratio (PAR) at the output of the correlator, but for PAR values over 10 dB, the receiver gave the correct code offset.

When the input was corrupted by noise only, an input SNR of greater than -18 dB gave a PAR of greater than 10 dB for all possible code offsets. The PAR for noise has a mean of 8.2 dB. For a PAR greater than 10 dB, coarse acquisition can occur.

The residual Doppler frequency determines how often a phase inversion occurs and the location the phase inversion determines how Doppler shift affects the PAR. For residual Doppler frequencies less than 500 Hz, a maximum of one phase inversion can in an epoch. But one phase inversion can prevent the maximum finder from determining the correct code offset. For residual Doppler frequencies greater than 500 Hz and less than 900 Hz, at least one phase inversion occurs in each epoch. For residual Doppler frequencies less than 900 Hz coarse acquisition is possible because the PAR does exceed 10 dB for at least one of the code offsets tested. For residual Doppler frequencies above 900 Hz, the PAR did not exceed 10 dB for any of the code offsets tested.

The padding of sequences to enable the use of efficient radix-2 FFT routines introduces distortions into the correlation. A second correlation peak is introduced; therefore, the index of the peak value from the correlation will not represent the code offset for all values of the code offset. The amount of code offset determines which peak will have the maximum value. For a code offset greater than 994, the actual code offset is two less than the index of the peak value. The value of the transition from one peak to the other given in this thesis may change for other satellites.

5.3 Recommendations

The research into the use of DSP methods to acquire the GPS C/A method should be continued with emphasis on non-radix-2 Fast Fourier Transform algorithms to perform the correlation. The padding of the sequences and the use of the radix-2 FFT introduced ambiguities that can be resolved in a laboratory environment but may prove difficult to overcome in the real world. The zero padding causes a second correlation peak, and the amount of code offset determines which correlation peak has the highest value. The separation of the two peaks caused by the zero padding is the same as the number of zeros used to pad the sequences. When the two peaks are nearly equal an ambiguity as to which peak should be used will exist.

5.4 Lessons Learned

The vector integrator is used at the output of the correlator to see if the PAR could be improved. Because all of the indices of the correlator output vector contain positive values the integration did not increase the PAR

The use of radix-2 FFTs to perform the correlation enabled signal acquisition, but the zero padding to reach the next power of two introduced distortion into the circular correlation process. The length of the sequence used in GPS is 1023 bits and when sampled at two samples per bit the resulting sequence is 2046 samples long. The number 2046 is a combination of the prime numbers 2, 3, 11, and 31. The use of computationally efficient methods of computing a 2, 3,

11, and 31 bit FFTs could be used to avoid zero padding and introduction of distortion into the circular correlation. The effect of the zero padding is determined by the location of where the zeros are inserted in to $x[n]$. This is shown by the change in the PAR as the code offset changes.

The maximum step size of the oscillator used to search through the frequency ambiguity caused by the Doppler shift can exceed 500 Hz. The PAR is used to determine if the location of the peak of the correlation is the correct offset between the received and reference signals. If the PAR of the first epoch of data is too low, a second epoch of data is examined before stepping the oscillator. This method of search is required because a phase inversion can prevent the PAR from exceeding 10 dB for any residual Doppler frequency. A low PAR for an epoch of data does not imply that the residual Doppler is preventing acquisition.

Appendix A: WORST CASE SIGNAL DYNAMICS

Overview

A Doppler shift arises from relative motion between the transmitter and the receiver. The Global Positioning System (GPS) satellite is not geosynchronous, therefore the velocity of the satellite relative to a stationary observer can be significant. If the GPS receiver is in a high performance jet aircraft, the motion of the receiver can contribute significantly to the Doppler shift.

Doppler Shift Calculations

For the GPS, Doppler shift comes from two main sources: the motion of the satellite, and the motion of the receiver. Worst case Doppler due to the satellite movement occurs as the satellite rises over the horizon and as it sets. The minimum height over the horizon to ensure reception is five degrees. A GPS satellite has a 20,183 km circular orbit and with a period of 12 hours. As the satellite rises over the horizon, the velocity towards a stationary receiver is approximately 700 meters per second (m/s). The equation for Doppler shift is:

$$\Delta f (t) = \frac{f_c}{c} v (t)$$

where

Δf = Doppler Shift from the Carrier Frequency in Hertz

f_c = Carrier Frequency in Hertz

c = Speed of Light in meters per second (3×10^8 m/s)

$v(t)$ = Relative Velocity Between the Receiver and Transmitter

Letting $f_c = 1.5$ GHz, the Doppler shift due to the velocity of the satellite, 700 m/s, is 3500 Hz. The Doppler shift from the satellite will decrease to zero as the satellite moves directly over head. As the satellite sets, the Doppler frequency decreases to -3500 Hz. Therefore, the Doppler range due to the motion of the satellite is 7000 Hz. A jet aircraft can attain speeds of up to 1200 m/s. The resulting Doppler for a jet aircraft is up to 6100 Hz.

Conclusion

The worst case Doppler from the motion of the receiver is when the receiver is travelling directly towards or away from the satellite. The worst case Doppler is when the satellite is rising and the aircraft is heading directly at the satellite, and when the satellite is setting and the aircraft is heading directly away from the satellite. The resulting Doppler can be up to ± 9600 Hz. or a range of 19200 Hz.

Appendix B SPW™ BLOCK AND DETAIL DRAWINGS

This appendix contains SPW™ drawings of the blocks explained in Section 4.2. There are two types of drawings in this appendix: symbol and detail. Symbol drawings represent the highest level of SPW™ blocks and are used to build a system such as the GPS coarse acquisition system. Each symbol contains several SPW™ detail blocks. The drawings that show more detail are called detail drawings. Some symbols have several layers of detail drawings, and each level, down to the basic SPW™ blocks, are shown. This appendix is arranged so that the symbol drawing is shown first, followed by the detail drawings that make up the symbol.

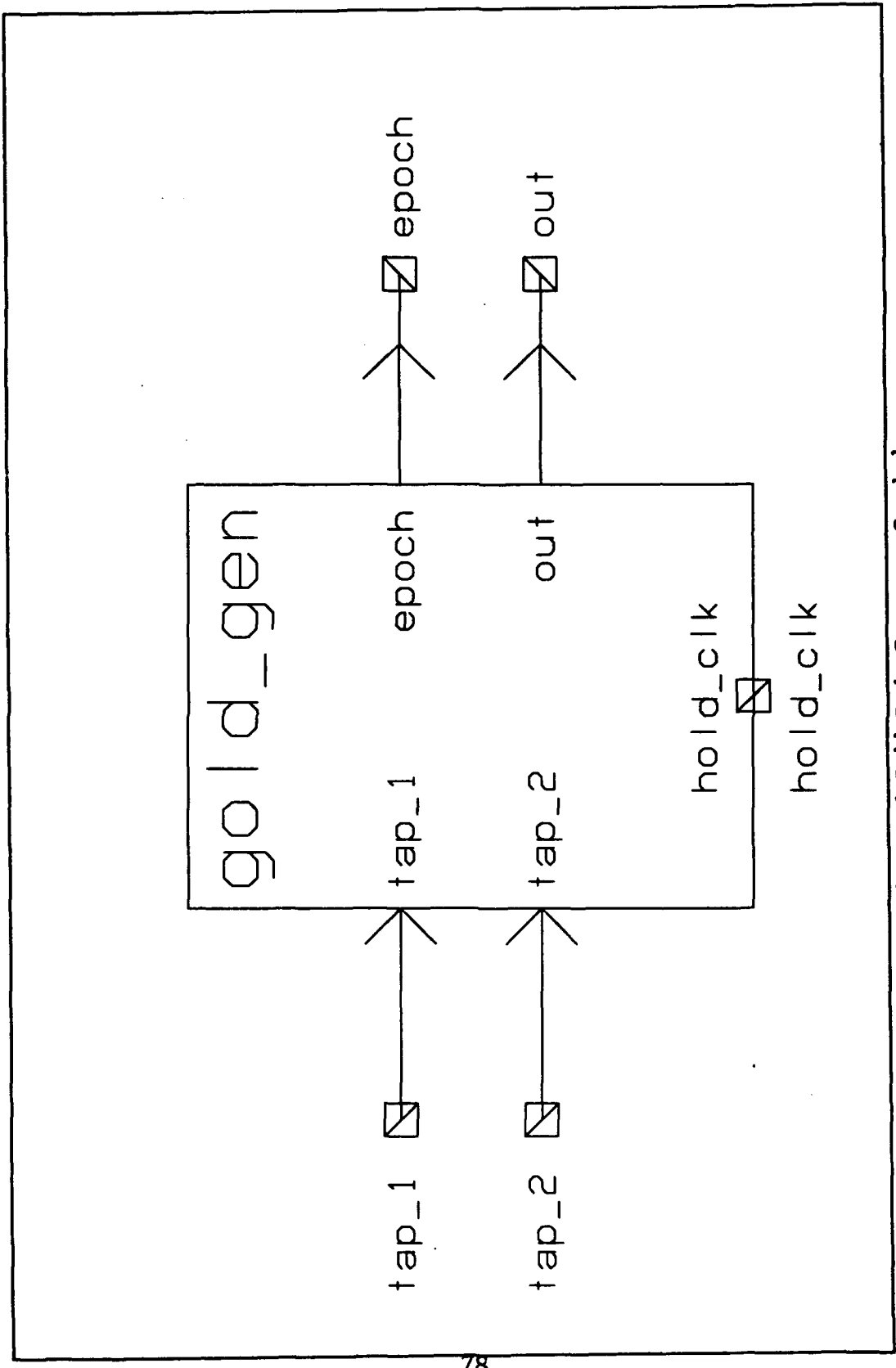


Figure 26 Gold Code Generator Symbol

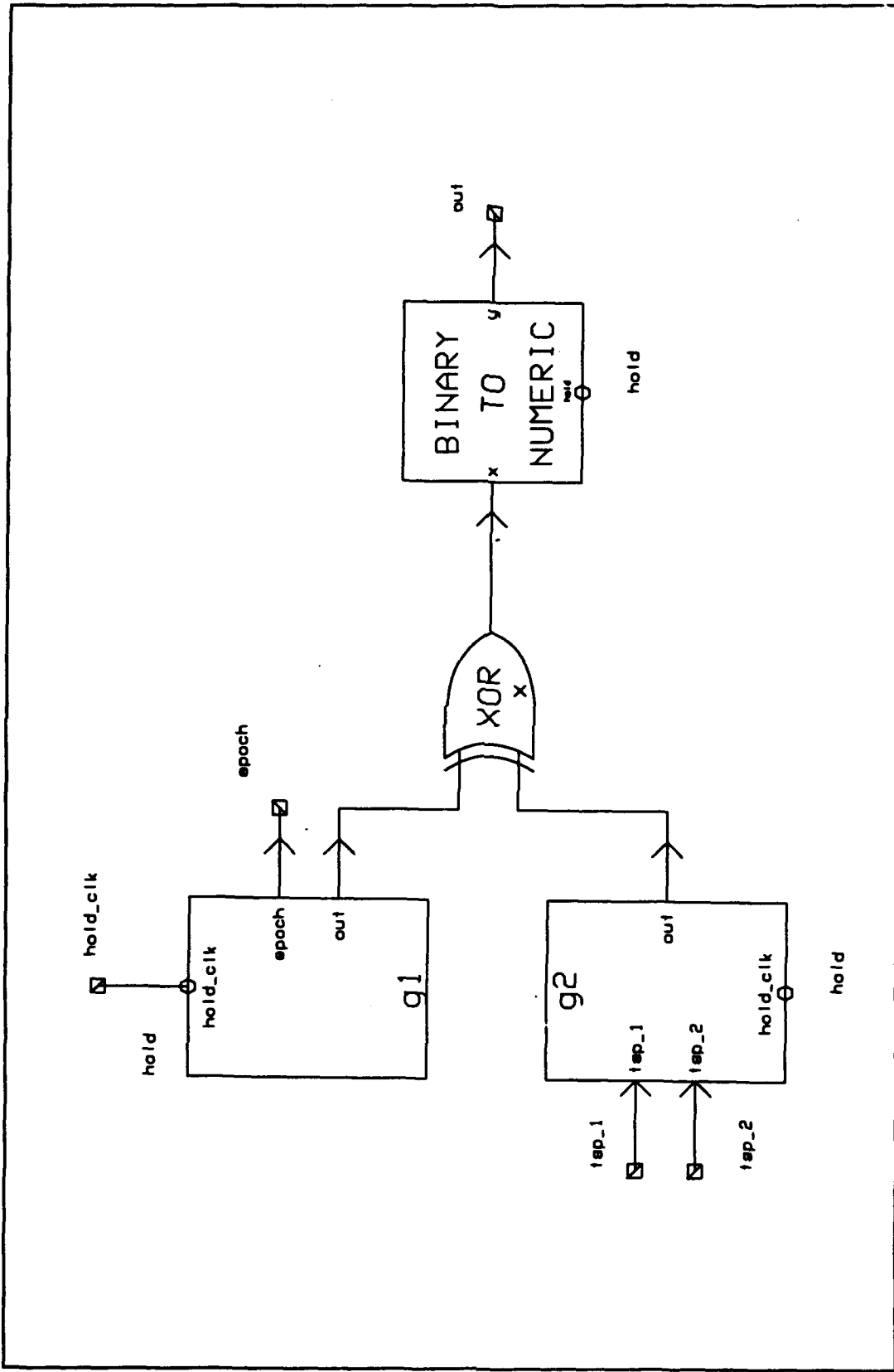


Figure 27 Gold Code Generator Detail

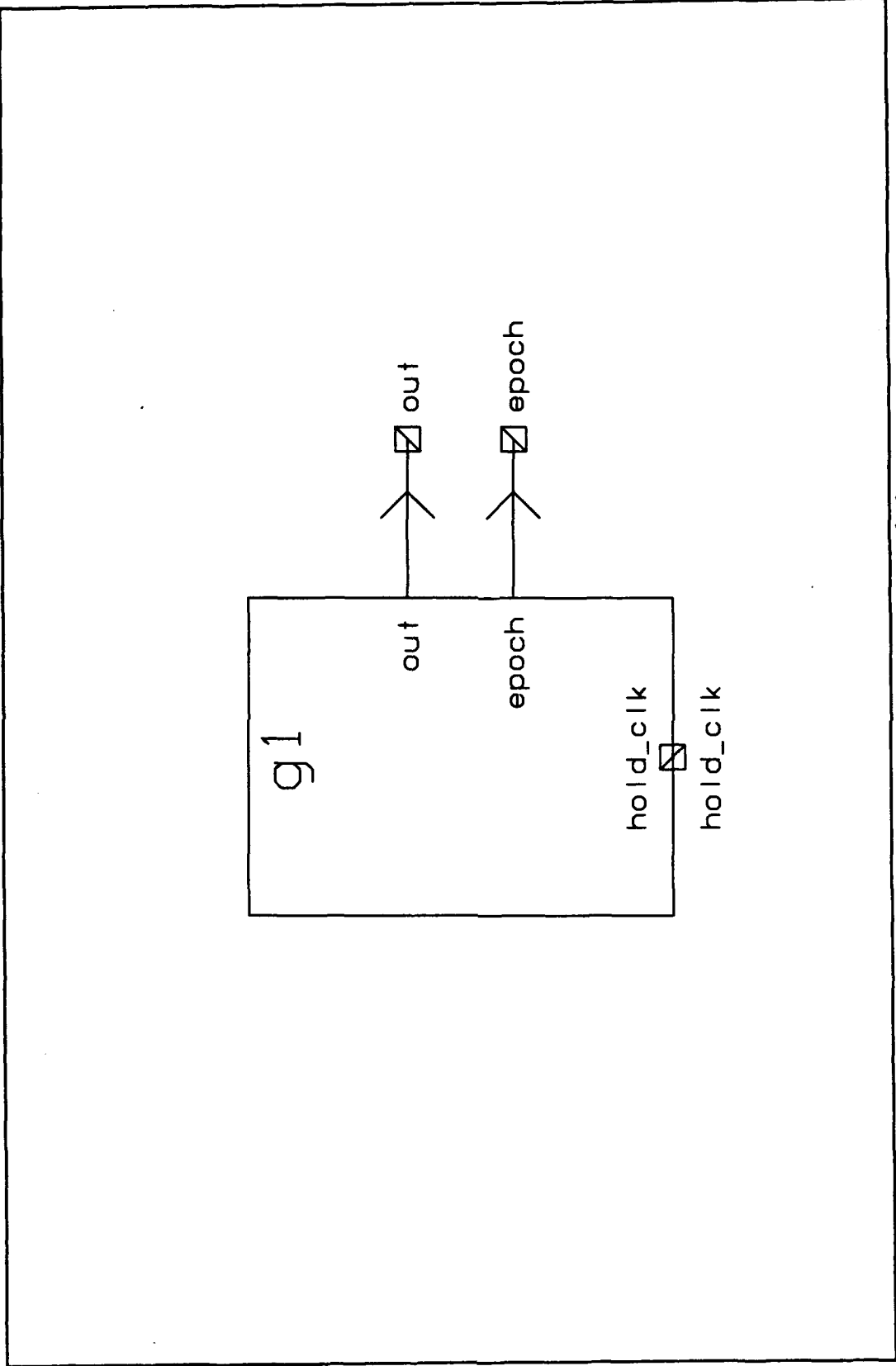


Figure 28 g1 Generator Symbol

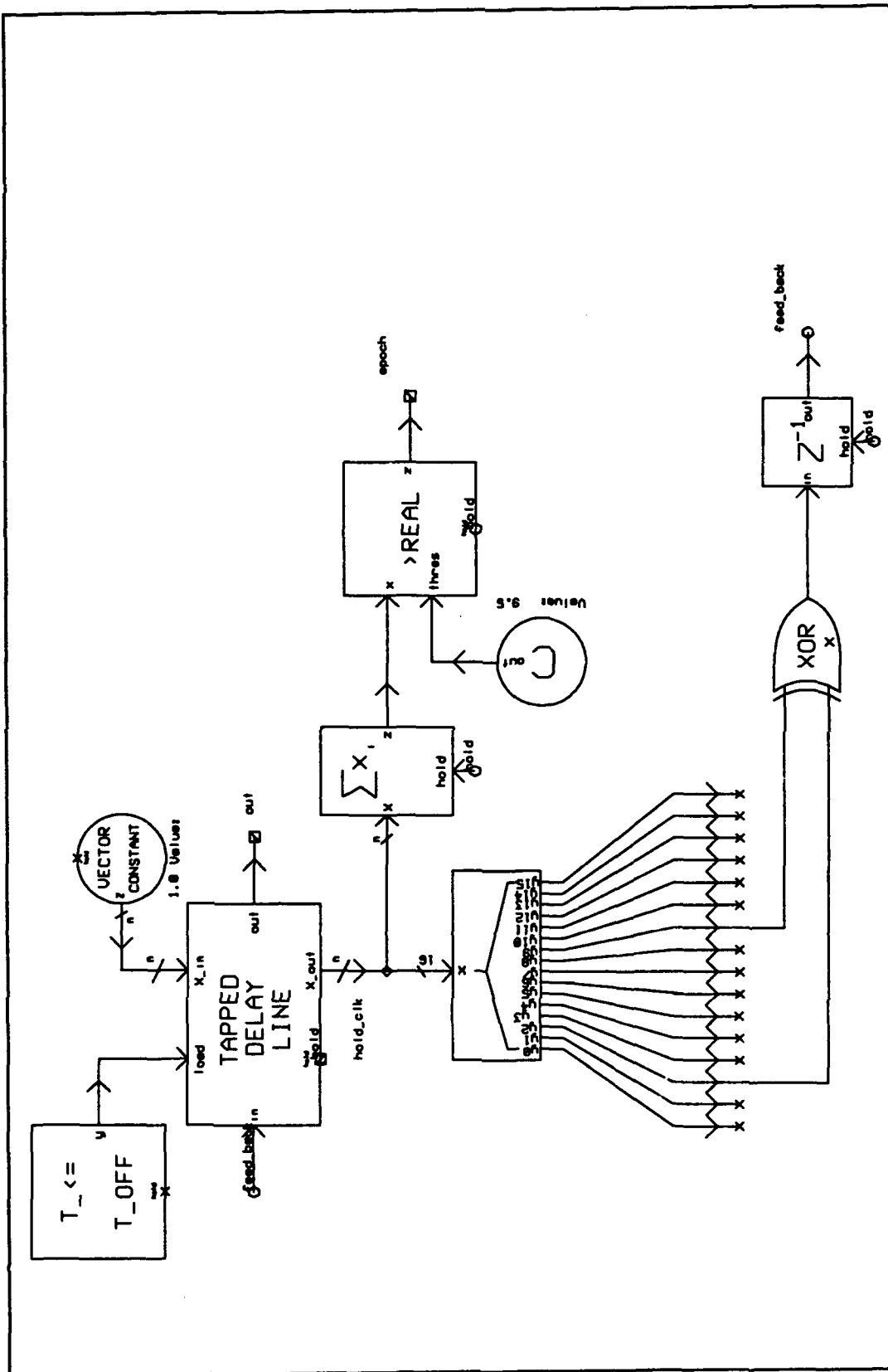


Figure 29 g1 Generator Detail

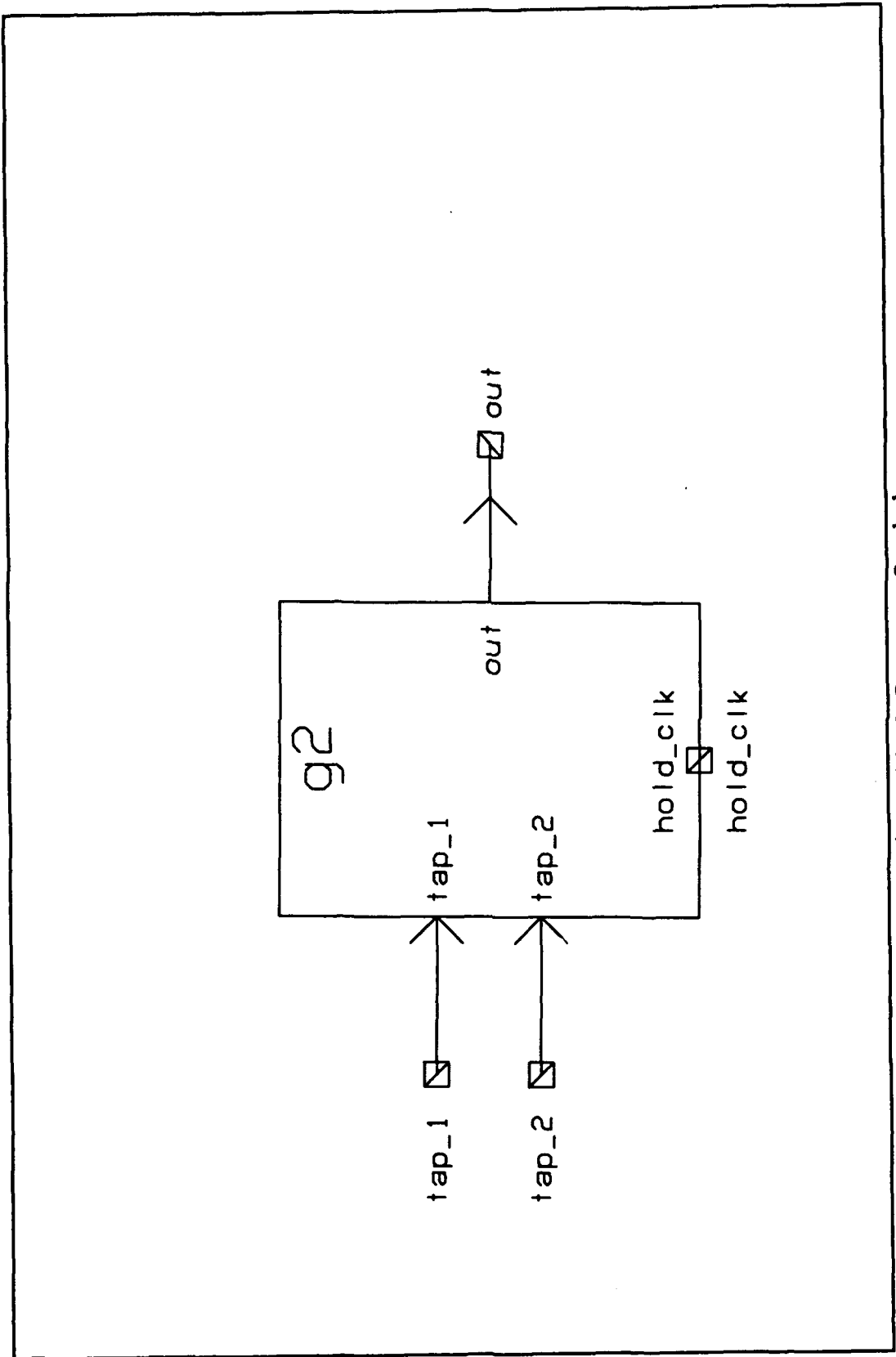


Figure 30 g2 Generator Symbol

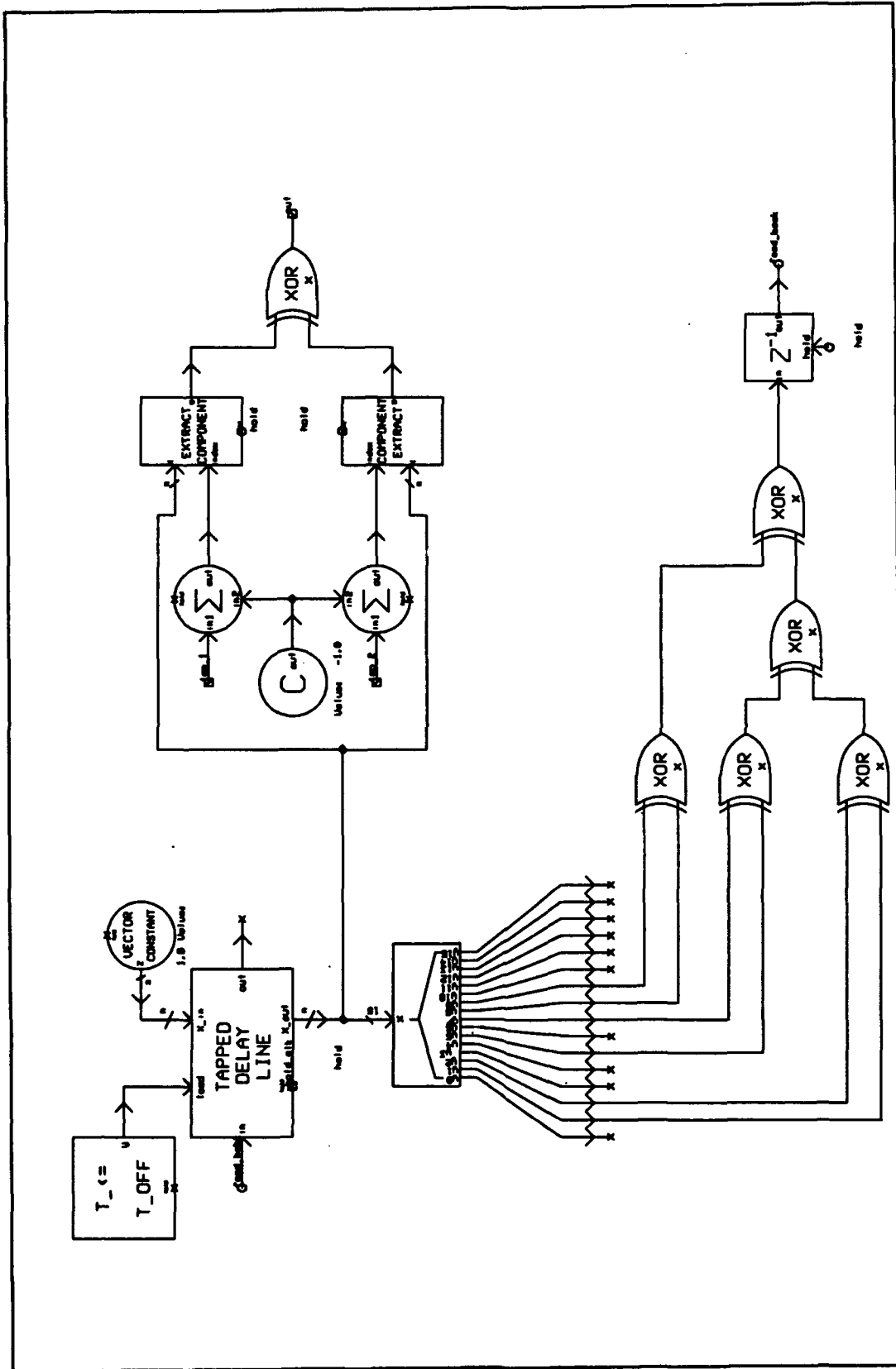


Figure 31 g2 Generator Detail

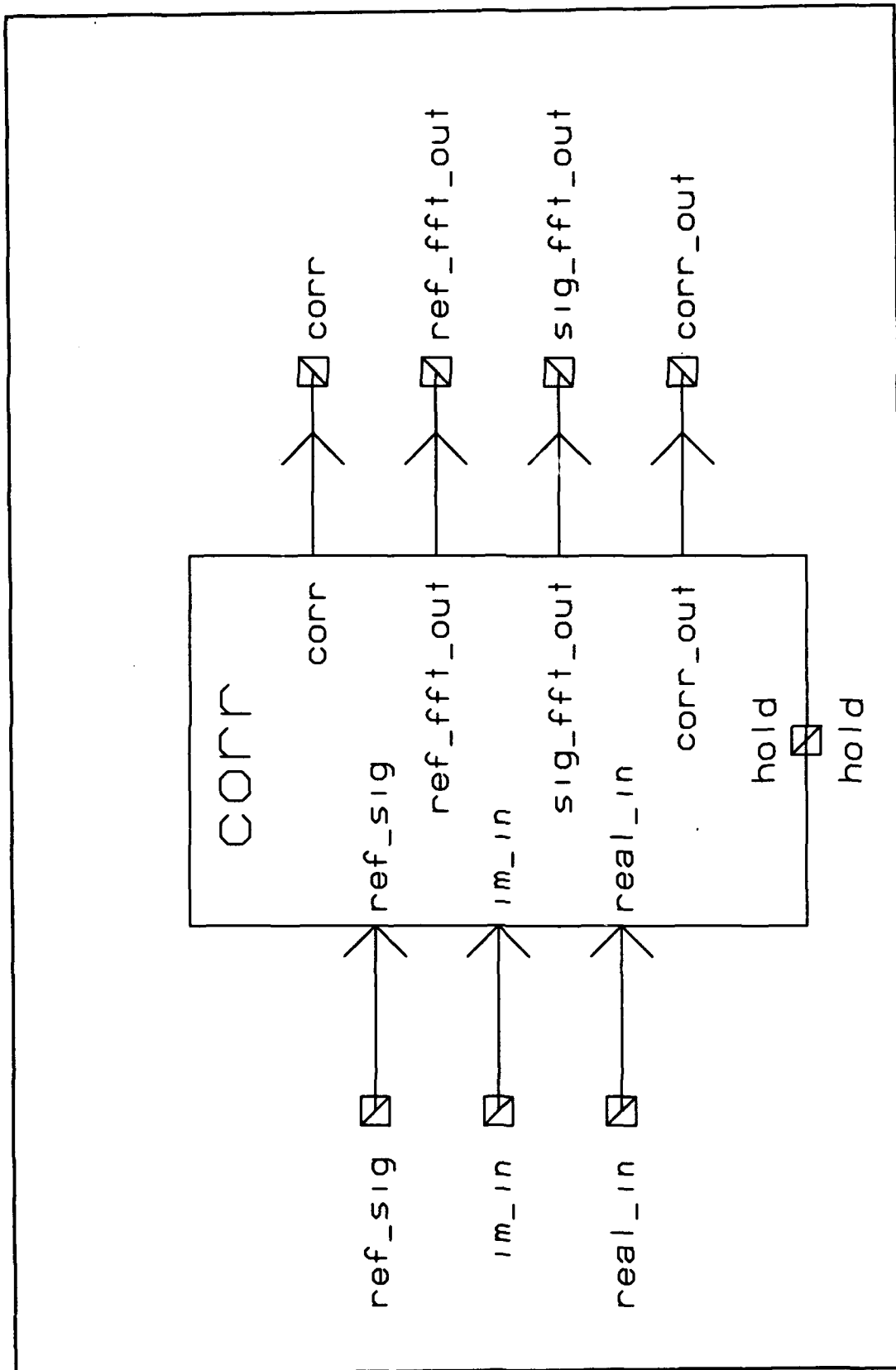


Figure 32 Correlator Symbol

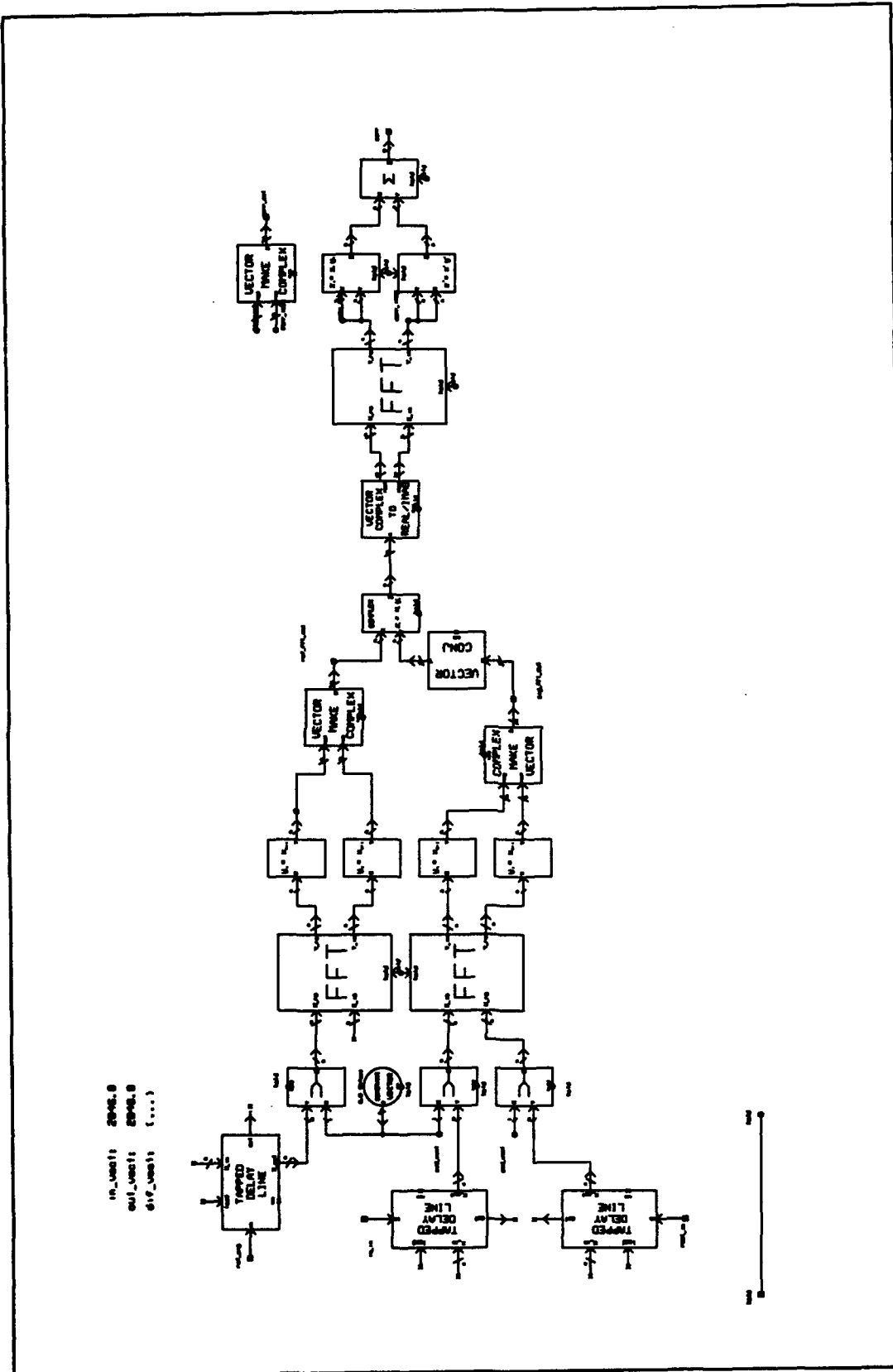


Figure 33 Correlator Detail

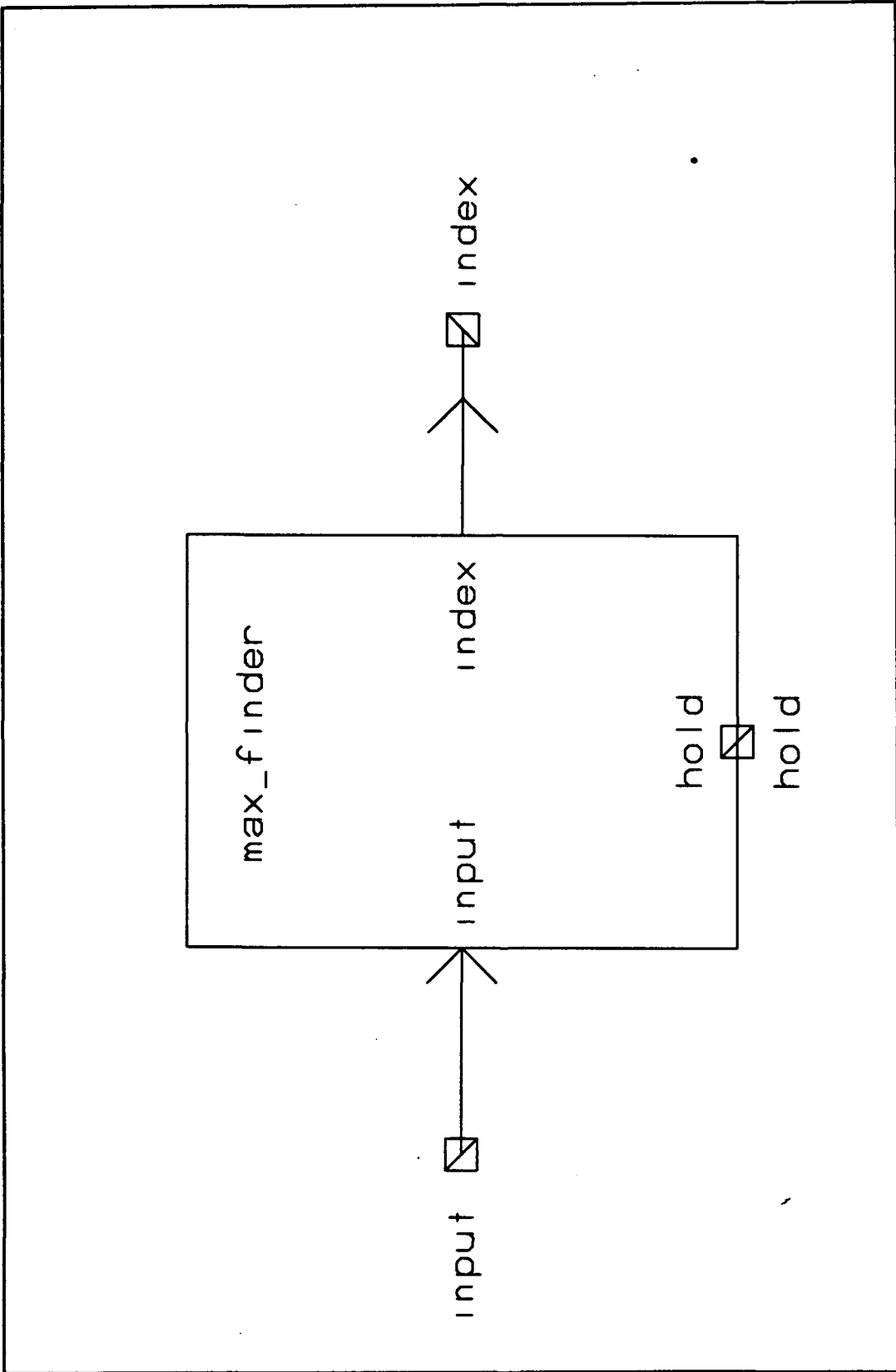


Figure 34 Maximum Finder Symbol

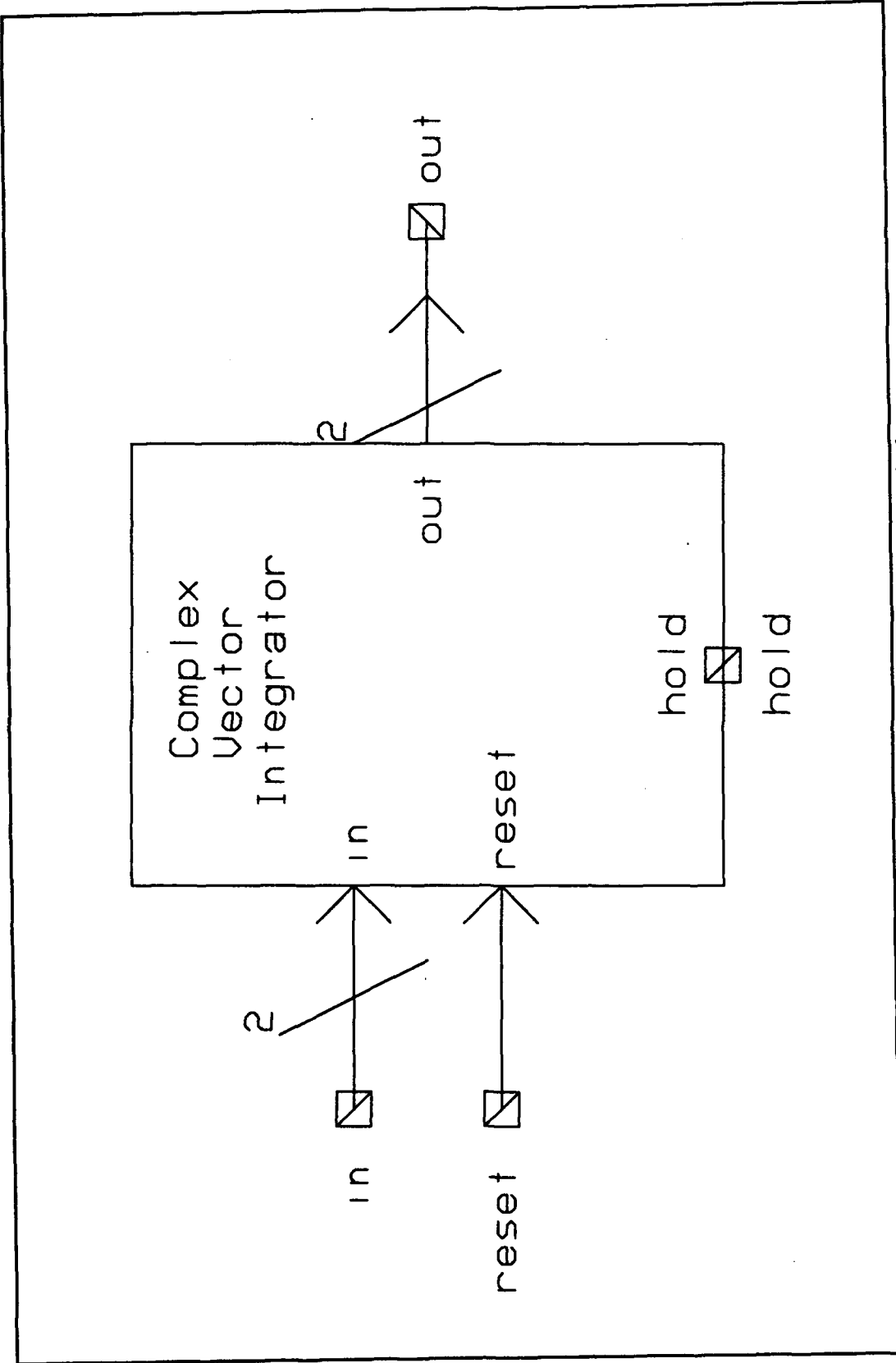


Figure 36 Complex Vector Finder Symbol

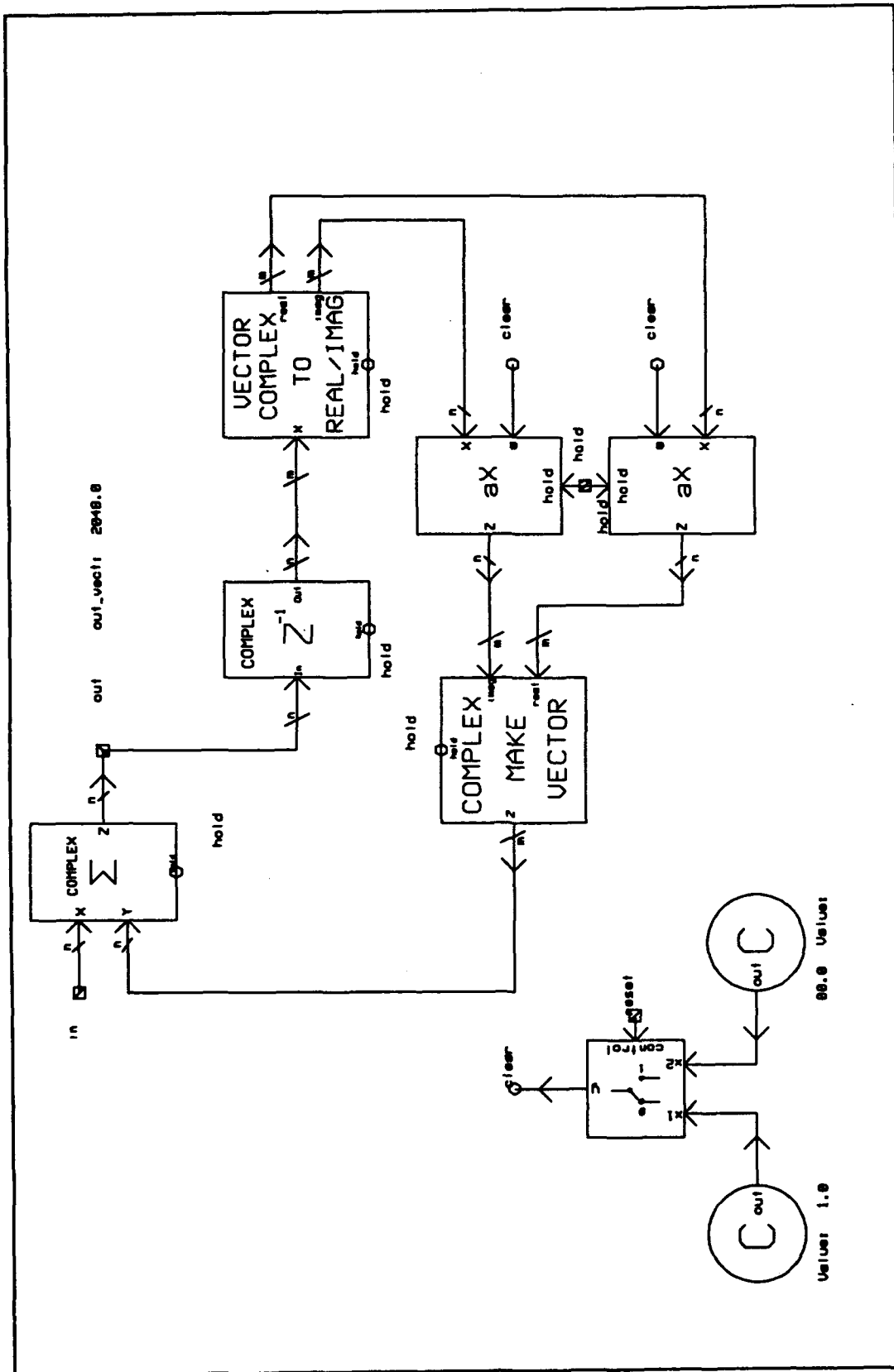


Figure 37 Complex Vector Integrator Detail

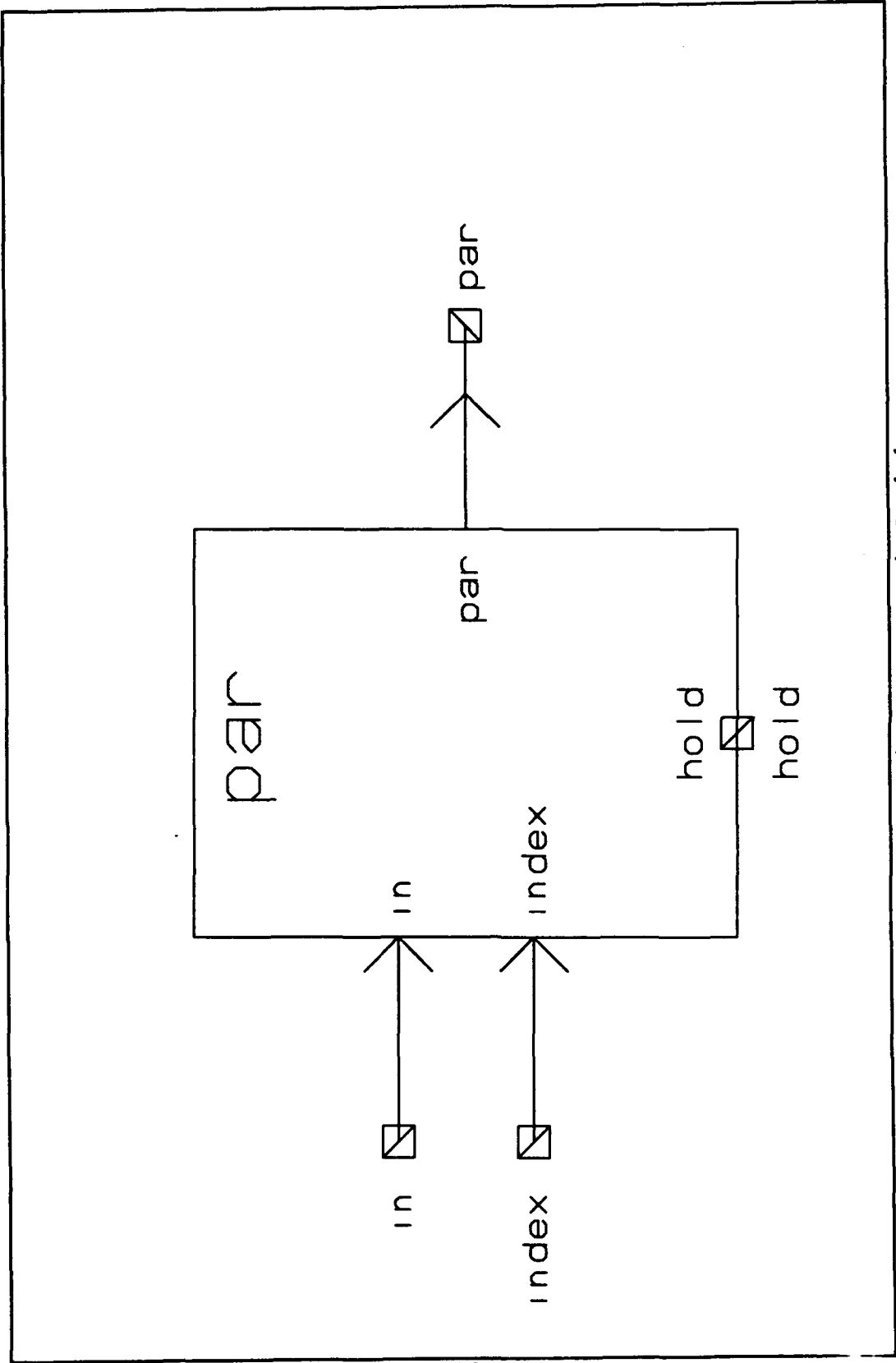


Figure 38 Peak-to-Average Ratio Symbol

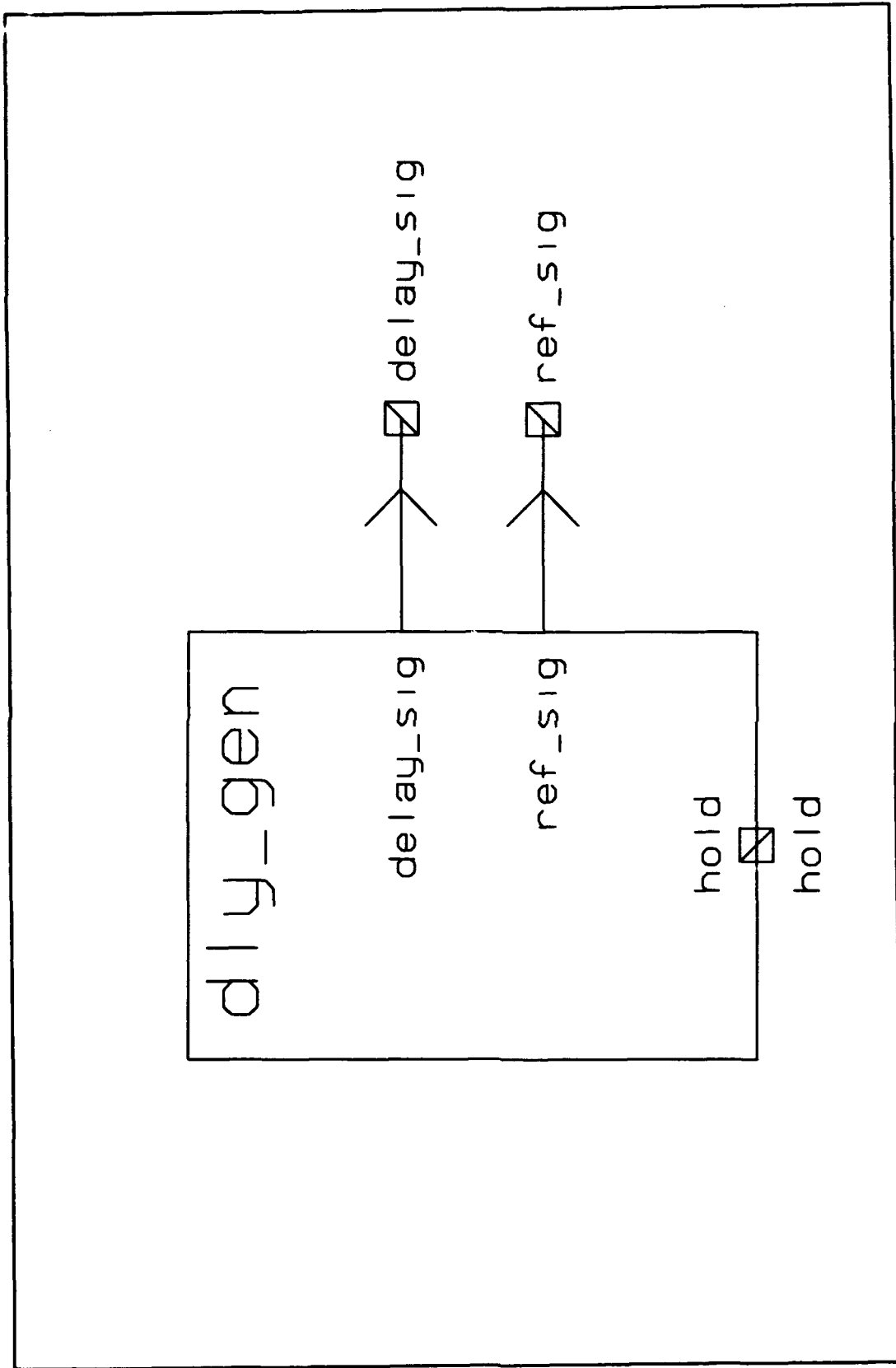


Figure 40 Delay Signal Generator Symbol

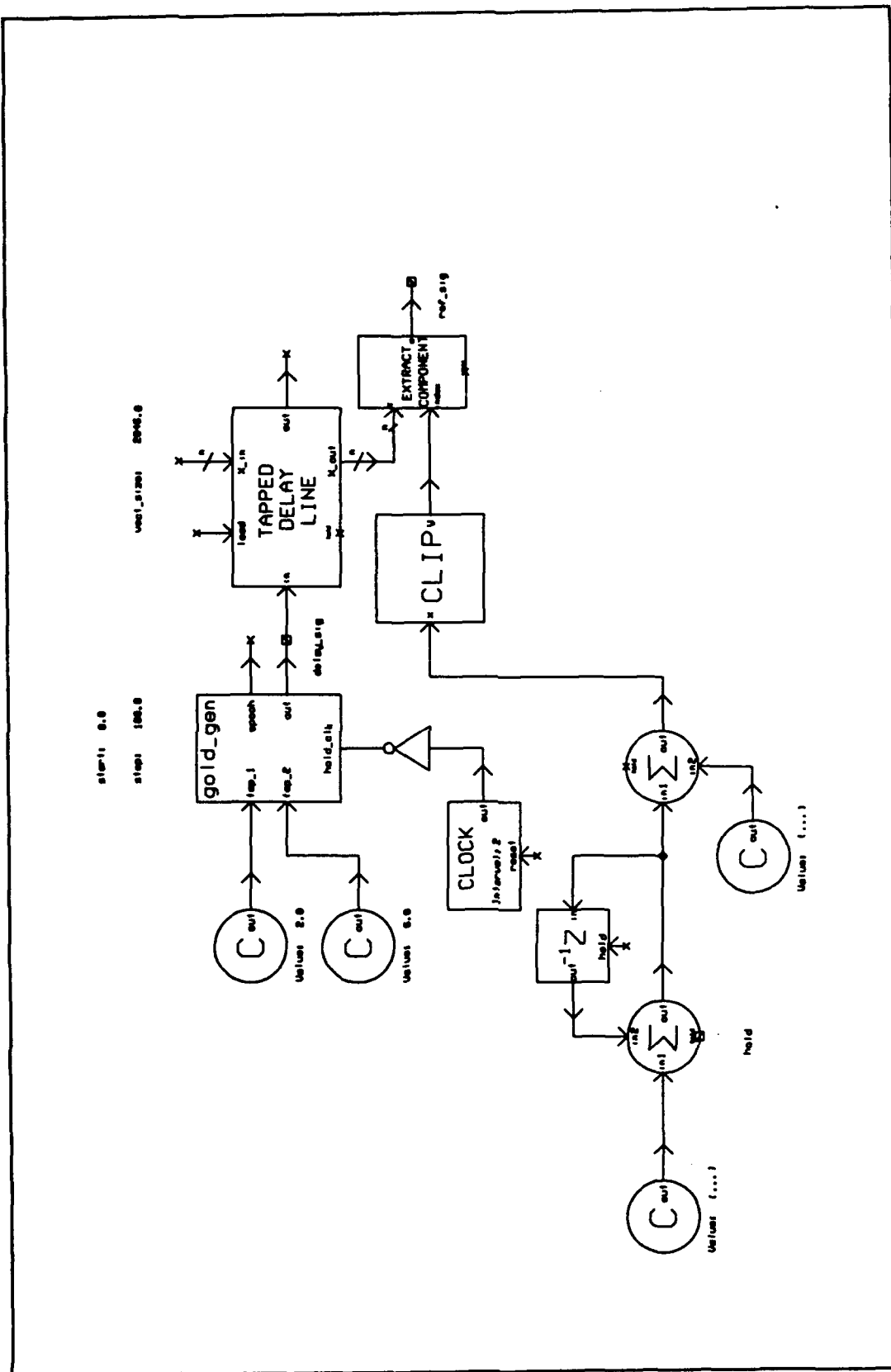


Figure 41 Delay Signal Generator Detail

Appendix C

THRESHOLD INPUT FOR VARIOUS DOPPLER FREQUENCIES

This appendix contains the inputs to the correlator for various residual Doppler shifts. As explained in Section 4.6, the frequency of the residual Doppler and the location of the phase shift from the residual Doppler shift determine the effect the Doppler shift has on the ability of the receiver to achieve coarse acquisition.

Figures 42 through 52 show the input to the threshold detector for 454 Hz residual Doppler and for θ from 0.0 to 1.0. Note that the location of the phase inversion increases in steps of 0.1. Also note that the PAR at the output of the correlator decreases as θ increases from 0.0 to 0.5, and as θ increases from 0.6 to 1.0 the PAR increases.

Figures 53 and 54 show the input to the threshold detector for 500 Hz residual Doppler. When the residual Doppler is 500 Hz, the location of the phase inversion does not change from epoch to epoch, as with the 454 Hz residual Doppler shown in Figures 42 through 52.

Figures 55 through 66 shows the input to the threshold detector for residual Doppler frequencies of 600 Hz to 900 Hz in 100 Hz steps. For each frequency, there are three figures. The first figure shows the input to the threshold detector for the lowest possible PAR at the out of the correlator. The next figure shows input to the threshold detector for the epoch of data following the epoch that

gives the lowest possible PAR. The last figure shows the input to the threshold detector for the highest possible PAR.

Figures 67 and 68 show the input to the correlator for 1000 Hz Doppler and two different inversion locations. Note that both figures have two phase inversions and the PAR is below 10 dB in both of the figures. Recall that a PAR of 10 dB is considered the minimum required PAR for achieving coarse acquisition.

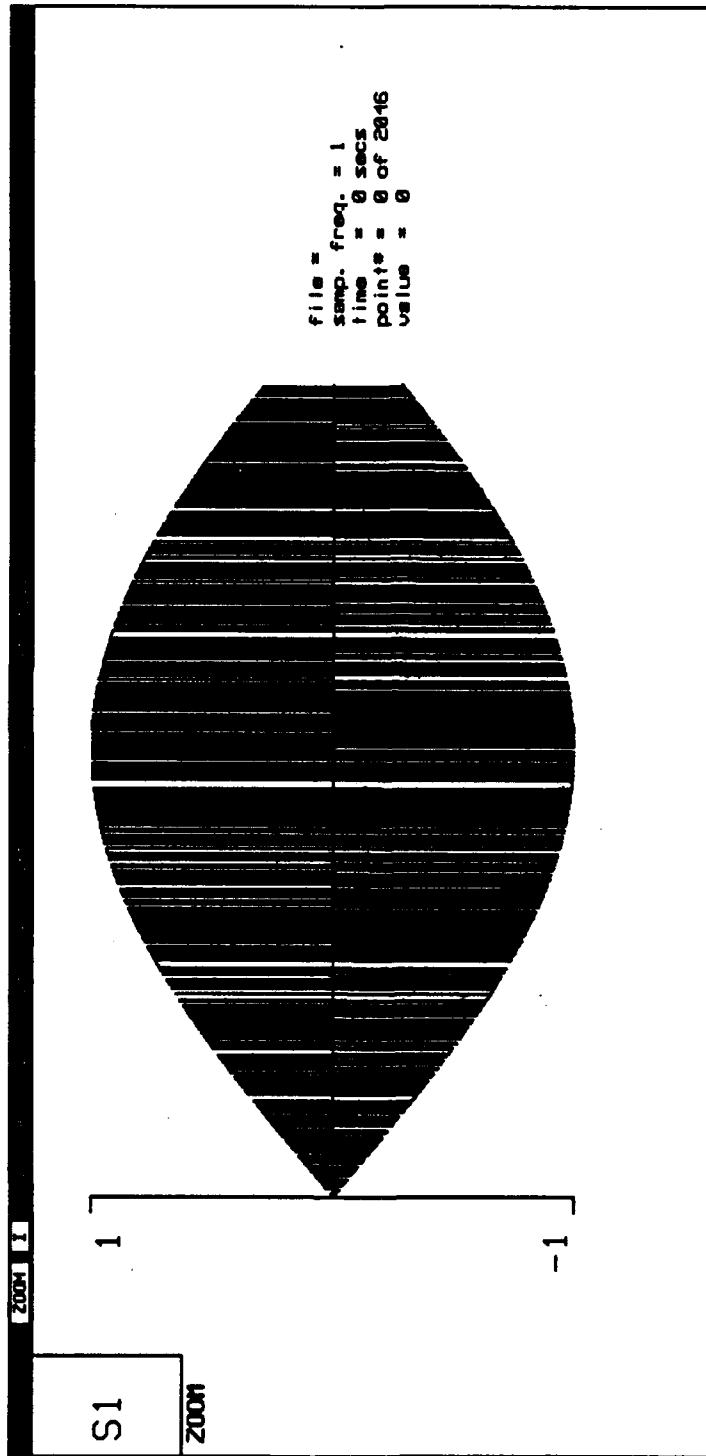


Figure 42 Input of Threshold Detector with 454 Hz Doppler and $\theta=0$

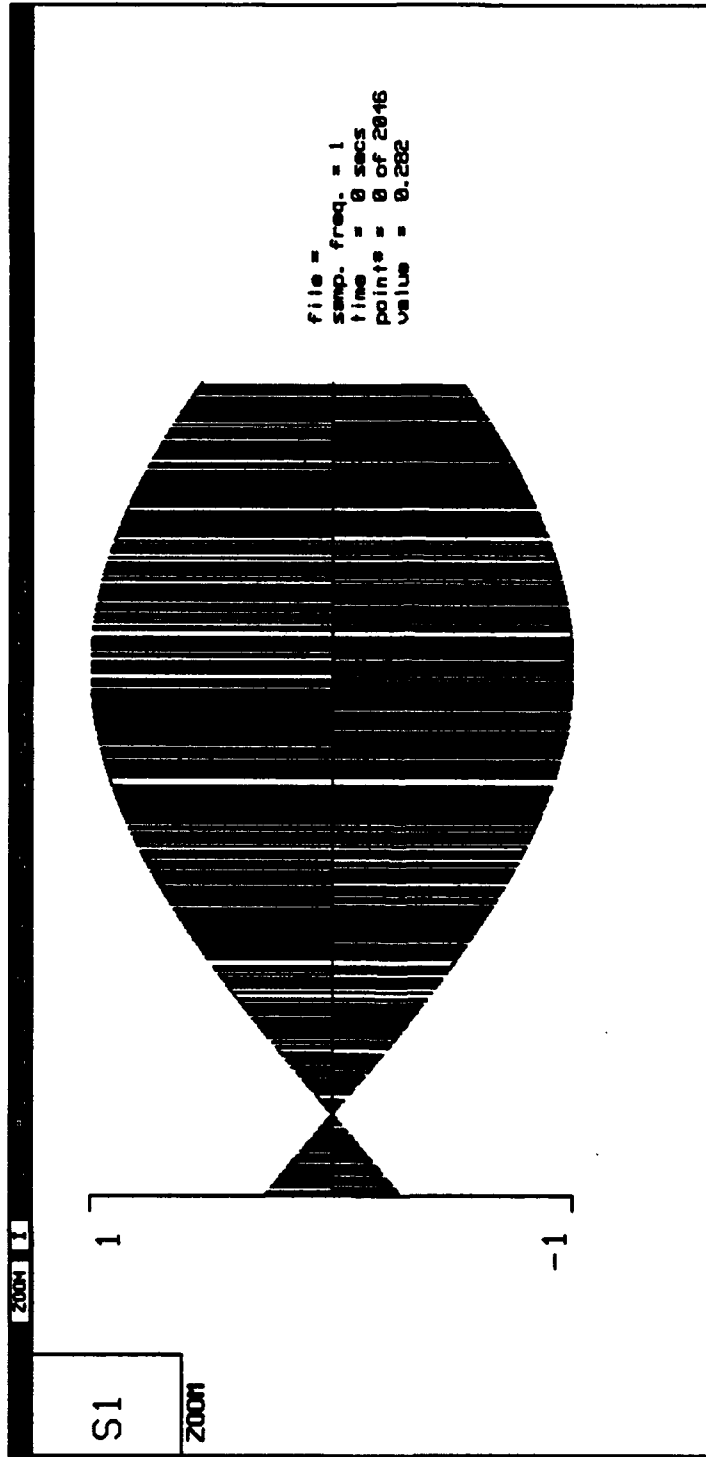


Figure 43 Input of Threshold Detector with 454 Hz Doppler and $\theta=0.1$

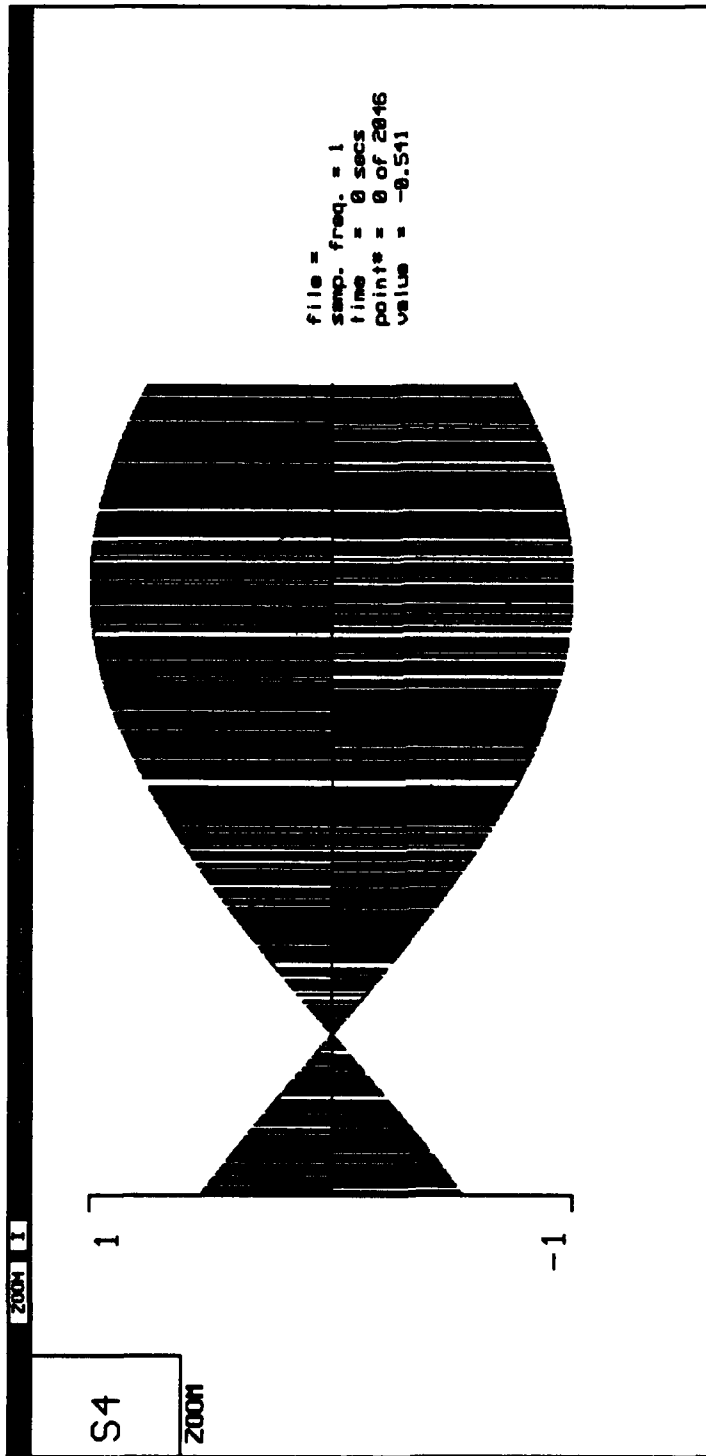


Figure 44 Input of Threshold Detector with 454 Hz Doppler and $\theta=0.2$

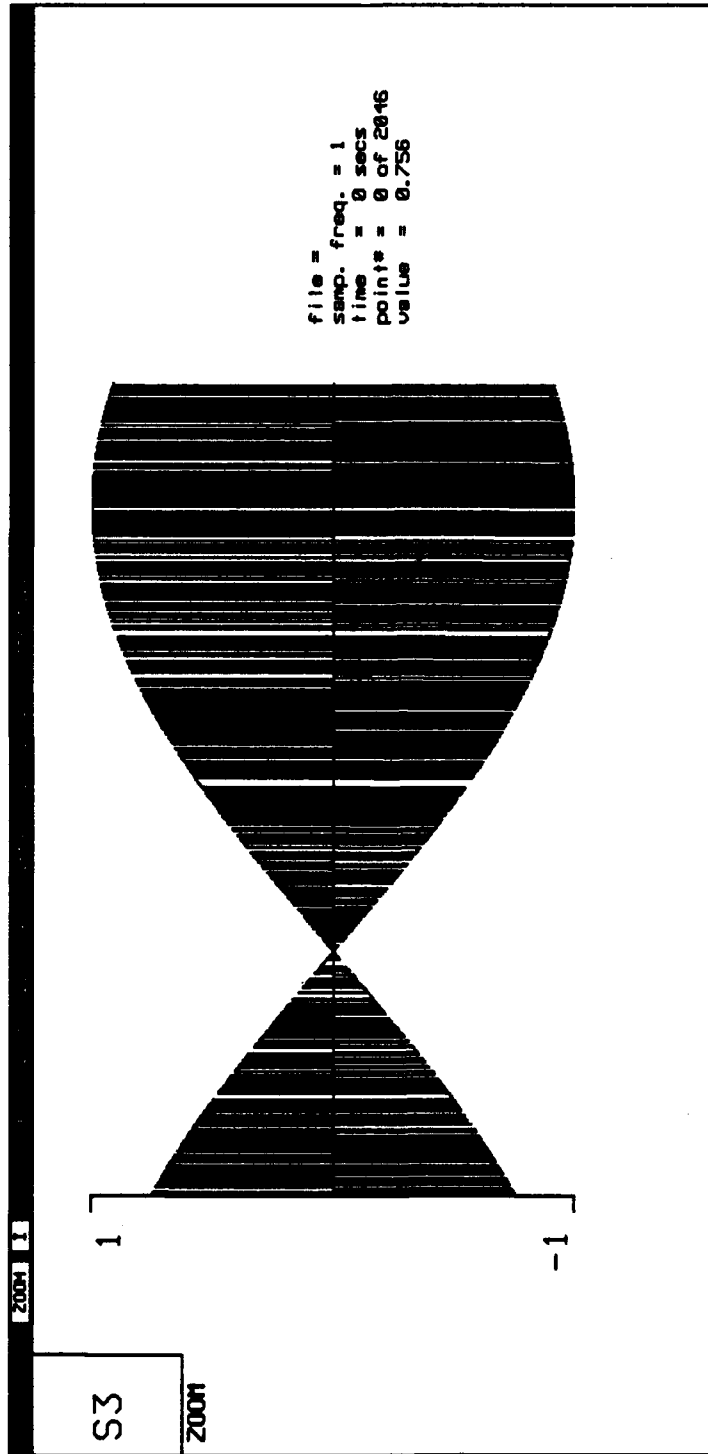


Figure 45 Input of Threshold Detector with 454 Hz Doppler and $\theta=0.3$

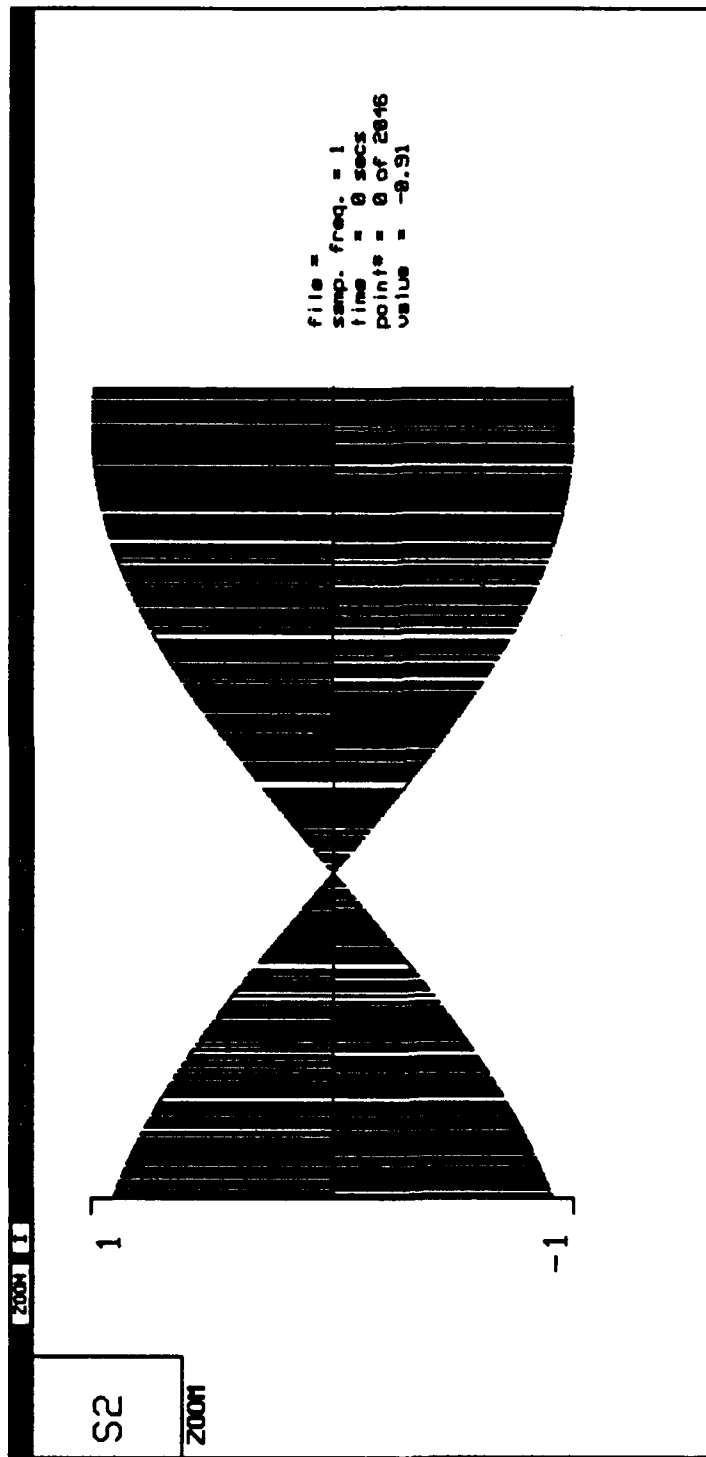


Figure 46 Input of Threshold Detector with 454 Hz Doppler and $\theta=0.4$

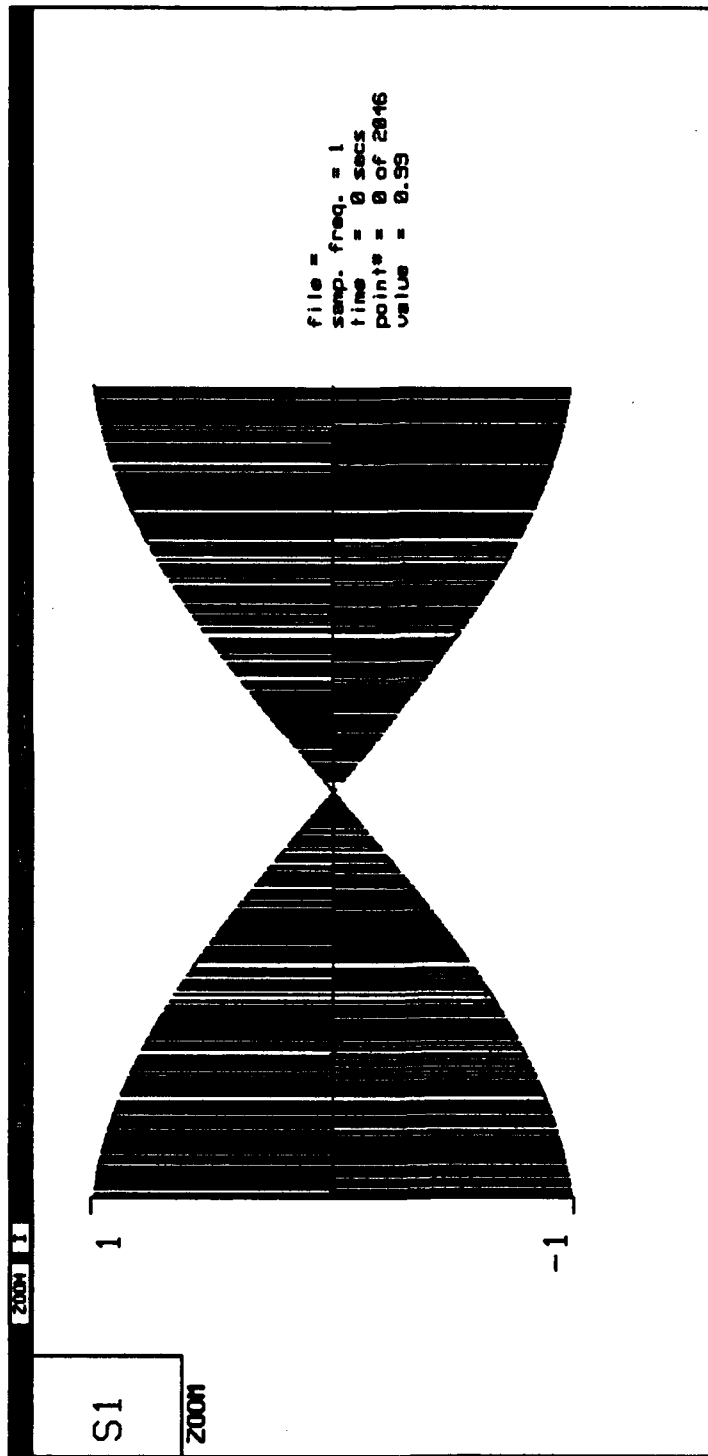


Figure 47 Input of Threshold Detector with 454 Hz Doppler and $\theta=0.5$

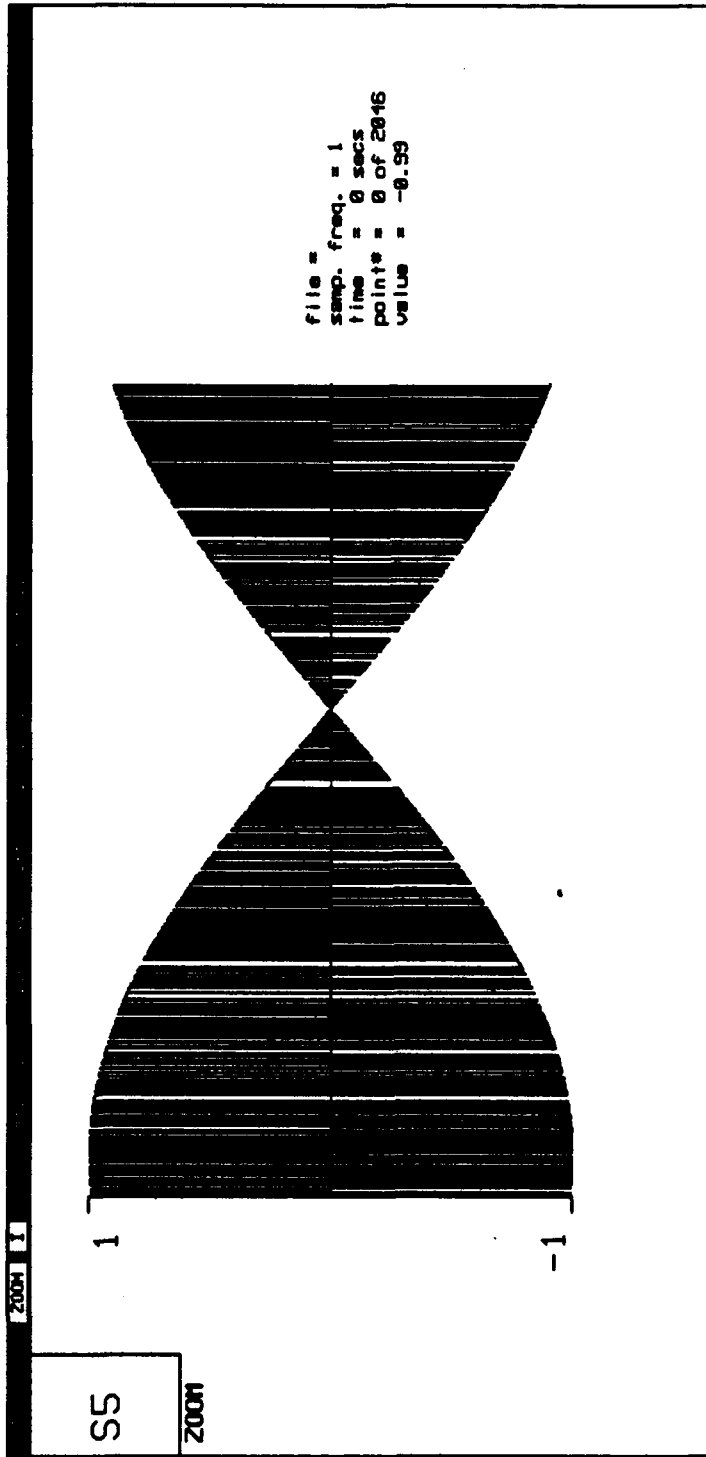


Figure 48 Input of Threshold Detector with 454 Hz Doppler and $\theta=0.6$

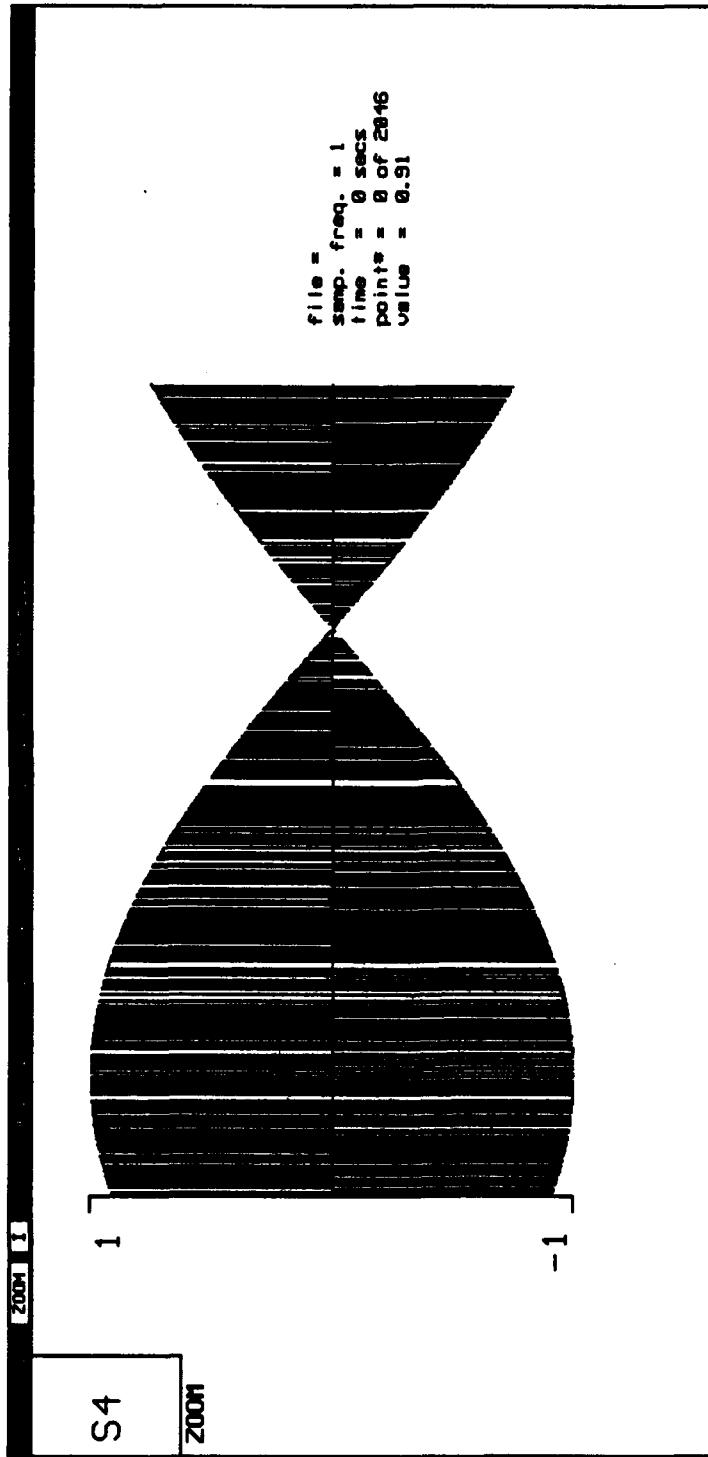


Figure 49 Input of Threshold Detector with 454 Hz Doppler and $\theta=0.7$

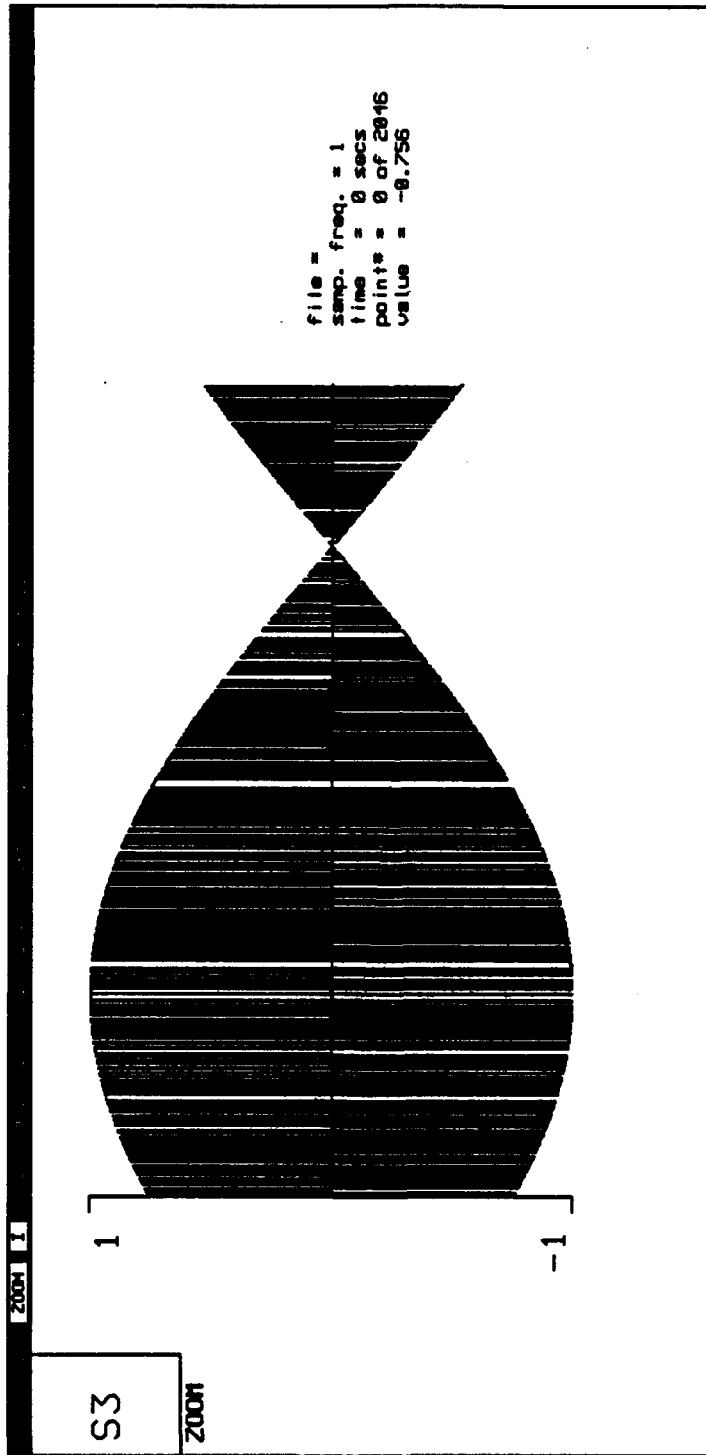


Figure 50 Input of Threshold Detector with 454 Hz Doppler and $\theta=0.8$

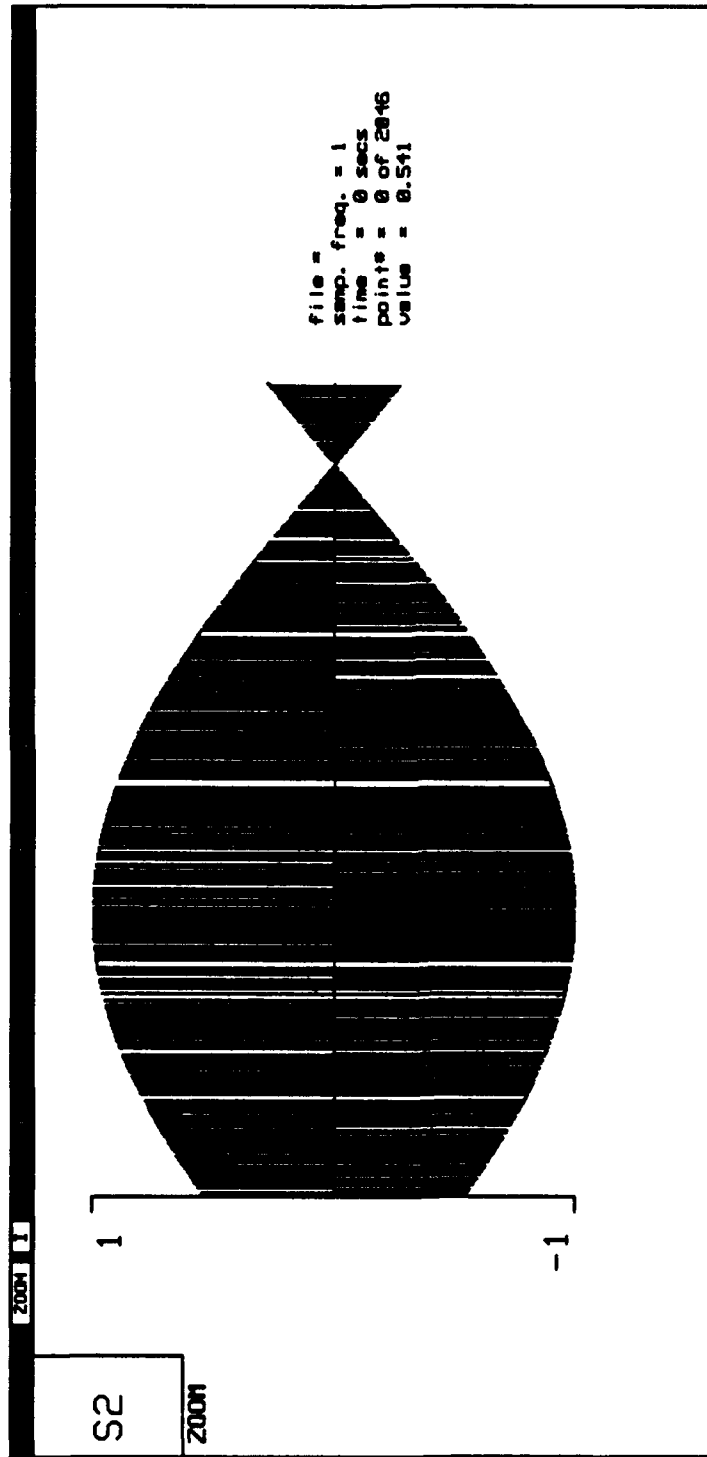


Figure 51 Input of Threshold Detector with 454 Hz Doppler and $\theta = 0.9$

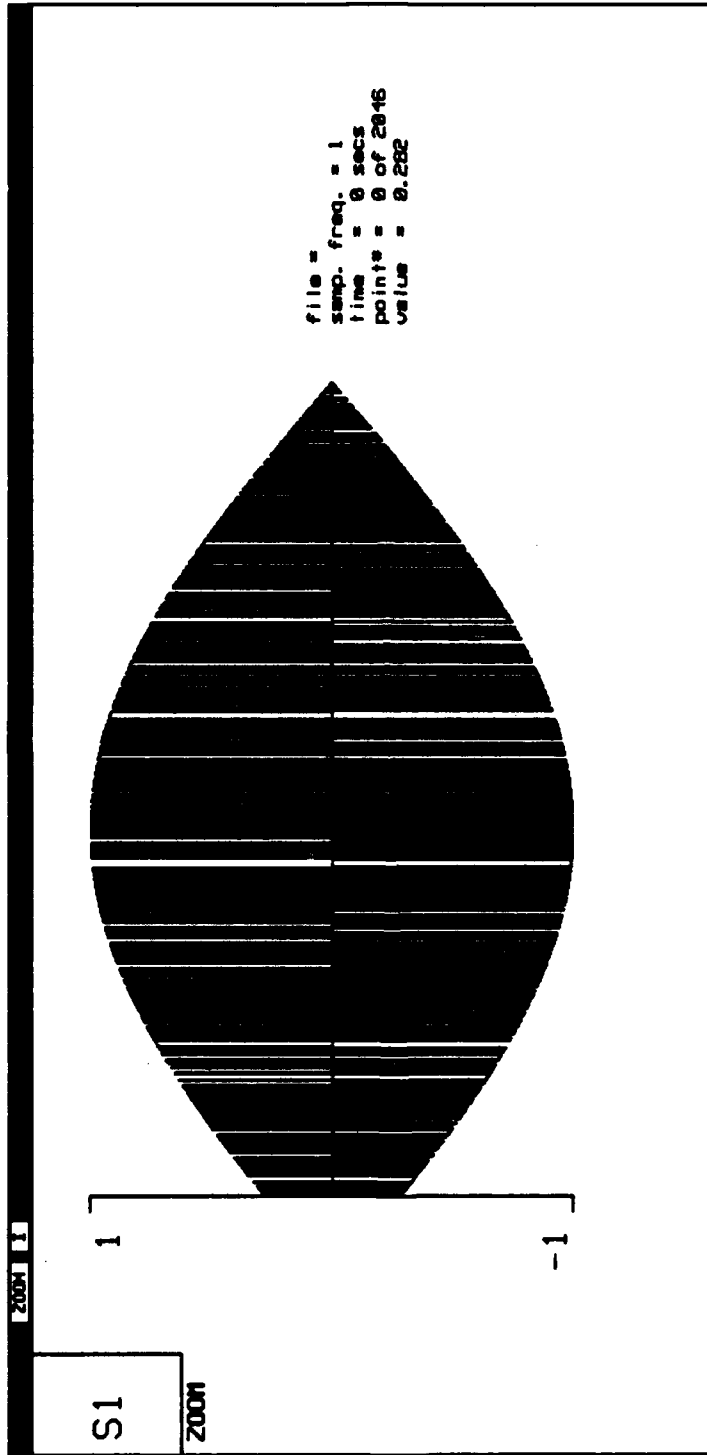


Figure 52 Input of Threshold Detector with 454 Hz Doppler and $\theta=1.0$

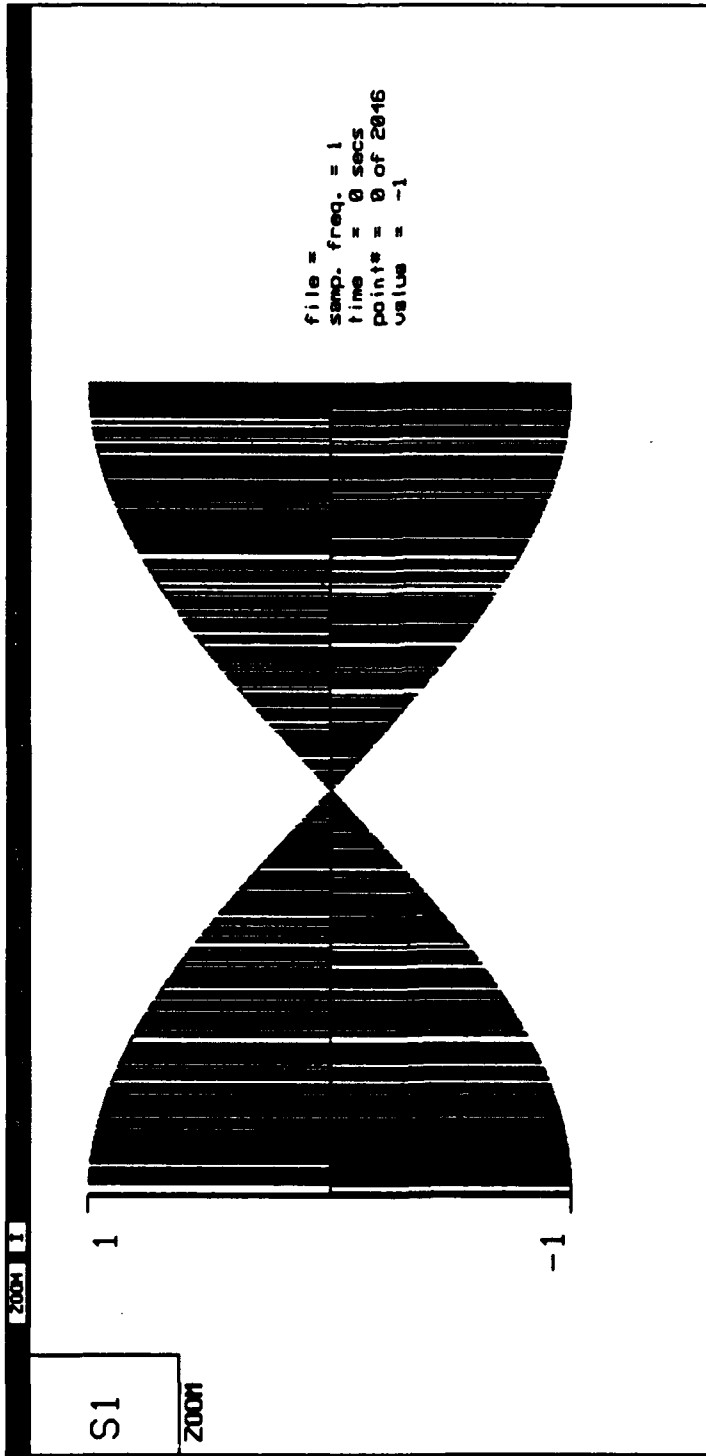


Figure 53 Input of Threshold Detector with 500 Hz Doppler and $\theta=0.5$. PAR=7.3 dB



Figure 54 Input of Threshold Detector with 500 Hz Doppler and $\theta=0.0$. PAR=31.4 dB

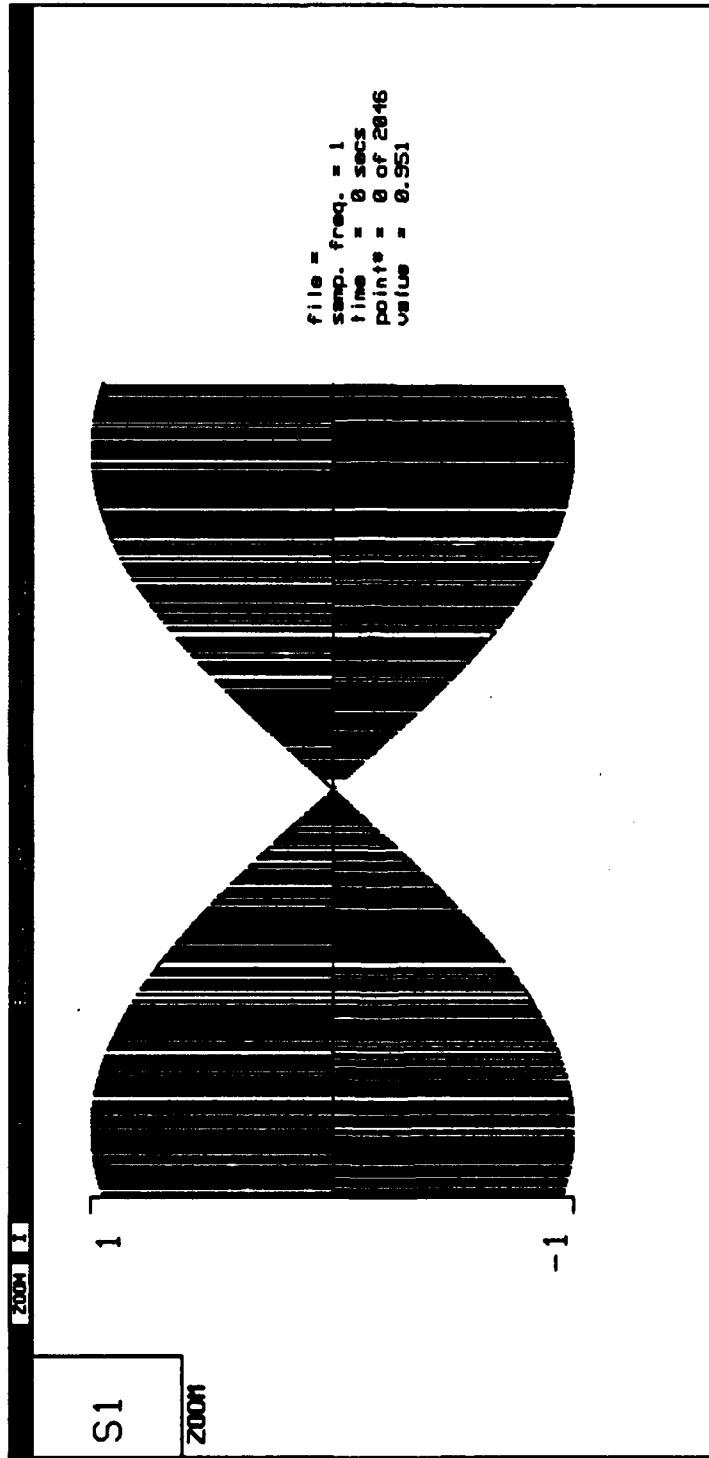


Figure 55 Input of Threshold Detector with 600 Hz Doppler and $\theta=0.5$. PAR=7.3 dB

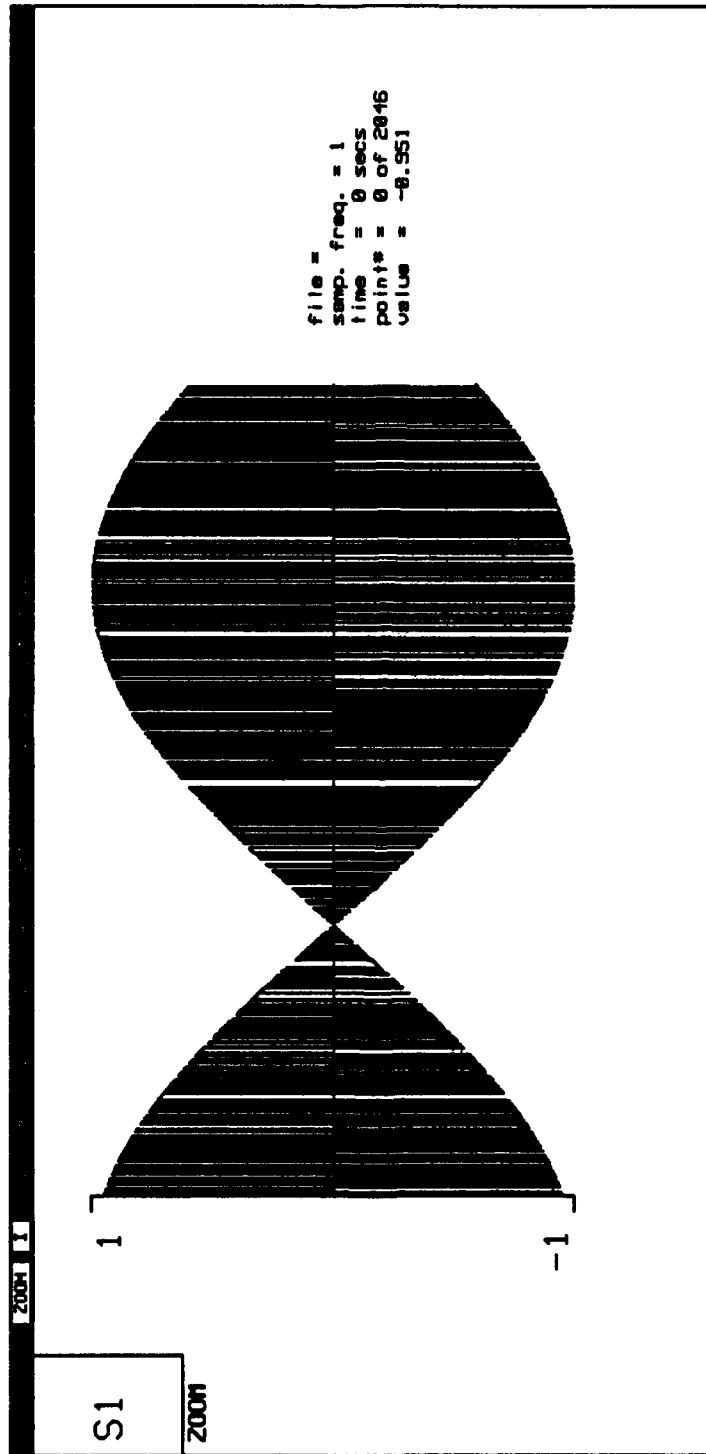


Figure 56 Input of Threshold Detector with 600 Hz Doppler and $\theta=0.3$. PAR=21.2 dB

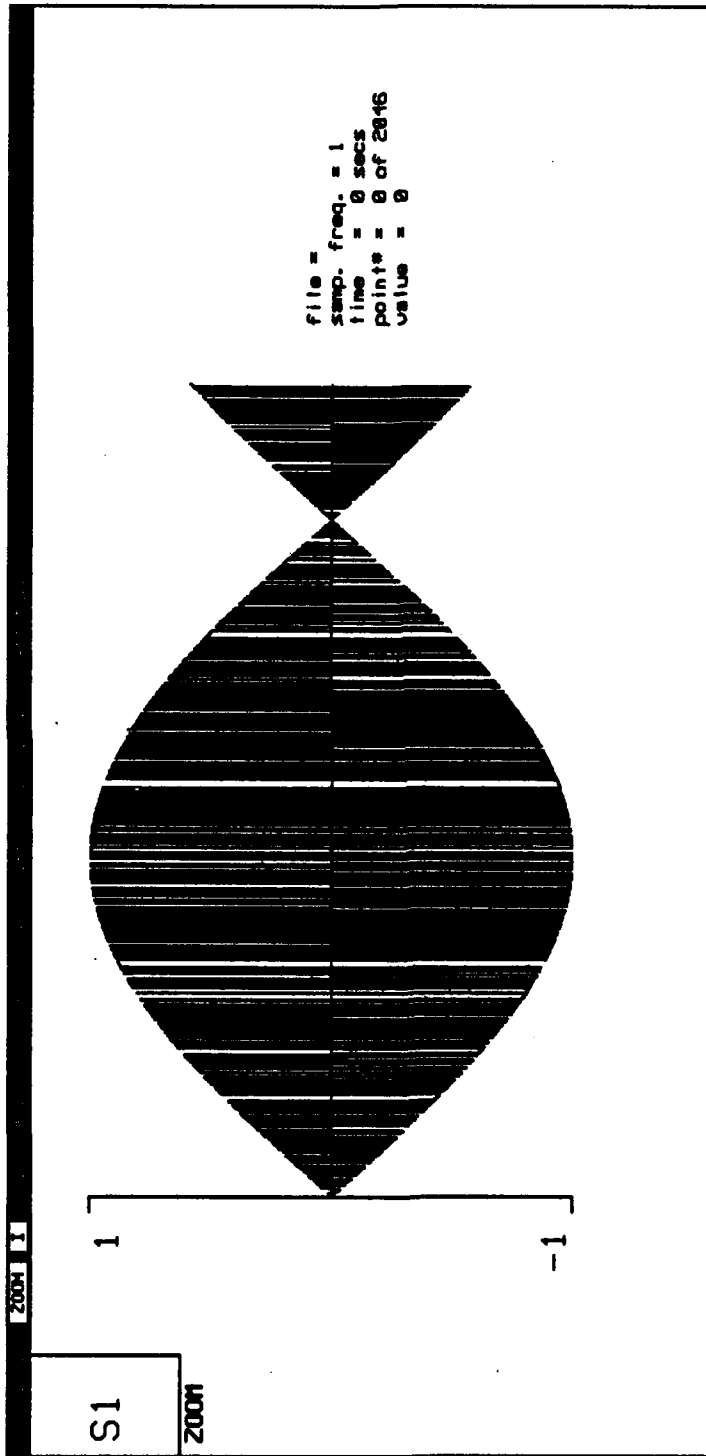


Figure 57 Input of Threshold Detector with 600 Hz Doppler and $\theta=0.8$. PAR=27.8 dB

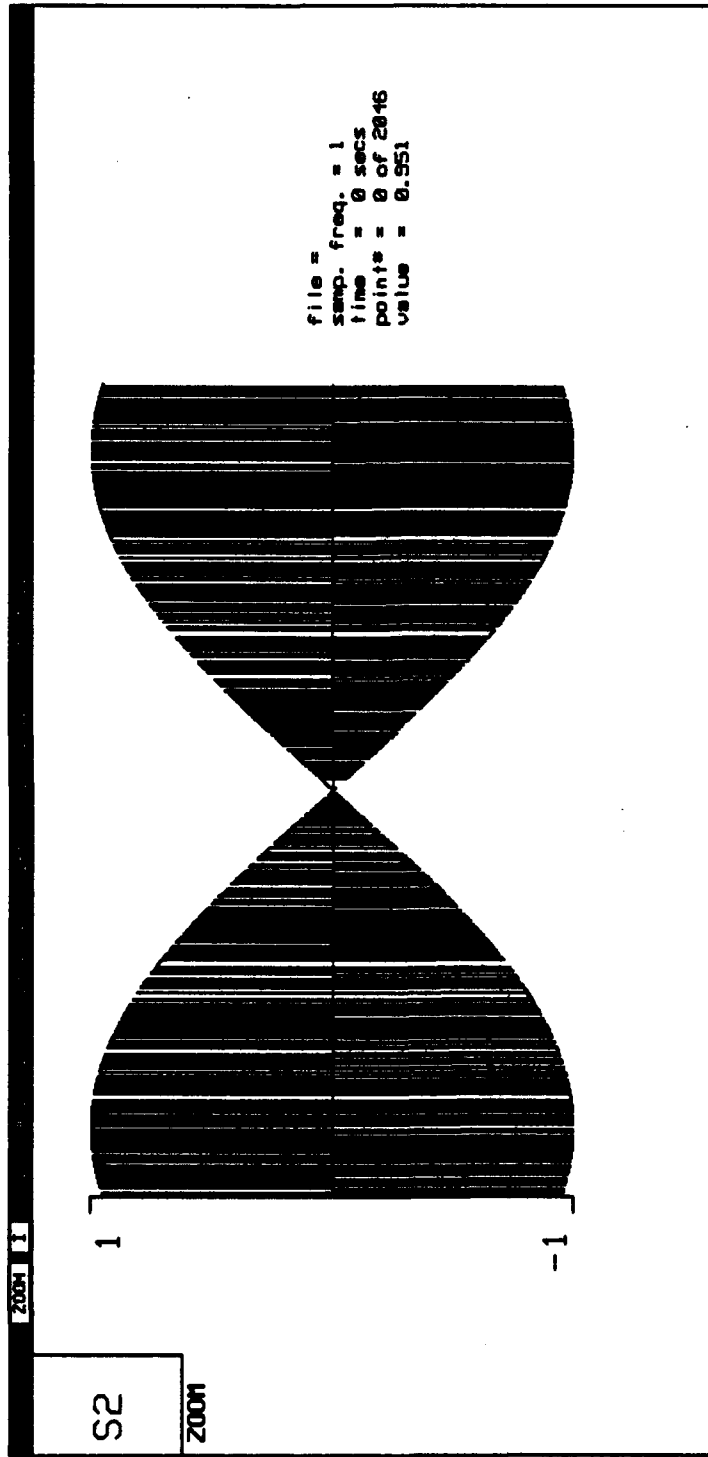


Figure 58 Input of Threshold Detector with 700 Hz Doppler and $\theta = 0.5$. PAR = 7.4 dB

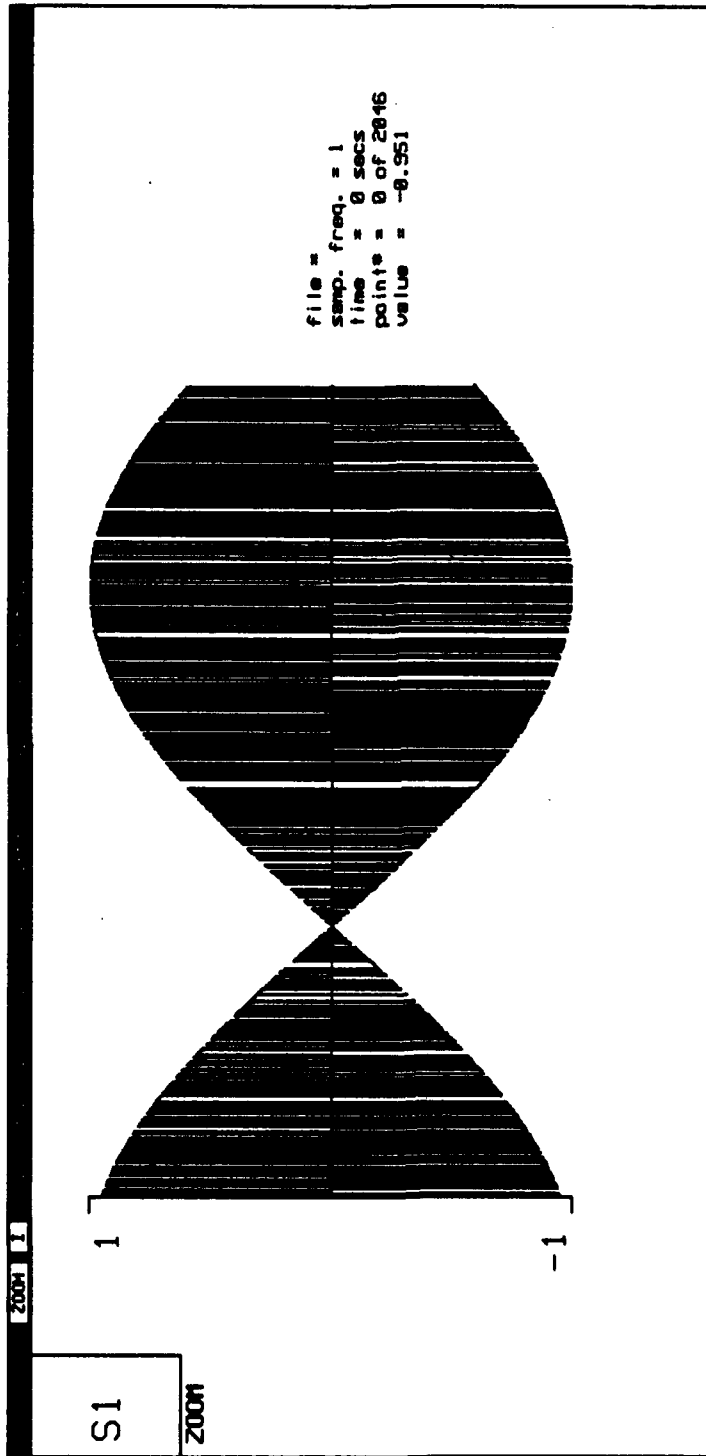


Figure 59 Input of Threshold Detector with 700 Hz Doppler. PAR=23.4 dB

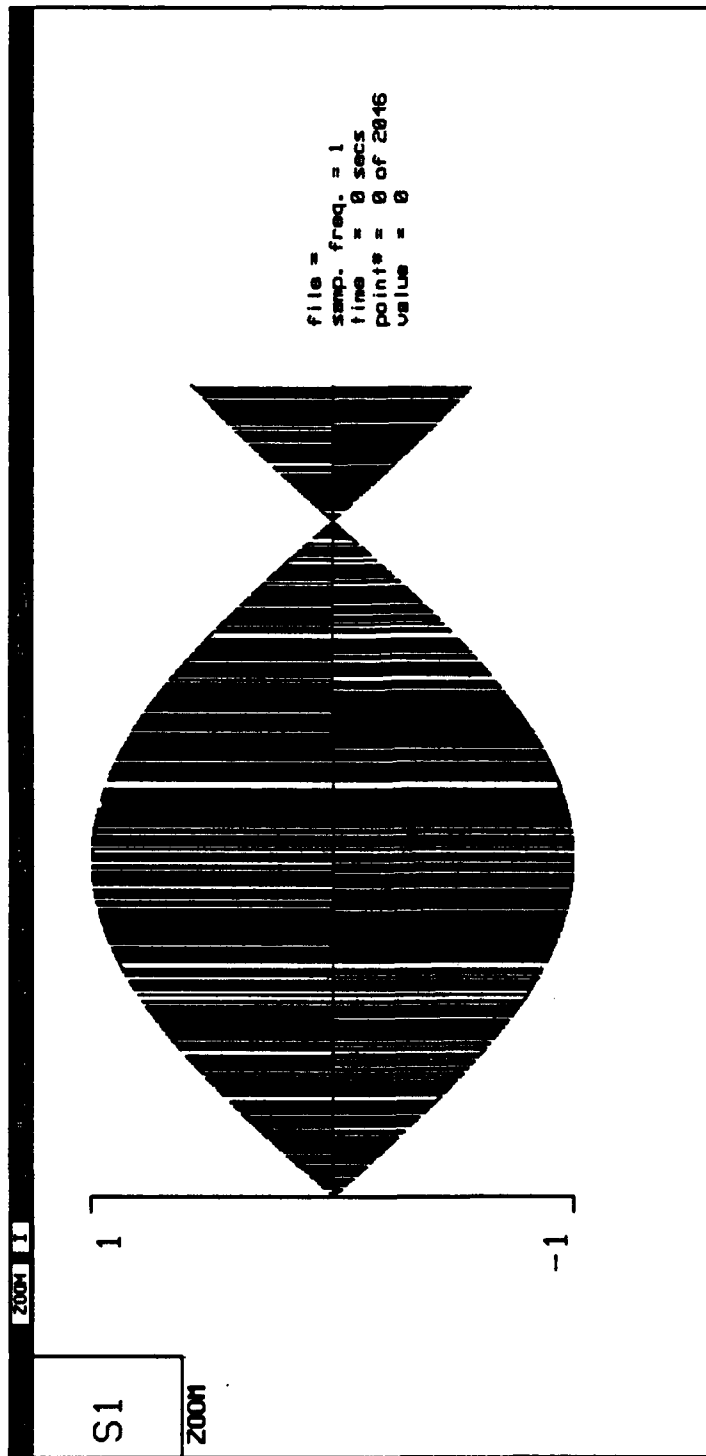


Figure 60 Input of Threshold Detector with 700 Hz Doppler and $\theta=0.7$. PAR=23.0 dB

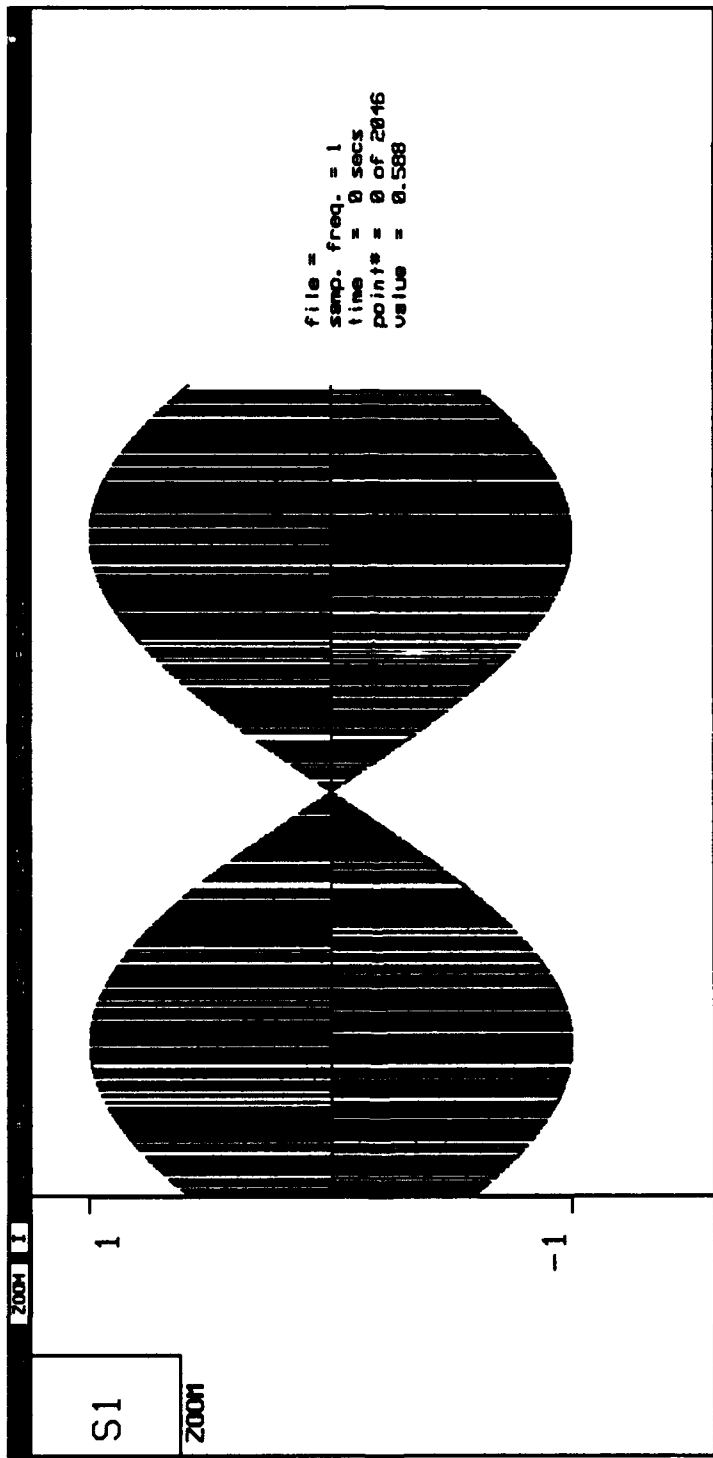


Figure 61 Input of Threshold Detector with 800 Hz Doppler and $\theta=0.5$. PAR=8.4 dB

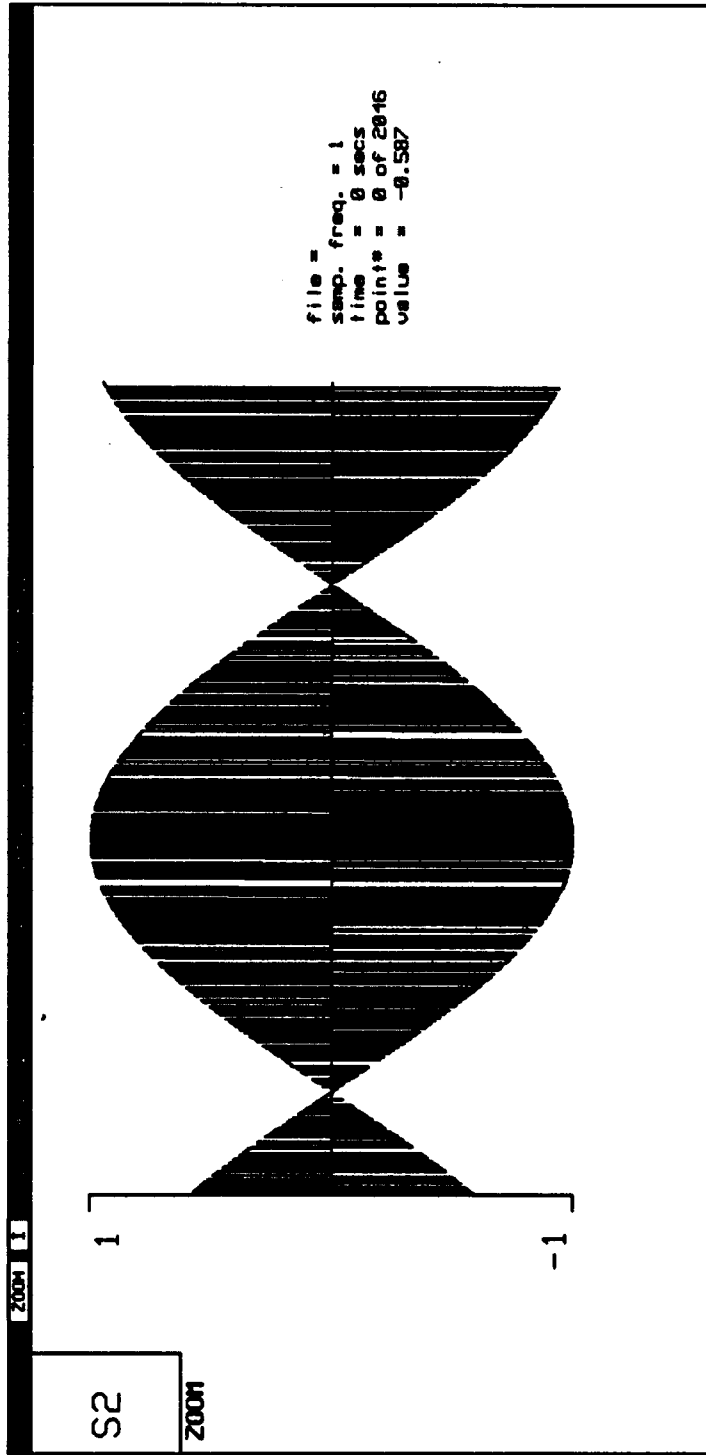


Figure 62 Input of Threshold Detector with 800 Hz Doppler. PAR=17.8 dB

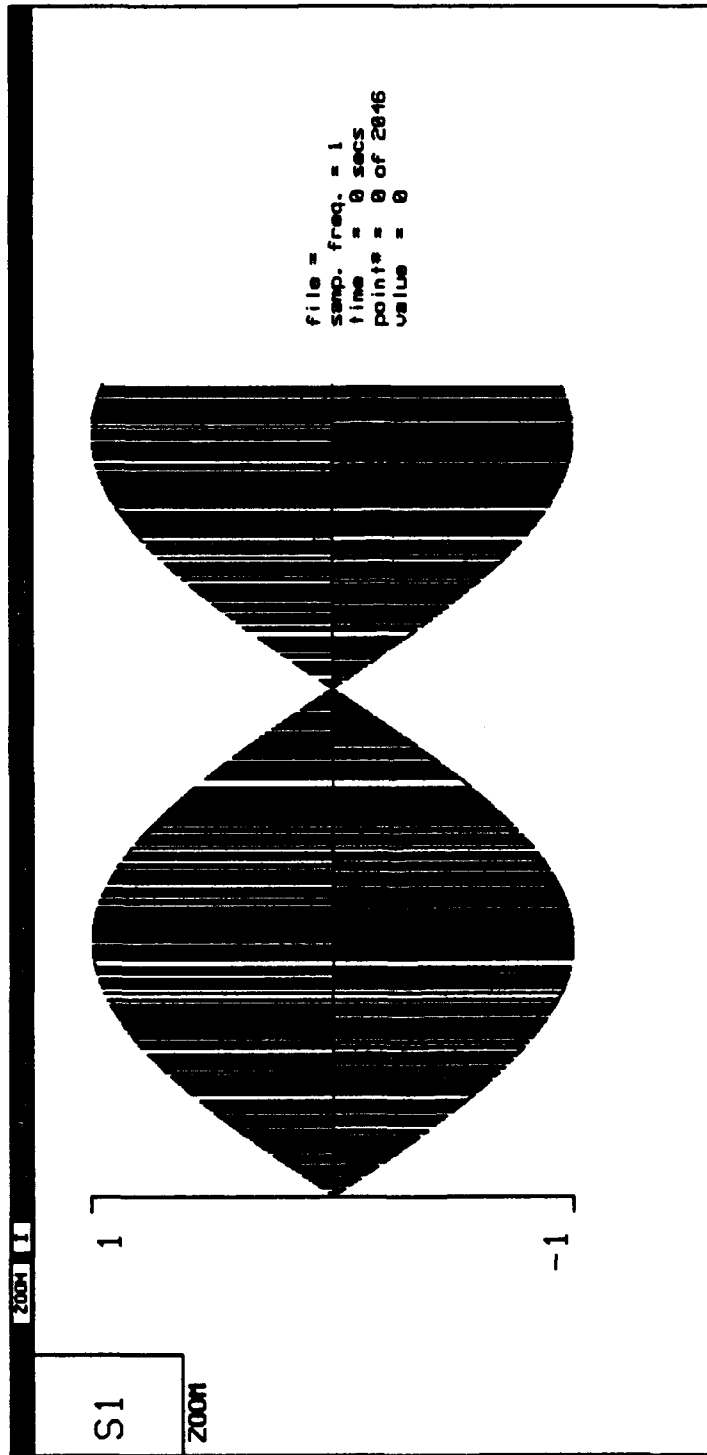


Figure 63 Input of Threshold Detector with 800 Hz Doppler and $\theta=0.6$. PAR=18.0 dB

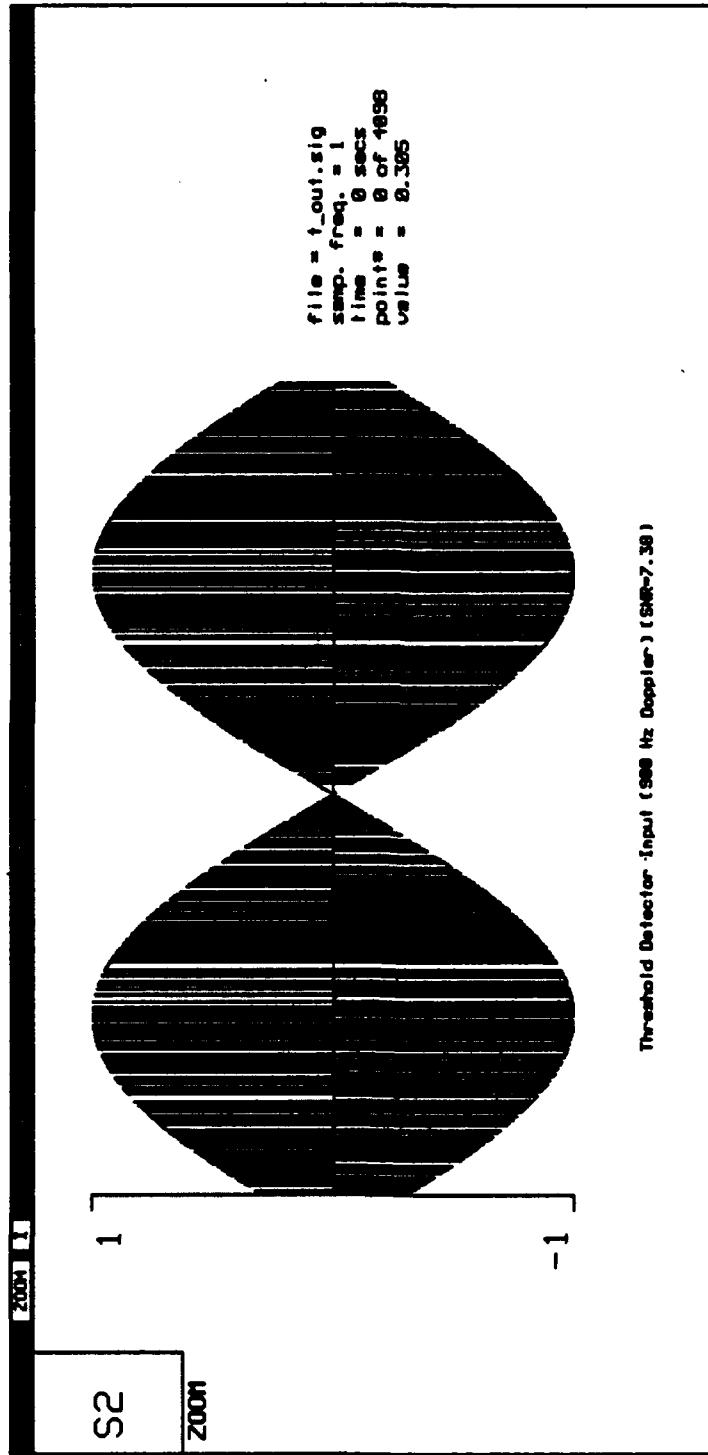


Figure 64 Input of Threshold Detector with 900 Hz Doppler and $\theta=0.5$ PAR=7.4 dB

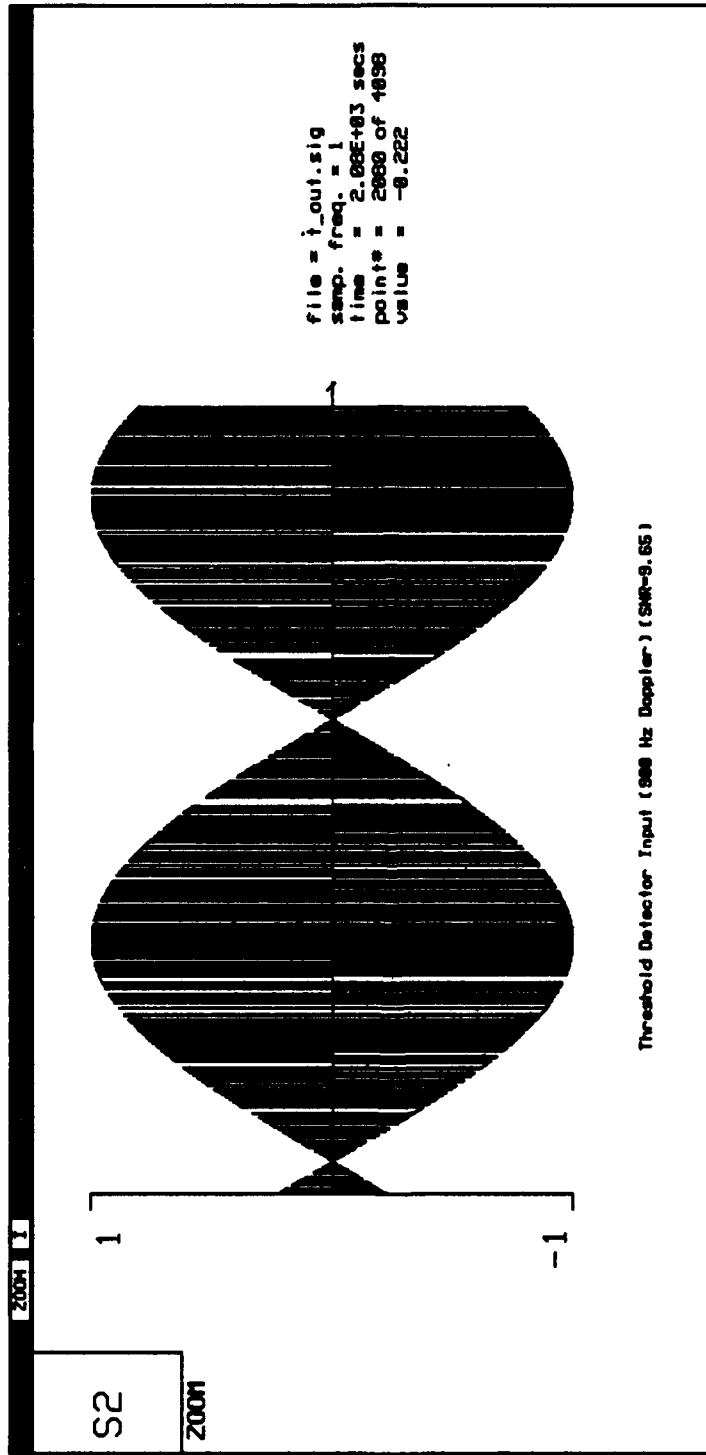


Figure 65 Input of Threshold Detector with 900 Hz Doppler. PAR=9.7 dB

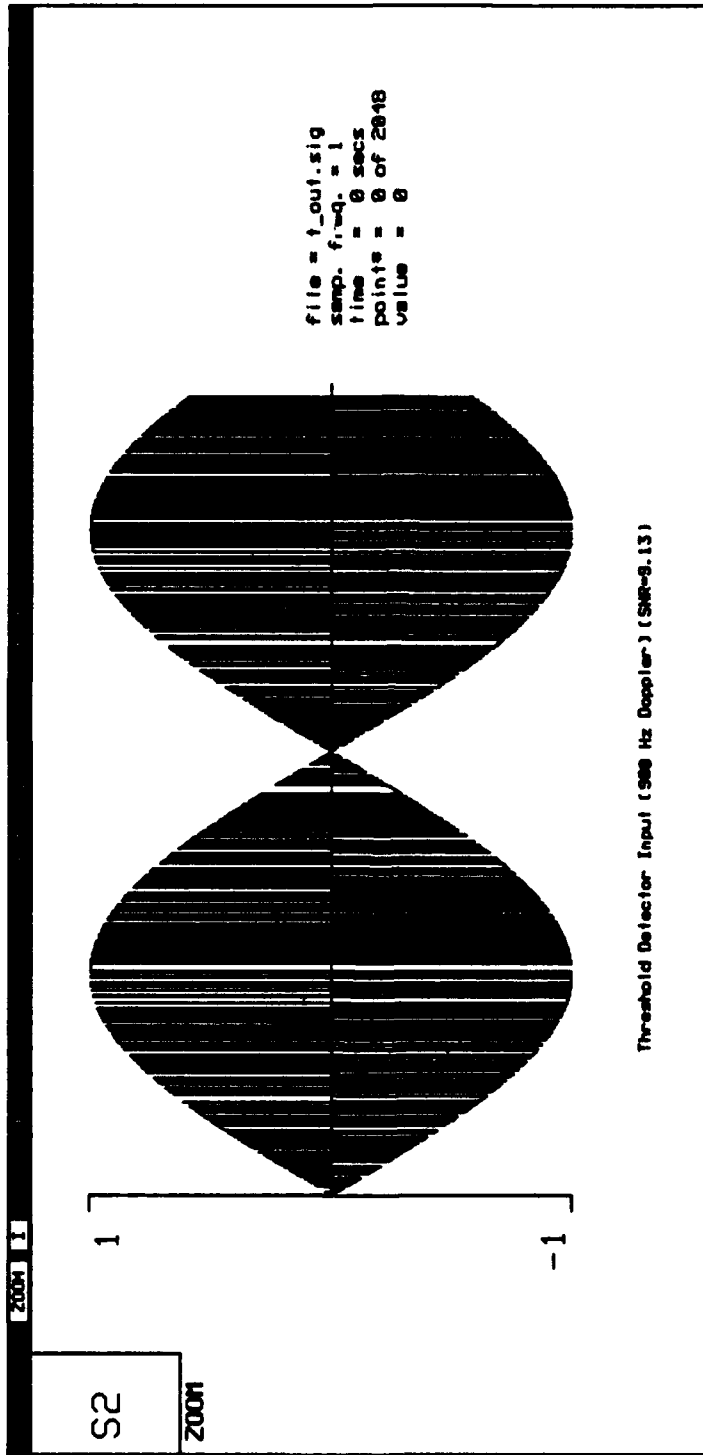


Figure 66 Input of Threshold Detector with 900 Hz Doppler. PAR=9.1 dB

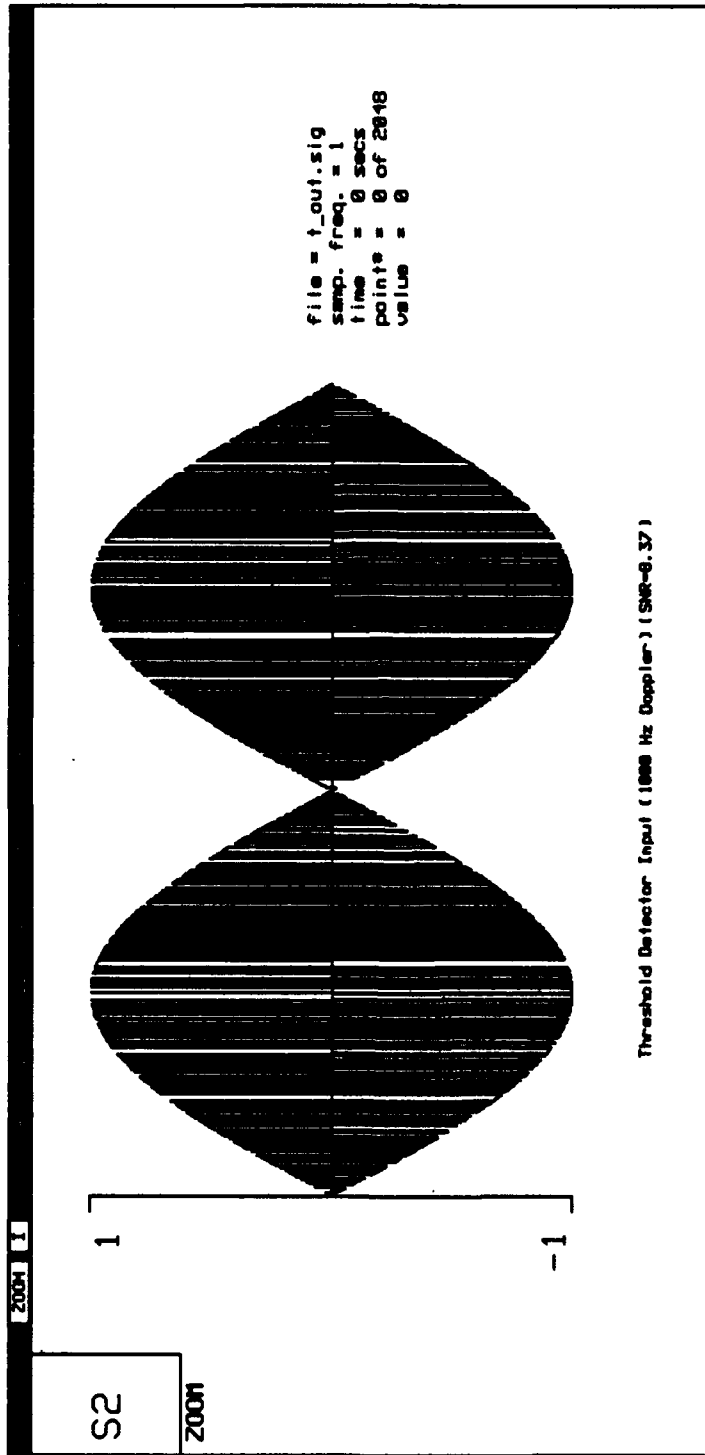


Figure 67 Input of Threshold Detector with 1000 Hz Doppler. PAR=8.4 dB

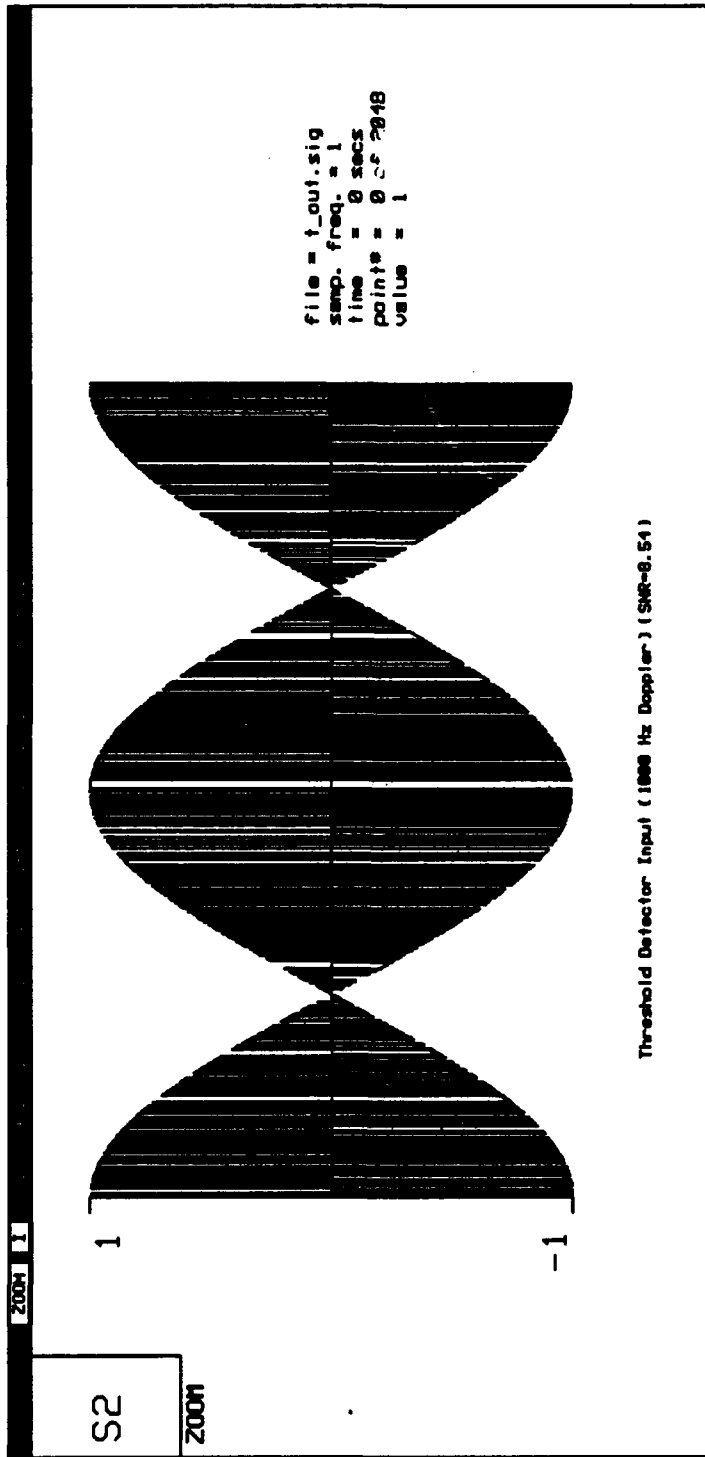


Figure 68 Input of Threshold Detector with 1000 Hz Doppler. PAR=8.5 dB

Bibliography

- 1 Janiczek, P. M. *Global Positioning System Volume I*, Washington DC: Institute of Navigation, 1980.
- 2 Cheng, U. and others. "Spread-Spectrum Code Acquisition in the Presence of Doppler Shift and Data Modulation." *IEEE Transactions on Communications*, 38: 241-250 (February 1990).
- 3 *Signal Processing Work Station™ Users Guide*. Foster City, CA: Comdisco System Inc, 1990
- 4 Dixon, R. C. *Spread Spectrum Systems*. New York: Wiley, 1976
- 5 Van Nee, D. and A. Coenen. "New Fast GPS Code-Acquisition Technique using FFT," *Electronic Letters* 27: 158-160 (January 1991).
- 6 Polydoros, A., and C. L. Weber. "A Unified Approach to serial Search Spread Spectrum Code Acquisition. Part I: General Theory." *IEEE Transaction on Communications Technology*. 32: 542-549 (1984)
- 7 Ward, R. B., and K. P. Yui "Acquisition of Pseudo Noise Signals by Recursion-Aided Sequential Estimation." *IEEE Transaction on Communication Technology*. 25: 784-794 (1977)
- 8 Jibrail W. W. and A. J. Houmad. "Acquisition of Direct Sequence Spread Spectrum Signals Using Sliding Correlators." *International Journal of Electronics*. 71: 733-743 (1991)
- 9 Davenport, Robert. "FFT Processing of Direct Sequence Spreading Codes Using Modern DSP Microprocessors," *IEEE Proceedings of the 1991 National Aerospace and Electronics Conference*. 98-105. New York: IEEE Press, 1991
- 10 Oppenheim, A. V. and Ronald W. Shafer. *Discrete-Time Signal Processing*. Englewood Cliffs, New Jersey: Prentice-Hall, Incorporated, 1989.
- 11 Elliot, D. *Handbook of Digital Signal Processing*. London: Academic Press Inc., 1987
- 12 Sklar, Bernard. *Digital Communications*. Englewood Cliffs, New Jersey: Prentice Hall, 1988

Bibliography (continued)

- 13 Gagliardi, Robert M. *Introduction to Communications Engineering*, New York: John Wiley and Sons, Incorporated, 1988
- 14 Gilbert, Stephen W. *Global Positioning System Volume III*, Washington DC: Institute of Navigation, 1980.
- 15 Stremler, Ferrel G. *Introductions to Communications Systems*, Reading, Massachusetts: Addison-Wesley Publishing Company, 1990
- 16 Gold, R. "Optimal Binary Sequences for Spread Spectrum Multiplexing," *IEEE Transactions on Information Theory*, 13: 619-621 (1967)

Vita

Captain Ronald E. Schmitz was born on 26 August 1955 in Coldwater, Ohio. He graduated from St Henry High School in St Henry, Ohio in May 1973 and enlisted in the U.S. Air Force in January 1976. After completion of training, he served as an Aircraft Control and Warning Radar Repairman. In August 1979, he was retrained into the Digital Flight Simulator Repairman career field and served as a Digital Flight Simulator Repairman. In 1983, he was selected for the Airmen Education and Commissioning Program and attended Michigan Technological University, graduating with a Bachelor of Science in Electrical Engineering in June 1986. Upon completion of Officer Training School in September 1986, he received a commission in the USAF and was assigned to the 1839th Engineering and Installation Group. There, he served as the division Chief of Readiness and Training and a communications engineer. In September 1988, he was transferred to the 1815th Operational Test and Evaluation Squadron and served as a Test and Evaluation Test Team Chief until entering the School of Engineering, Air Force Institute of Technology in May 1991.

Permanent Address:

705 Spruce Street

Hubbell, MI 49934

REPORT DOCUMENTATION PAGE

Form Approved
OMB No. 0704-0188

Public reporting burden for this collection of information is estimated to average 1 hour per response, including the time for reviewing instructions, searching existing data sources, gathering and maintaining the data needed, and completing and reviewing the collection of information. Send comments regarding this burden estimate or any other aspect of this collection of information, including suggestions for reducing this burden, to Washington Headquarters Services, Directorate for Information Operations and Reports, 1215 Jefferson Davis Highway, Suite 1204, Arlington, VA 22202-4302, and to the Office of Management and Budget, Paperwork Reduction Project (0704-0188), Washington, DC 20503.

1. AGENCY USE ONLY (Leave blank)	2. REPORT DATE December 1992	3. REPORT TYPE AND DATES COVERED Master's Thesis	
4. TITLE AND SUBTITLE ACQUISITION OF DIRECT SEQUENCE SPREAD SPECTRUM SIGNALS USING DIGITAL SIGNAL PROCESSING TECHNIQUES		5. FUNDING NUMBERS	
6. AUTHOR(S) Ronald E. Schmitz		8. PERFORMING ORGANIZATION REPORT NUMBER AFIT/GE/ENG/92D-35	
7. PERFORMING ORGANIZATION NAME(S) AND ADDRESS(ES) Air Force Institute of Technology, WPAFB OH 45433-6583		10. SPONSORING / MONITORING AGENCY REPORT NUMBER	
9. SPONSORING / MONITORING AGENCY NAME(S) AND ADDRESS(ES) Lt Col Wiernle 6585th Test Group Guidance Test Division Holloman AFB, NM 88330-5000		11. SUPPLEMENTARY NOTES	
12a. DISTRIBUTION / AVAILABILITY STATEMENT Approved for public release; Distribution Unlimited		12b. DISTRIBUTION CODE	
13. ABSTRACT (Maximum 200 words) This thesis investigates the use of digital signal processing (DSP) techniques to achieve initial synchronization with Global Positioning System (GPS) Pseudo-Noise (PN) signals. Synchronization with the transmitted PN signal is essential to the despreading of the transmitted Direct Sequence Spread Spectrum (DS/SS) signals and decoding of the transmitted satellite data. The use of DSP methods to decrease the time required to achieve initial synchronization is investigated. This thesis proposes an initial acquisition section of the GPS receiver and derives the equations to show the method is mathematically feasible. Computer simulations of the proposed receiver using received signals corrupted by Doppler shifts and noise and having various code offsets, show that coarse acquisition of GPS signals can be achieved using DSP methods. However, the correlation of the sequences is distorted by zero padding to allow the use of radix-2 FFTs. This distortion can be accounted for and proper coarse acquisition is still achieved.			
14. SUBJECT TERMS GPS, Spread Spectrum, FFT, Acquisition Doppler Shift		15. NUMBER OF PAGES 141	
17. SECURITY CLASSIFICATION OF REPORT UNCLASSIFIED		16. PRICE CODE	
18. SECURITY CLASSIFICATION OF THIS PAGE UNCLASSIFIED		20. LIMITATION OF ABSTRACT UL	
19. SECURITY CLASSIFICATION OF ABSTRACT UNCLASSIFIED			